Investigating the Rotational Catalytic Mechanism of the *Escherichia coli* F_1-ATPase

Joanne Amanda Baylis Scanlon
Charlottesville, Virginia

B.S. Physics, College of Charleston, 1998

A Dissertation presented to the Graduate Faculty
of the University of Virginia in Candidacy for the Degree of
Doctor of Philosophy

Biophysics Program

University of Virginia
August, 2008

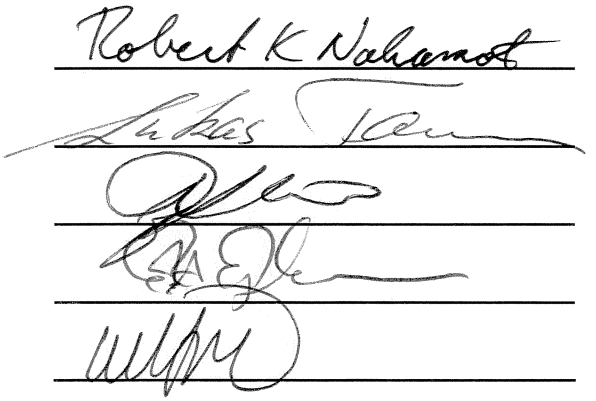

ABSTRACT

The F_OF_1 is a multi-subunit enzyme that functions as a mechanical motor using rotation to efficiently couple the chemical energy from ATP synthesis/hydrolysis to ion translocation across the membrane. Steady state ATP hydrolysis in the F_1-ATPase involves rotation of the central γ subunit relative to the catalytic sites in the $\alpha_3\beta_3$ pseudo hexamer. In order to understand the role of γ subunit rotation in the catalytic mechanism, the pre-steady state kinetics of Mg·ATP hydrolysis upon rapid filling of all three catalytic sites was determined in the F_1-ATPase. The experimentally accessible partial reactions leading up to the rate limiting step and continuing through to the steady state mode were obtained for the first time. Analysis of the burst kinetics of Mg·ATP hydrolysis indicated that the rate limiting step follows hydrolysis and precedes the release of products Pi and ADP. The burst kinetics and steady state hydrolysis for a range of Mg·ATP concentrations provided adequate constraints for a unique minimal kinetic model which can fit all the data and satisfied extensive sensitivity tests. Consistent with the single molecule analysis of Yasuda *et al.* [Yasuda, R., Noji, H., Yoshida, M., Kinosita, K., and Itoh, H. (2001) *Nature* 410, 898-904], we propose that the rate-limiting step involves a partial rotation of the γ subunit; hence this step was named k_γ. Moreover, our model suggests that reversible hydrolysis/synthesis can only occur in the active site of the β_{TP} conformer [Abrahams, J. P., Leslie, A. G. W., Lutter, R., and Walker, J. E. (1994) *Nature 370*, 621-628].

To directly test the model two single cysteine mutants, βD380C and βE381C, were used, which can reversibly inhibit rotation upon formation of a cross-link with the

conserved γCys87. In the pre-steady state, the γ-β cross-linked enzyme at high Mg·ATP conditions retained the burst of hydrolysis but was not able to release Pi. These data show that the rate-limiting rotation step, k_γ, occurs after hydrolysis and before Pi release. This analysis provides additional insights into how the enzyme achieves efficient coupling and implicates the βGlu381 residue for proper formation of the rate-limiting transition state involving γ subunit rotation.

TABLE OF CONTENTS

ACKNOWLEGEMENTS

I have to confess that writing this section, while liberating because of lack of restraints on form and content, is also a daunting one to write. Truly, to name all the many people who have helped me through this graduate school process would take a lengthy chapter, particularly as I tend not to be the most succinct of writers!

First, I would like to thank my committee members: Lukas Tamm, William Guilford, Zhifeng Shao, Edward Egelman and John Bushweller, for their thoughtful consideration of my research, their trenchant insights, advice, and also their encouragement and criticisms which ultimately improved both the quality of my work and my understanding of it.

Thank you to Dr. Bob Nakamoto, my advisor. A favourite memory is him walking up and down the middle hallway of Jordan Hall trying to soothe a screaming eight week old baby – who was ravenously hungry and whose mother was furiously trying to finish the long experiment involving radioactivity, which absolutely HAD to be done yesterday! Bob and I have enjoyed chats on a wide range of topics from the scientific community and scientific careers, to golf, and everything in between. He has been greatly considerate of family life, and graciously agreed for me to take the summer off after the birth of my daughter. I am truly grateful for the many hours he spent reading manuscripts and giving feedback. Writing is one of his fortés, and I am deeply grateful for all I have learned about scientific writing from him. Two of his other characteristics are the excitement he shows for interesting data and an eagerness to know the results of important experiments. These qualities are a great encouragement, and motivating. I am grateful for the opportunity to work in his lab.

Thank you to Marwan Al-Shawi for the innumberable hours he spent with me troubleshooting and vehemently discussing (perhaps arguing?) my experimental design, results and conclusions. Where would I be without Marwan, who patiently listened to interminable details surrounding a variety of experimental, instrumental and computational issues I encountered? He always responded with equally detailed instructions on topics I should research and ways to proceed. The man has a penchant for pedantic tendencies, which I am sure I too have acquired, and which have enabled me to see this work through. He also spent a rather large number of days holding eppendorf tubes for kinetic experiments, also weighing and processing samples collected on the quench-flow instrument (a.k.a. the bane of my existence!). It was indeed a dog's life!

I am grateful to the Nakamoto lab members past and present during my tenure: Dr. Scott Andrews, Dr. Hiroshi Omote, Ming Liang Liu, Xiaopu Liu, Dr. Mikhail Galkin, Serhiy Vitko, Nazir Bareksi, Dr. Shimei Gong, Dr. Elaine Etter, Kimberly DiGiandomenico, Dr. Phi Nga Le, Dr. Yelena Peskova, Dr. Edith Sievers, Dr. Jürgen Sievers, Julie Teater, Dannon Smith, Nazir Bareksi, Molly Wingerd, Natalie Negrey, and Dorothy Zhang. I am grateful to them all for sharing laughter and jokes and for many valuable conversations. Edith and Jürgen are wonderful, generous, funny friends, who now live in Germany. Their tenure in the lab is one of the highlights of my time in the lab. Nazir and Serhiy are great additions to the lab. I appreciate their friendship and humour. I have enjoyed my conversations with Misha on F_OF_1, and wish I had spent more time learning from him. I would like to specifically mention several lab members for their direct impact on my work or development as a scientist. I would like to acknowledge Julie Teater and Dorothy Zhang for their assistance with protein

purification, and Julie for helping to lay the groundwork for optimizing the conditions for cross-linking the F_1 mutant proteins.

I am deeply grateful to Phi Nga Le, known to our lab as Le. She is responsible in large part for my development as a scientist. I benefitted directly from her initial work on this project, which I took over, and which ultimately became the bulk of my thesis. Shin-Kai Lin has been my fellow traveler on this graduate school journey. His support, willingness to share advice on protocol details, lunch trips to Qdoba, and discussions on all aspects of the F_OF ATP synthase have enhanced my understanding of the topic. I have enjoyed our friendship, and hope to remain friends after we both graduate. I am grateful to Lena, who ruled the lab with an iron fist when I first joined, and has evolved into a mother hen who has supported Kai and me immensely. Thank you to our former neighbours, the members of the Perozo lab, especially Luis Cuello, Christopher Ptak, Valeria Vasquez, Julio Cordera, Marien Cortes, and Sudha Chakrapani. I enjoyed many discussions with them on scientific and life topics. I miss them.

I am grateful to my fellow graduate students and friends, Kimberley Parrot, Anne Allison, Quyen Aoh, Melissa Fredette, Matthew Zimmerman, Andrea Stith, Margaret Bolton and Ron Neppl, who have been willing to grab coffee and talk about science, graduate school, nerves, dissertation schedules, and life issues in general, especially Anne and Kim, who have supported me in multiple ways. I would also like to acknowledge Angela Otero, Cathy Black, Carol Yowell, Ann Folsom, Pamela Mullinex for their support and encouragement and the Graduate Programs Office, particularly, Susan Amato. I would also like to thank John Chapman for his computer expertise, particularly in the final stages of the dissertation. He effectively dealt with many dramas!

There truly have been too many friends who have supported me through this to be able to name them all. I am deeply grateful to Amy Graeser, Edward and Felicia Song, Kristine Harmon, Melissa Fredette, Judith and David Kovacs, Brian and Beth Vander Wel, Brett Ferrell, Susan and David Murphy, Amanda Woodiel, Dannon Smith, Lauren Winner, Carey Morton, Monica Shenouda, Lillian Huang, Bill Wilder, Quyen Aoh, Abigail Flower, and the group of younger folks from the 11 o'clock Christ Church service. I need to particularly mention Amy Graeser, as none has helped me as much as she. Amy has encouraged me, prayed for me, baked for me, cooked for me, cleaned for me, cared for my daughter and in many countless ways been a true friend. For the abundance of her care and support I am deeply grateful.

I am thankful for my family, my in-laws, the Scanlons, who have embraced me and welcomed me. Bill and Barb Scanlon, Jen and Mark Semioli, Kelly and Jesse Wild, and the girls, they have added much richness to my life. My brothers and sister-in-law Mike Baylis and Steve and Natalie Baylis, have always been encouraging, even when they tease – I take them as they are, and love them for it. I have so much fun when we are together, my great sadness is that we live on three different continents now. To Cherry Baylis, my step-grandmother, who is a bright and vibrant woman, and who has been supportive, encouraging and enthusiastic of my endeavours, a heartfelt thank you.

To my husband, and best friend, Todd, who knows me well, yet loves me still. It has been a long journey for him too, but we have grown together through the whole process. Thank you for your support in the ups and downs. I remember how you would accompany me into the lab at midnight, and fall asleep waiting for me to finish the

labwork I had to do. Words cannot express how much you, and your love and support, have meant to me.

I am very grateful for my daughter Lauren, who has brought so much joy to our lives. She gives us perspective and is a grounding influence. She makes us laugh. She is a delight. She brings me more joy, and whom I love more than I could have ever imagined.

This work is dedicated to my Mum and Dad, who have worked harder, and sacrificed more than I think I will ever know, to give me opportunities they never had. I am grateful that they have raised me to value compassion, empathy and kindness for everyone, but particularly for those less fortunate. Their generosity and hospitality are awe-inspiring. I am grateful for their support, encouragement, but mostly for their unconditional love. This thesis is also dedicated in memoriam of my childhood friend Lewis Muridzo Chitengwa and my grandfather, my favourite, William (Bill) Baylis. I am grateful for their influence in my life, and they continue to inspire me.

LIST OF FIGURES

LIST OF TABLES

ABBREVIATIONS

AMP PNP: adenosine 5′-(β,γ-imido)triphosphate

ATPγS: adenosine 5′-O-(3-thio)triphosphate

BMN: benzylidene malononitrile

CCCP: carbonyl cyanide 3-chlorophenylhydrazone

CM: N-[4-[7-(diethylamino)-4-methyl]coumarin-3-yl)]maleimide

Cy3-nucleotide: 2'-O-Cy3-EDA-nucleotide

DCCD: dicyclohexylcarbodiimide

DTNB: 5,5′-dithiobis(2-nitrobenzoic acid)

DTT: DL-dithiothreitol

FRET: fluorescence resonance energy transfer

MDCC-PBP: 7-diethylamino-3-((((2-maleimidyl)ethyl)amino)carbonyl) coumarin)-labeled phosphate binding protein

MEG: 7-methylguanosine

MOPS: 3-(N-morpholino)propanesulfonic acid

MSC: Model Selection Criterion

PDRM: phosphodeoxiribomutase

PEP: phospho(enol)pyruvate

PNPase: purine nucleoside phosphorylase;

TCEP: tris(2-carboxyethyl)phosphine hydrochloride; TES: 2-[(2-hydroxy-1,1-bis(hydroxymethyl)ethyl)amino]ethanesulfonic acid.

TMH: transmembrane helix

1. Introduction

1.1 Overview

1.1.1 Physiological role of the FoF_1 ATPase

Electron transport mechanisms use reducing equivalents generated from metabolic processes, light or other coupled reactions to generate the proton (or in some organisms, sodium) motive force ($\Delta\mu_{H^+}$, or $\Delta\mu_{Na^+}$). At the cellular level, most activities that require energy derive it from adenosine triphosphate (ATP), specifically the phosphoanhydride bond of ATP. The ATP synthase generates ATP, from ADP and Pi, by utilizing energy derived from transporting protons (or in some organisms, Na^+) across the membrane down their electrochemical potential energy gradient. This coupling between ion movement and ATP synthesis was described by Mitchell in his chemiosmotic hypothesis (Mitchell, 1974; Mitchell and Moyle, 1967). The nearly ubiquitous F_OF_1 ATP synthase is located on the plasma membrane of bacteria, the inner membrane of mitochondria, and the thylakoid membrane of chloroplasts. It is one of the most remarkably well-conserved proteins during evolution and shares a high amino acid sequence identity and overall structure in all organisms from bacteria to humans. There are a few additional subunits and domains in the mitochondrial enzyme (Table 1.1.1), which are thought to play roles in regulation or assembly. Formation of supramolecular complexes of the mitochondrial ATP synthase (Complex V) have been observed (Allen *et al.*, 1989; Buzhynskyy *et al.*, 2007; Nicastro *et al.*, 2000), mediated through F_O subunits *e*

Table I. Subunit nomenclature for the bacterial, chloroplast, and mitochondrial ATP synthase complexes.

	Bacteria	Mitochondria	Chloroplast
F_1 Stator	α	α	α
	β	β	β
F_1 Stator Peripheral Stalk	δ	OSCP[1]	δ
F_1 Rotor, Central Stalk	γ	γ	γ
	ε	δ	ε
		ε	
F_O Stator	*A*	*a*, *e*, *f*, *g*, A6L	*A*
F_O Stator Peripheral Stalk	b_2, or *bb'*	b_2, *d*, F6	*bb'*
F_O Rotor, Central Stalk	$c_{10\text{-}15}$	c_{10}	$c_{10\text{-}15}$

[1]OSCP, Oligomycin Sensitivity Conferral Protein

and *g* (Arselin *et al.*, 2003; Bustos and Velours, 2005; Paumard *et al.*, 2002), and several other newly identified subunits in yeast (Arnold *et al.*, 1998). Electron microscopy revealed that dimers of the mitochondrial enzyme, form at an angle relative to each other causing the membrane to bend (Dudkina *et al.*, 2005; Dudkina *et al.*, 2006; Minauro-Sanmiguel *et al.*, 2005) supporting the role of the ATP synthase oligomerization in cistae morphology of the inner mitochondrial membrane (Giraud *et al.*, 2002; Paumard *et al.*, 2002). These ATP synthase supracomplexes, along with supercomplexes of electron transport chain enzymes, function to stabilize the complexes in the membrane and optimize energy transduction (reviewed in (Vonck and Schaefer, 2008)).

Depending on the conditions, the bacterial F_OF_1 can function in reverse coupling the hydrolysis of ATP to the generation of the electrochemical gradient for subsequent use in nutrient uptake, secondary transport and flagellar rotation. It has also been shown that, under certain circumstances in mitochondria, the enzyme functions as a H^+ pump (Lefebvre-Legendre *et al.*, 2003; Matsuyama *et al.*, 1998; St-Pierre *et al.*, 2000).

1.1.2 Quarternary arrangement of subunits

The fundamental idea behind structural studies in molecular biology is that establishing the structure or structural changes of a biological macromolecule grants insight into its function, commonly termed the structure-function relationship. This has certainly been true for the ATP synthase. Since the early 1970s efforts have been focused on solving the high-resolution structure of the F_OF_1 enzyme from a number of sources using a variety of techniques such as crystallography, nuclear magnetic resonance spectroscopy and electron microscopy. Several high resolution structures are solved for

several of the subunits and subcomplexes, but high resolution structures of the entire complex remains the holy grail of structural studies of the ATP synthase. Relevant structural data that have provided much insight into molecular mechanisms of the enzyme will be highlighted throughout this chapter.

The ATP synthase is traditionally divided into two parts, the membrane embedded F_O sector and the extramembranous F_1 sector, which extends from the membrane surface and projects as a knob-like image in electron micrographs. The *E. coli* transmembranous F_O sector consists of three subunits with one copy of *a*, two of *b*, and 10 copies of the *c* subunit, and facilitates the transport of H^+ across the membrane. The F_1-ATPase is the catalytic portion of the enzyme and consists of five subunits in the following stoichiometry $\alpha_3\beta_3\gamma_1\delta_1\varepsilon_1$. These two sectors are structurally and functionally distinct, separated by *ca.* 100 Å, and are joined only by the two stalk regions. Mitochondria and chloroplasts contain homologous subunits to all the subunits found in the bacterial enzyme, but the F_O portion in particular is more complex in mitochondria, with several additional subunits (Collinson *et al.*, 1994). The quarternary relationship of the subunits for the *E. coli* enzyme is shown in Fig. 1.1.1.

The relative positions of the subunits were determined using various methods before any high resolution structures were solved (for a review see (Capaldi *et al.*, 1992)). The subunits that compose the F_1 globular portion were imaged by electron microscopy, showing a hexameric ring of six densities, which were identified as alternating α and β subunits through the use of subunit specific antibodies (Gogol *et al.*, 1989a; Lündsdorf *et al.*, 1984).

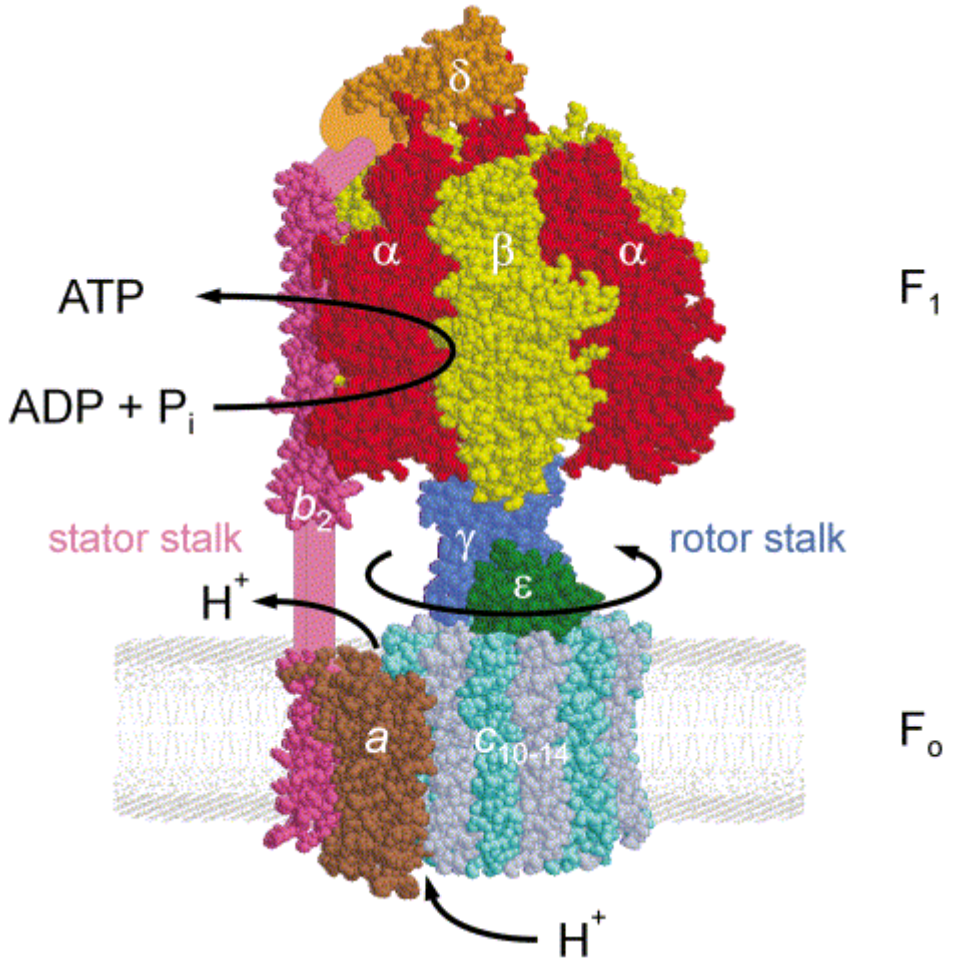

Figure 1.1.1. Structure of *E. coli* F_1F_0-ATP synthase.

The solvent exposed F_1 sector of *E. coli* ATP synthase consists of $\alpha_3\beta_3\delta\varepsilon$. The F_o sector consists of the membraneous subunits: ab_2c_{10}. The three catalytic β subunits alternate with the three non-catalytic α subunits. The nucleotide binding sites are located at the α/β subunit interfaces. The γ subunit interacts with *c* and ε, and its long helical coiled-coil (not shown) extends almost to the top of the central cavity within the $\alpha_3\beta_3$ hexagon. The δ-subunit is situated on top of F_1. The *a*-subunit interacts with, and lies outside the *c*-ring. Functionally it is divided into rotor and stator. The rotor consists of γε and a ring of 10 *c* subunits, the stator consists of $b_2\delta$ and the $\alpha_3\beta_3$ hexamer. The structure shown here is a model (Rastogi and Girvin, 1999). High-resolution structures have been determined for all subunits except *a*-subunit, the C-terminal domain of δ, and portions of the *b*-subunits (Del Rizzo *et al.*, 2002; Dmitriev *et al.*, 1999; Fillingame *et al.*, 2000a; Fillingame *et al.*, 2000b; Gibbons *et al.*, 2000; Menz *et al.*, 2001; Uhlin *et al.*, 1997; Wilkens *et al.*, 1997). Figure from (Weber, 2003).

Similarly, the position of the γ subunit within the $\alpha_3\beta_3$ hexameric ring was determined by electron microscopy (Gogol *et al.*, 1989b). Cross-linking studies and mutagenesis determined the position of the ε subunit as part of the central stalk with γ (reviewed in (Capaldi and Schulenberg, 2000; Vik, 2000). In the F_O sector atomic force microscopic and electron microscopic low-resolution images suggested the *c* oligomer formed a ring-like arrangement with subunits *a* and *b* lying at the periphery (Birkenhäger *et al.*, 1995; Singh *et al.*, 1996; Takeyasu *et al.*, 1996). The oligomeric *c* subunit ring model was supported by the crystallographic structure of the yeast mitochondrial enzyme at 3.9 Å (Stock *et al.*, 1999). The second peripheral stalk, formed by the two *b* subunits extending from F_O to F_1 was seen in electron micrographs (Bottcher *et al.*, 1998; Wilkens and Capaldi, 1998a).

1.1.3 Function of the F_OF_1 ATPase

Mechanistically the F_OF_1 has remained conserved from eubacteria to mitochondria, and has been shown to function using a unique rotary mechanism ((Kato-Yamada *et al.*, 1998) reviewed in (Nakamoto *et al.*, 2008; Nakamoto *et al.*, 1999)). Considering this, the molecular motor F_OF_1 ATPase can be divided into two counter-rotating assemblies. In *E. coli* the assembly defined as the stator consists of the α_3, β_3, δ, a, b_2 subunits and the rotor is composed of the γ, ε, c_{10} subunits.

The F_O and F_1 each individually function as a motor. By itself F_1 is able to hydrolyze, but not synthesize ATP, and F_O alone can passively conduct protons. Together F_OF_1 links the two functions of active proton transport and synthesis/hydrolysis of ATP. In the synthesis mode the F_O motor converts the electrochemical energy stored

in the ion motive force into mechanical energy of rotation of the *c*-subunit ring. Rotation of the *c*-ring generates torque in the F_1 rotor subunits, ε, and the asymmetric γ subunit which drives conformational/binding changes in the catalytic β subunits. The conformational changes lead to formation of ATP from ADP and Pi, and its subsequent release from the catalytic sites. F_1 therefore converts the rotational energy into chemical energy by generating the phosphoanydride bond of ATP. Each motor exchanges energy with the other, in an incredibly efficient manner, through mechanical rotation of the central stalk. In hydrolysis the reaction and rotation occur in reverse. Oster and Wang compiled the kinetic, biochemical and structural data into a mathematical model to describe the energy transduction in the F_OF_1 motors where binding energy of the nucleotide is translated into elastic strain in the enzyme and is released to drive rotation (Elston *et al.*, 1998; Oster and Wang, 2003). In mitochondria, the high efficiency of the glucose metabolic pathway is dependent on the high efficiency of this final step of oxidative phosphorylation, since most ATP is generated via this pathway and the ATP synthase.

The communication between the two physically and functionally distinct portions of the enzyme involves many complicated subunit-subunit interactions, and an important goal of studies on this enzyme involves understanding the mechanism which links or couples the two disparate functions of catalysis and transport. On a more fundamental level are the questions of how the F_1 sector converts the chemical energy stored in ATP to rotational mechanical energy, termed chemomechanical coupling, and how the F_O

sector converts the electrical and chemical energy of the potential gradient stored across the membrane, into rotational energy, termed electro-chemomechanical coupling.

1.2 Transport Through F_O

Structurally the F_O sector is the least well-defined part of the ATP synthase. In order to fully describe the molecular mechanism of transport through the F_O motor, a high resolution structure is needed. Fig. 1.2.1 illustrates the general features of the proposed transport pathway through F_O.

1.2.1 The c subunit: the proton carrier

Multiple copies of the small (8.3 kDa), hydrophobic *c* subunit are present in the F_O complex. The number of *c* subunits is variable and controversial with proposed stochiometries ranging from 10-15 for different species (Jiang *et al.*, 2001; Meier *et al.*, 2003; Pogoryelov *et al.*, 2005; Seelert *et al.*, 2000; Stahlberg *et al.*, 2001; Stock *et al.*, 1999). However improved experimental design yielded a stochiometry of 10 for the *E. coli* enzyme, based upon functional, co-expressed, genetically fused trimers and tetramers (Jiang *et al.*, 2001). Consistent with this is the structure of the yeast mitochondrial subcomplex composed of F_1 and 10 *c* subunits (Stock *et al.*, 1999), and the stochiometry of 10 *c* found in the thermophilic Bacillus PS3 (Mitome *et al.*, 2004). However the high resolution structure of the *c*-ring of the Na^+-transporting F-ATPase of *Ilyobacter tartaricus* was solved and consisted of 11 *c* subunits (Meier *et al.*, 2005). In current models of transport, the number of subunits in the *c*-ring corresponds to the number of H^+ (or Na^+) transported per 360º rotation, and three ATP synthesized, therefore the

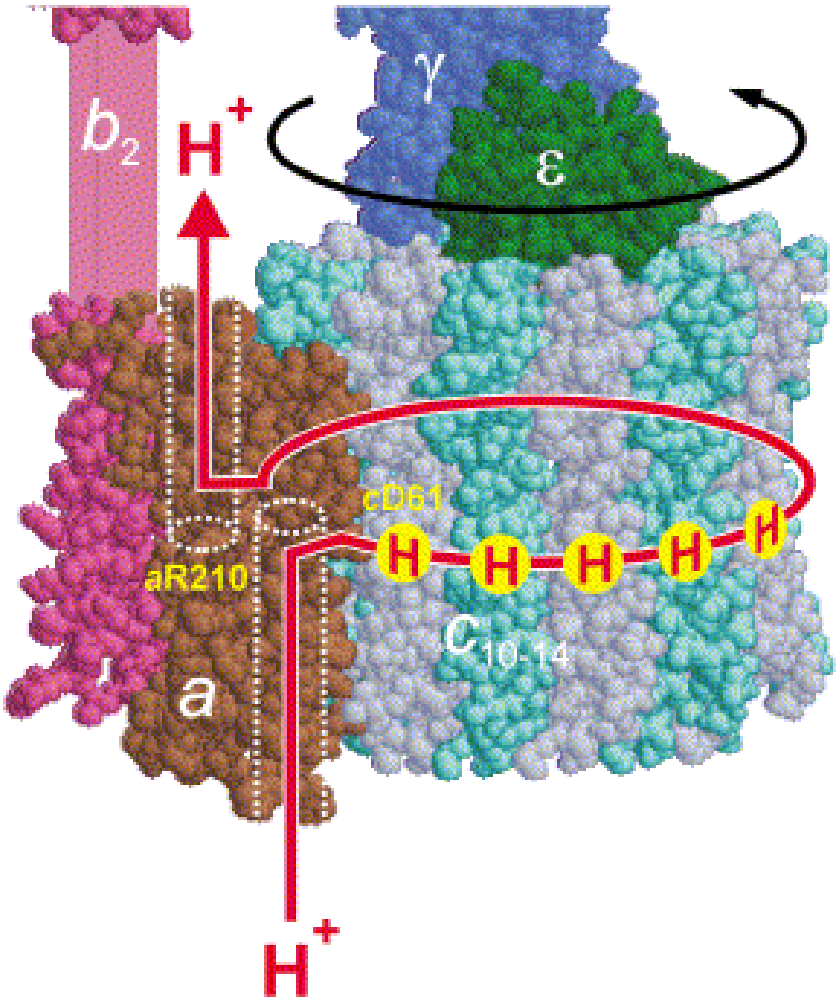

Figure 1.2.1. Structure and proposed proton transport pathway through F_O.
The conserved residues *c*Asp61 and *a*Arg210 are located in the middle of the bilayer at the interface of *a* and *c*-ring. The interaction of these two residues is required for proton translocation coupled to rotation, and is described in the text. Putative proton access inlet and outlet half-channels are shown. The direction indicated for rotation and H^+ pumping shown is for synthesis. Protons enter from the periplasmic inlet half-channel, protonate and neutralize *c*Asp61, this residue thus neutralized can enter the hydrophobic lipid environment to allow the next *c*Asp61 to be protonated. The *c*-ring carries protons around until they exit from the cytoplasmic outlet half-channel. Figure from (Weber, 2003).

variability seen may be due to the advantage a higher *c* subunit stochiometry would afford ion pumping bacteria under low ion motive force conditions. In the ATP synthesis direction, the coupling ratio, or the number of *c* subunits divided by three (the number of ATP synthesized/hydrolyzed per 360º rotation), dictates the ion-motive force required to synthesize ATP. The number and whether it varies within a complex is still a topic of some debate (Krebstakies *et al.*, 2008; Pati *et al.*, 1991).

The high resolution structure of the monomeric *c* subunit was solved by NMR in a membrane-mimicking solvent composed of chloroform:methanol:water (4:4:1) at pH 5 (Girvin *et al.*, 1998), Fig. 1.2.2. The subunit folds as a hairpin of two closely packed, parallel α helices connected by a seven residue, conserved polar loop, oriented on the cytoplasmic side of the membrane towards F_1. The loop plays a role in binding of F_1 to F_O (Fraga and Fillingame, 1991; Fraga and Fillingame, 1989; Fraga *et al.*, 1994b) and *c*Arg41-Gln42-Pro43-Asp44 (*E. coli* sequence numbering) interact with the F_1 γ and ε subunits (Fraga *et al.*, 1994b; Hermolin *et al.*, 1999; Watts *et al.*, 1996; Zhang and Fillingame, 1995; Zhang *et al.*, 1994) described more fully in section *1.6.1.1*). The N-terminal transmembrane helix (*c*Helix-1) is Gly and Ala rich and consequently has a smaller diameter than the C-terminal α-helix (*c*Helix-2), which contains the conserved *c*Asp61, located in the middle of the helix (Hermolin and Fillingame, 1989). The *c* subunit hairpin molecules are oval-shaped due to the close interactions between the

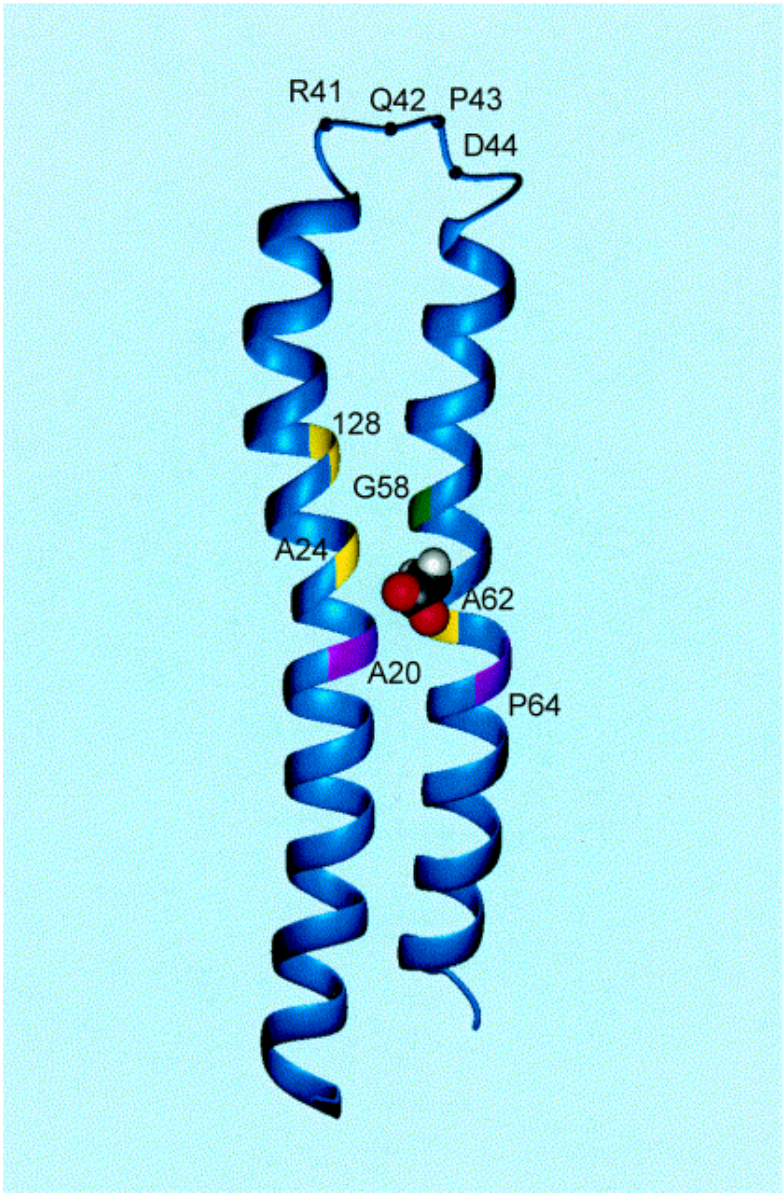

Figure 1.2.2. NMR structure of subunit *c* at pH 5.

Subunit *c* exhibits a hairpin-like fold. In this structure the Asp^{61} is protonated (Girvin *et al.*, 1998), and the side chain packs towards the "front" of the structure with the Ala^{24} and Ile^{28} side chains (not shown) packing towards the "back" of the structure. The positions of key residues are indicated. Structure depicted from PDB entry 1c0v (Rastogi and Girvin, 1999) by (Fillingame and Dmitriev, 2002).

residues. Molecular dynamics and energy minimization calculations were used to model the *E. coli* oligomeric *c* subunits using the monomeric NMR structure and inter-subunit distance constraints derived from native F_OF_1 cross-linking data (Dmitriev *et al.*, 1999b), and were shown to pack front-to-back with *c*Helix-1 inside and *c*Helix-2 outside the ring (Dmitriev *et al.*, 1999b; Jiang and Fillingame, 1998; Jones *et al.*, 1998). The structure of the *I. tartaricus* undecameric complex was mostly consistent with this arrangement revealing a cylindrical hour-glass shaped ring with the 11 *c*Helices-1 forming a tight inner ring, and the 11 *c*Helices-2 packed into the grooves, forming an outer ring (Meier *et al.*, 2005), Fig. 1.2.3. In the membrane environment the inner lumen is thought to be filled with lipids (Meier *et al.*, 2005; Oberfeld *et al.*, 2006), although this is still a topic of debate, and in the absence of F_1, F_O allows passive conductance of protons.

The key functional residue of subunit *c* is Asp61, the proton binding site and carrier. Covalent modification of *c*Asp61 by inhibits the enzyme, and mutagenesis indicates the necessity of an ionizable group for proton transport (Hermolin and Fillingame, 1989). In addition, proton transport function was retained when the Asp at position 61 on *c*Helix-2 was interchanged with residue 24, the corresponding position on *c*Helix-1, this mutant is usually termed the D24N61 mutant (Miller *et al.*, 1990; Zhang and Fillingame, 1994). The unusually high pKa of the *c*Asp61 carboxyl group, 7.1 compared with values below 6 for other carboxyl groups in the subunit (Assadi-Porter and Fillingame, 1995), suggested it was buried in a hydrophobic pocket and protonated at pH 5, and almost completely deprotonated at pH 8. The solution structure of the *c*

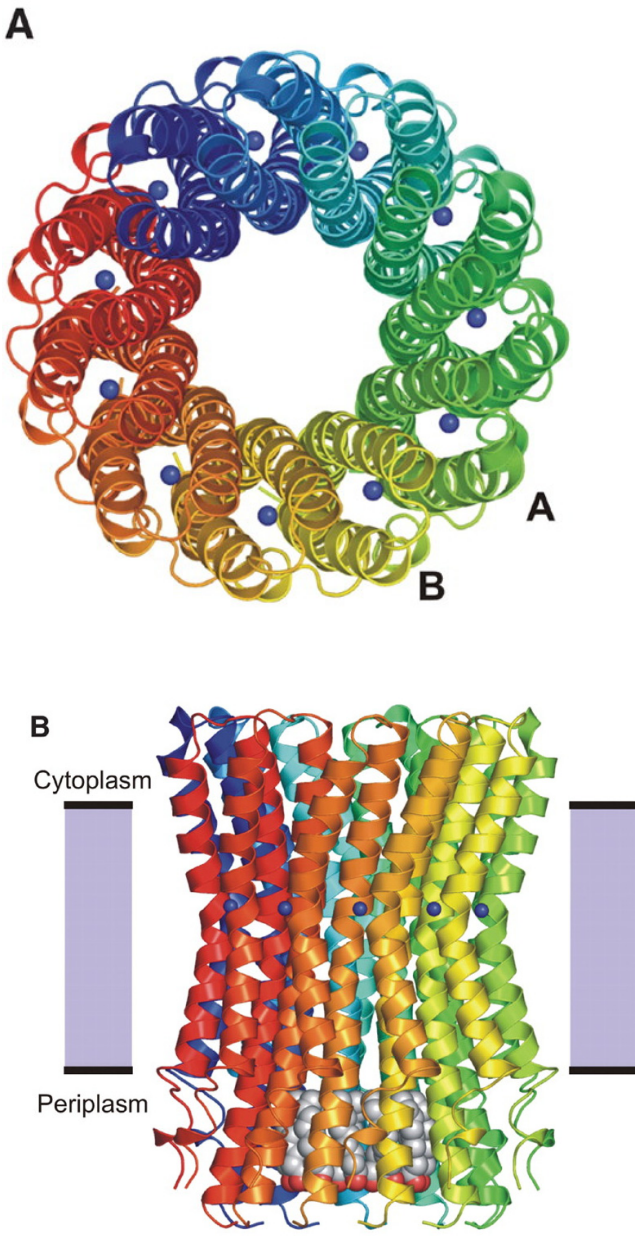

Figure 1.2.3. Ribbon representation of the structure of the c_{11} ring from the Na^+ transporting variant *I. tartaricus*.

Subunits are shown in different colors. (**A**) View from the cytoplasmic side, perpendicular to the membrane, with two labeled subunits. (**B**) Side view showing the hour-glass-like structure. The blue spheres represent the bound Na^+ ions. The position of the membrane is illustrated by the gray shaded bar. (Meier *et al.*, 2005).

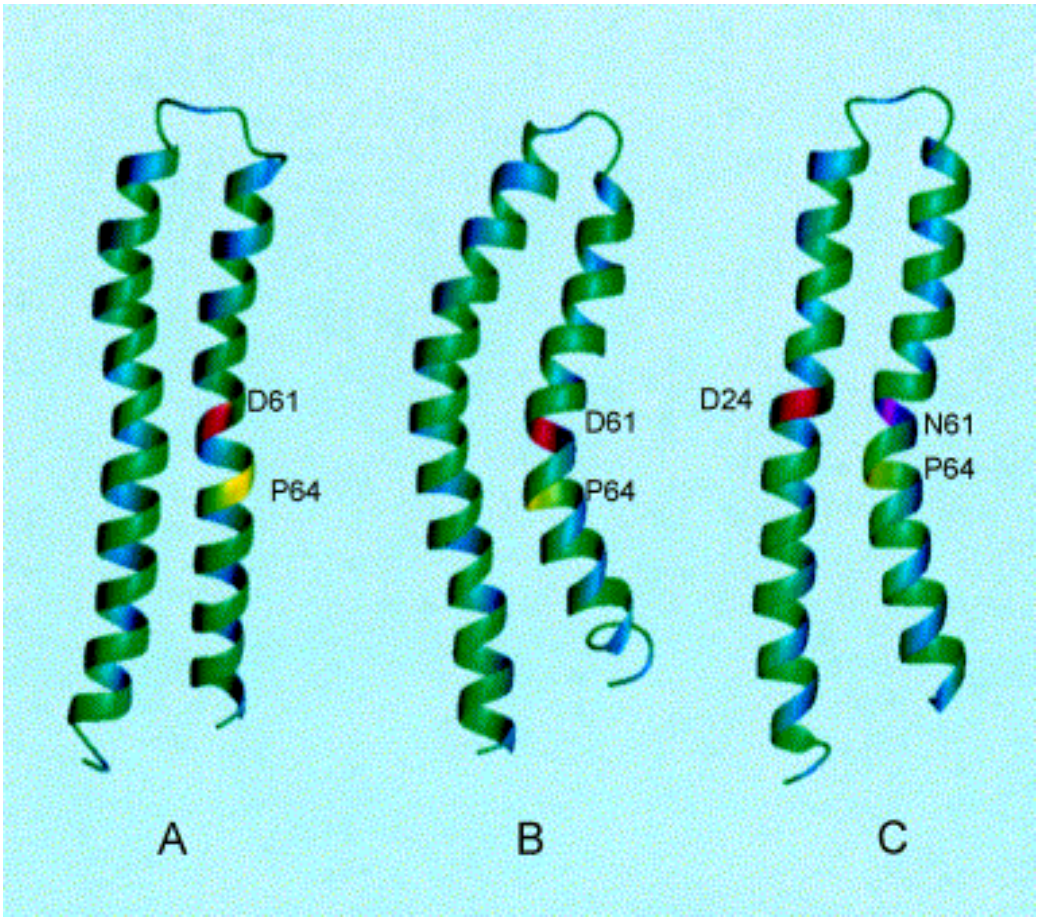

Figure 1.2.4. Ribbon diagram comparing structures of subunit *c*.

(A) Structure of the wild-type subunit *c* at pH 5 (PBD entry 1c0v (Rastogi and Girvin, 1999)). (B) Structure of wild-type subunit *c* at pH 8 (PBD entry 1c99 (Rastogi and Girvin, 1999)). (C) Structure of the functional interchange mutant, D24N61 subunit *c* at pH 5 (PBD entry 1L6T (Dmitriev *et al.*, 2002)). Figure from (Fillingame and Dmitriev, 2002).

subunit monomer was solved at pH 8, in the chloroform-methanol-water solvent (Rastogi and Girvin, 1999), revealing a 140° rotation of *c*Helix-2 relative to *c*Helix-1, Fig 1.2.4B. This was consistent with large structural changes which had been seen in the region of the loop occurring over the pH range for Asp61 ionization (Assadi-Porter and Fillingame, 1995). Interestingly the structure of the functional interchange mutant, D24N61, at pH 5, (known to be protonated at this pH) was very similar to the structure of the wild-type *c* subunit at pH 8 (Dmitriev *et al.*, 2002), Fig 1.2.4C. The swivel of the helices caused a reorientation of Asp61 from facing towards the "front" of the hairpin to facing towards the "back." This helical rotation is thought to play a role in driving the rotation of the *c* subunit ring (Angevine *et al.*, 2003; Fillingame *et al.*, 2003).

1.2.2 The a subunit: mediation of the access half-channels

Subunit *a* is a highly hydrophobic protein with five transmembrane helices (TMH) (Long *et al.*, 1998; Valiyaveetil and Fillingame, 1998; Wada *et al.*, 1999), located at the periphery of the *c*-ring with which it forms a stable, yet dynamic interface allowing almost frictionless rotation of the *c*-ring against it (Ueno *et al.*, 2005). It is thought to be the major component of the H^+ access half-channels from the cytoplasm and periplasm to the center of the membrane to allow interaction with *c*Asp61 (illustrated schematically in Figure 1.2.1). The three-dimensional structure has not been solved and not much is known of the packing its helices. Residues important in forming the aqueous half-channels were determined by reacting substituted cysteines with Ag^+, which inhibits activity, and N-ethylmaleimide, to define the solvent accessibility (Angevine and Fillingame, 2003; Angevine *et al.*, 2003; Angevine *et al.*, 2007; Fillingame *et al.*, 2002).

The two residues thought to form the ends of the access pathways are *a*Ser206 and *a*Asn214 (Angevine and Fillingame, 2003; Fillingame *et al.*, 2002). The Ag^+ sensitive pathway was mapped to the interior surfaces of a bundle of four transmembrane helices (TMH) bundle of subunit *a*, *a*TMH-2-5, the arrangement of which was predicted by cross-linking and second-site suppressor studies (Schwem and Fillingame, 2006). This cluster forms a continuum of Ag^+ sensitive residues extending to each side of the membrane and a swiveling of the helices was proposed as a gating mechanism (Fillingame *et al.*, 2002). Interestingly, a recent study using the same techniques mapped Ag^+ sensitivity to regions of the cytoplasmic loops (Moore *et al.*, 2008). These were determined by cross-linking to form a closely packed cluster of loops, and a role for this single domain in gating H^+ release to the cytoplasm was proposed (Moore *et al.*, 2008).

Located near the middle of the membrane on *a*TMH-4 is the only absolutely essential residue in *a* for function, *a*Arg210 (Cain and Simoni, 1989; Lightowlers *et al.*, 1987). It is thought to lower the pKa of *c*Asp61 and force deprotonation of the *c* subunit residue as it passes the *a* subunit stator (Elston *et al.*, 1998; Fraga *et al.*, 1994a). Interaction between the *a* and *c* subunits is vital for transport as revealed by mutational studies where activity of the double mutant *c*Asp24/*c*Gly61 was enhanced by third-site mutations in *a*, near *a*Arg210 (Friedl *et al.*, 1983; Schneider and Altendorf, 1985). The close interaction of *a*TMH-4 and *c*Helix-2 was confirmed by cross-linking studies (Jiang and Fillingame, 1998). Importantly, the face of the *c*Helix-2 that cross-links with *a* packs against the *c*Helix-1 in the solution structure of the monomeric *c* subunit at pH 5 (Girvin *et al.*, 1998), and in the c-ring model and structure (Dmitriev *et al.*, 1999b; Meier *et al.*,

2005). In additional it packs against the adjacent *c* subunit in the oligomeric model and structure (Figure 1.2.3) and is therefore inaccessible to subunit *a*. However in the NMR solution structure of *c* at pH 8 (Rastogi and Girvin, 1999), and the double mutant *c*Asp24/*c*NAsn61 (D24N61) at pH 5 (Dmetriev 2002), the rotation of *c*Helix-2 allows *c*Asp61 access to *a*Arg210, Fig. 1.2.4, which has led to the refinement of models for proton translocation through F_O, as described in the next section.

1.2.3 Model of H^+ transport through F_O

Single molecule experiments allowed direct observation of rotation by probes attached to the *c*-ring when F_OF_1 was anchored through tags on the β subunits (Pänke *et al.*, 2000; Sambongi *et al.*, 1999), and also in the reverse orientation, rotation of the α-β subunits was visualized when the anchoring tags were on the amino-termini of the *c* subunits (Nishio *et al.*, 2002). Transport-driven rotation was conclusively shown in F_OF_1 by fluorescence energy transfer between γ and *b* subunits (Zimmermann *et al.*, 2006). Taken together, results from the single molecule experiments and the structural and functional studies of individual subunits have allowed the development of models for transport through F_O (Aksimentiev *et al.*, 2004; Dimroth *et al.*, 2006; Fillingame and Dmitriev, 2002; Junge *et al.*, 1997; Rastogi and Girvin, 1999; Vik *et al.*, 2000; Wang and Oster, 1998). There seems to be a general consensus of the main features of the mechanism, although the intricate nature of the interactions between *a* and *c* subunits that drive rotation and ion translocation and the molecular specifics of the different models differ widely.

The c-ring rotor undergoes thermal fluctuations, rotating within a narrow range in both directions, and in an idling mode it can transport ions across the membrane. The pH gradient across the membrane biases the direction of *c*-ring rotation because the proton binding site exposed to the access channel on the side with the higher proton concentration will have a greater probability of being protonated (Junge *et al.*, 1997). Coupling the direction of *c*-ring rotation to the direction of proton flow across the membrane requires that the half-channels from either side of the membrane lead to adjacent *c* subunits. In the ATP synthesis direction, another requirement for H^+ transport is the electrical ($\Delta\psi$) component of the electrochemical ion gradient ($\Delta\mu_{H+}$). Dimroth and coworkers determined that a threshold electrical potential was required to drive ATP synthesis (Dimroth *et al.*, 2000; Kaim and Dimroth, 1999). To take this into account they have incorporated a horizontal component of the potential into their model of ion transport. This potential is thought to act horizontally in the middle of the membrane, in the region between the two aqueous access channels, which are conductive and have essentially the same potential as the side of the membrane to which they are connected (Dimroth *et al.*, 2003).

In ATP synthesis, the concentration of H^+ is high on the periplasmic side of the membrane and protons enter the inlet half channel, which terminates in *a*Asn214, and are transferred from *a*Asn214 to the deprotonated *c*Asp61 (the proton carrier) at the *a*-*c* interface (Aksimentiev *et al.*, 2004). If the *c*Asp61 does not bind a proton, the unprotonated site acts as a ratchet preventing backwards movement of the negatively charged *c*Asp61 because of the energetic penalty of inserting a charged residue into the

hydrophobic environment of the membrane (Junge *et al.*, 1997; Vik and Antonio, 1994). The negatively charged, deprotonated *c*Asp61 is attacted by the *a*Arg210 into the a-c interface where it has an equal probability of moving towards either access channel. It has been proposed that the horizontal component of the membrane potential provides the external driving force to bias the direction of the rotor, by attracting the *c*Asp61 towards the access channel where it can bind a proton. The newly reprotonated (neutral) *c*Asp61 may then leave the *a*-*c* interface and enter the low dielectric environment of the bilayer (Junge *et al.*, 1997), and the cycle occurs again for the following *c* subunit. Rotation of the *c*-ring, driven by the proton gradient, almost completes a revolution, whereupon the proton binding site, *c*Asp61, approaches the *a*-subunit arginine which dissociates the proton due to electrostatic repulsion. The proton is transferred to the *a*Ser206 and released to the cytoplasmic side of the membrane, through the outlet half-channel. The cAsp61 is now negatively charged. The proton pathway is schematically represented in Fig. 1.2.1

In the lipid bilayer each *c*Asp61 residue in the ring is protonated (neutral), and because the *c* subunits are composed mainly of hydrophobic residues, the protonation state of *c*Asp61 can only be changed when interacting with *a*Arg210 on *a*TMH-4. The NMR structure of the interchange double mutant *c*Asp24/*c*NAsn61 (D24N61) (described in *1.2.1*) which is protonated at pH 5 (Dmitriev *et al.*, 2002), was very similar to the wild-type deprotonated *c* subunit, at pH 8 (Rastogi and Girvin, 1999), Fig.1.2.4 and led to the postulation that the large *c*Helix-2 rotation, seen in these structures, occurs before deprotonation (Fillingame and Dmitriev, 2002). This was shown in the model of the *a*-*c*

interaction and the molecular mechanism of H^+ transport through F_O, which was probed through a molecular dynamics simulation and mathematical modeling approach (Aksimentiev *et al.*, 2004). Helical rotation of *c*Helix-2 exposed *c*Asp61, as it approached *a*Arg210 in *a*TMH-4, and caused deprotonation of the *c*Asp61site due to the close proximity to the positive *a*Arg210, as proposed previously (Fillingame *et al.*, 2002). It was found that at the *a*-*c* interface two *c*Asp61 were deprotonated by *a*Arg210 forming a bidentate salt bridge at the center of the bilayer. This allowed a more energetically favorable salt bridge transfer from one *c*Asp61 to the next, and also meant that one *c*Asp61 was always deprotonated (Aksimentiev *et al.*, 2004). It was postulated that *a*TMH-4 inserts between subunits of the *c* oligomer similar to meshed gears (Fillingame *et al.*, 2000; Jiang and Fillingame, 1998). Also that swiveling movements of *a* may be coupled to closing and opening of inlet and outlet channels of the *a* subunits (Fillingame and Dmitriev, 2002). These are still consistent with the molecular modeling data, but the motions may be more subtle than was previously thought. The molecular dynamics revealed (Aksimentiev *et al.*, 2004) that the interaction of the *a*Arg210 and *c*Asp61 also regulate the access of the proton donor and acceptor sites at the ends of the half-channels, *a*Asn214 and *a*Ser206, which in turn regulate access to the pathways while also preventing a short circuit of protons between the two channels.

In summary the proton motive force drives a concerted swiveling of individual *c* subunit helices that are coupled to the protonation state of two neighboring *c*Asp61 residues by salt bridge formation with *a*Arg210, and the rotation of the entire *c*

oligomeric ring. The pH gradient determines the direction of rotation and the membrane potential is the main driving force for torque generation in the ATP synthesis direction.

1.3 The Peripheral Stator Stalk

1.3.1 The δ subunit

In *E.coli*, the δ subunit has a molecular weight of approximately 19 kDa, and its location near the top of the $\alpha_3\beta_3$ hexamer, was determined by cross-linking studies (Lill *et al.*, 1996; Ogilvie *et al.*, 1997). It is required for reconstitution of F_1 to F_O (Smith and Sternweis, 1977), and forms part of the stator-stalk and as such functions to prevent co-rotation of the catalytic $\alpha_3\beta_3$ domain with the rotor. δ connects to the b subunits C-termini *via* its C-terminus (McLachlin *et al.*, 1998) in a Mg^{2+} dependent manner (Weber *et al.*, 2004). The affinity between δ and *b* C-termini are not strong enough to withstand the torque generated by the rotor, so it is thought that additional interaction between *b* and the α/β hexamer strengthens the peripheral stator interaction (Weber, 2006). The N-terminal domain of δ binds to the N-terminal 22 residues of α (Dunn *et al.*, 1980; Weber *et al.*, 2003) with very high affinity (Hasler *et al.*, 1999; Weber *et al.*, 2002). The high resolution structure of the N-terminal domain of δ bound to a 22 residue peptide, which mimicked the binding region of α, was solved by NMR (Wilkens *et al.*, 2005), shown in Fig. 1.3.1.

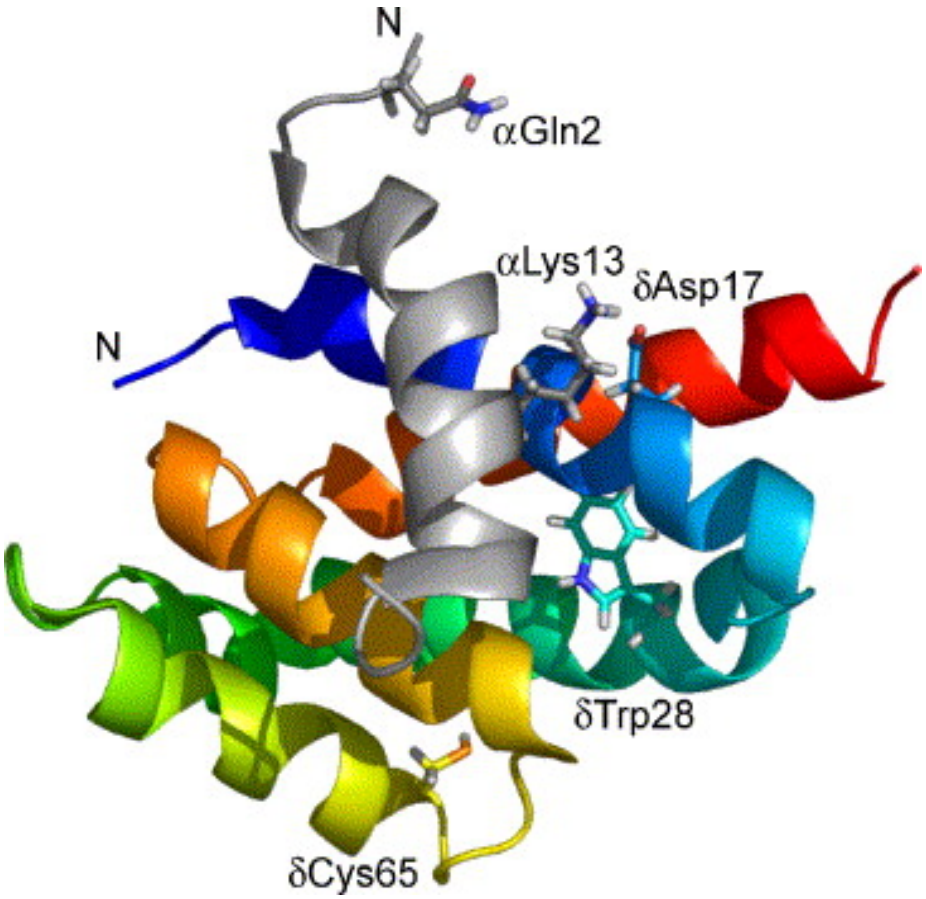

Figure 1.3.1 Interaction of δ with the N-terminal helix of α.

Ribbon diagram of the high resolution NMR solution structure of the N-terminal domain of the δ subunit, shown in rainbow colors. This forms a complex with a peptide (shown in gray). mimicking the N-terminal 22 residues of the α subunit (Wilkens *et al.*, 2005). Highlighted residues are those shown previously to play a role in the δ-α interaction. (Ogilvie *et al.*, 1997). Figure from (Weber, 2006).

It revealed that the N-terminal domain of δ consists of a six α-helical bundle, while the C-terminal domain appears to be unfolded. The amphipathic, α-helical, 22-residue peptide was nestled between two helices of δ, implicating important residues for the subunit-subunit interaction.

Although the structures of the stator differ markedly between mitochondria and *E. coli* (Weber, 2006), the homologous subunit to δ, termed OSCP for Oligomycin Sensitivity Conferral Protein, has a similar structure and a similar mode of high affinity binding to the N-terminal of α (Carbajo *et al.*, 2005; Hundal *et al.*, 1983). This emphasizes that the δ subunit is important for F_OF_1 function.

1.3.2 The b subunit

In the *E. coli* F_OF_1, as in most bacerial ATPases, the 156 residue *b* subunit is present as an identical homodimer, b_2 (McLachlin and Dunn, 1997). It is an amphipathic subunit with a hydrophobic N-terminus tethering it to the membrane, and a long hydrophilic α-helical region of approximately 110 residues which extends up to connect with F_1 *via.* δ and α subunits (Dunn and Chandler, 1998; McLachlin *et al.*, 1998; Rodgers and Capaldi, 1998). Functionally it has been divided into four domains, listed in order from the amino-terminus to the carboxy-terminus: the membrane domain, the tether region, the dimerisation domain and the δ-binding domain (Dunn *et al.*, 2000), illustrated in Fig. 1.3.2.

In contrast to most of the essential functional units of the ATP synthase, which are conserved through evolution, the stator stalk differs greatly between the bacterial,

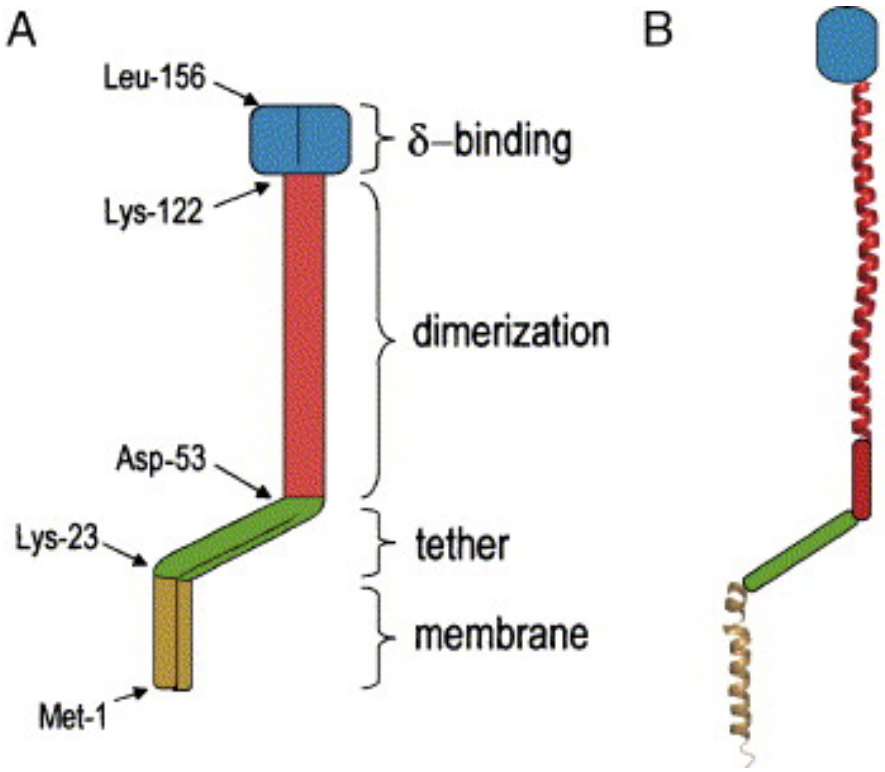

Figure 1.3.2. A single homodimer of *E. coli b* subunit.

(A) The proposed functional domains of subunit *b*. The labelled residues are at the junctions between domains. The subunit is mostly α-helical (adapted from (Dunn *et al.*, 2000)). (B) A monomer of subunit *b* showing the regions for which structures have been solved: the membrane domain determined by NMR (PDB entry 1B9U; (Dmitriev *et al.*, 1999)) and the dimerization domain determined by X-ray crystallography(PDB entry 1L2P; (Del Rizzo *et al.*, 2002)). Figure from (Walker and Dickson, 2006).

mitochondrial and chloroplast enzymes (Walker and Dickson, 2006). The chloroplast and photosynthetic bacterial forms of the *b*-stalk contain two homologous, but non-identical forms, *b* and *b'*, termed subunits I and II in chloroplasts. The mitochondrial stator stalk contains a subcomplex consisting of *b*, *d* and F_6 subunits. Homologues of the latter two subunits are not present in bacterial or chloroplast F_O sectors. Structurally, only the membrane domain and a fragment including the dimerization domain of the stalk have been solved for the *E. coli* enzyme (Del Rizzo *et al.*, 2002; Dmitriev *et al.*, 1999a), but a large portion of the mitochondrial stalk complex was solved by x-ray crystalography (Dickson *et al.*, 2006), revealing a curved shape to the stalk, which fits well into the low resolution cryo-electron microscopy structure (Rubinstein *et al.*, 2003).

1.3.3 Function of the stator stalk

The stator stalk needs to function similarly in all species despite differences in architecture. The *b* subunit is necessary for F_1 binding to F_O (Hoppe *et al.*, 1983), and while not directly involved, it is important for active H^+ transport. The ATP synthase consists of two connected motors which require rotation of rotor subunits, γ, ε, *c*-ring relative to the stator subunits $\alpha_3\beta_3$ and *a*. The *b* subunits and δ form the peripheral stator-stalk which plays a vital role in ATP synthase function by affixing the stators of F_1 and F_O, to prevent co-rotation of the stator assembly. This means that the stator-stator interfaces, between *b*-*a*, *b*-δ (perhaps with additional interactions between *b*-*a*), and δ-α, must withstand the tremendous torque that is built up during the course of the catalytic cycle. Fig. 1.3.3 shows the regions of interaction between *b* and δ.

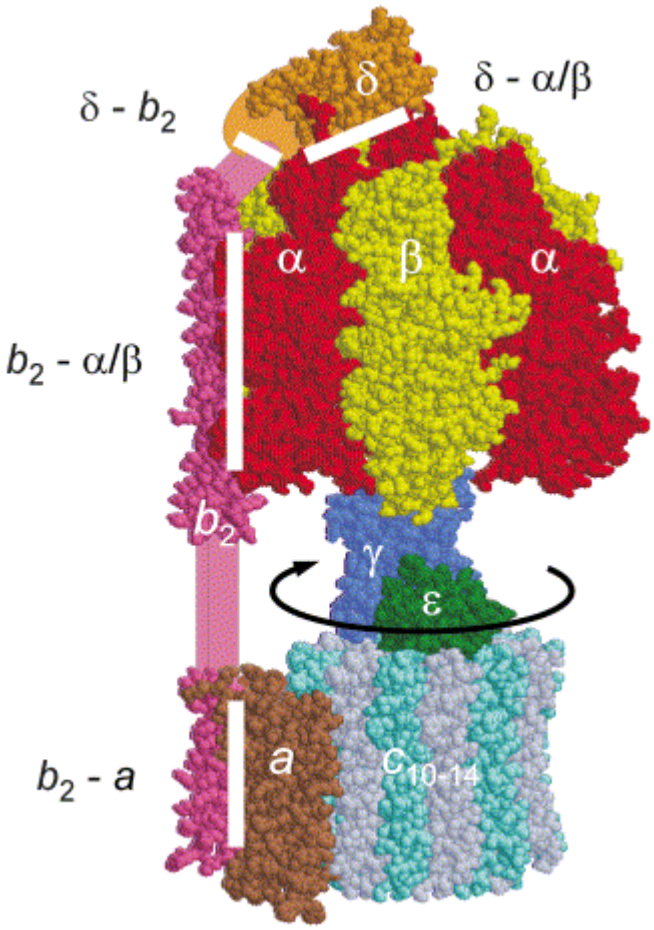

Figure 1.3.3. The stator interactions.

The white rectangles show regions of stator interactions on the contrived structure of *E. coli* ATP synthase, described in section *1.3.3*. Figure from (Weber, 2003).

Elasticity is needed to efficiently couple two motors with mis-matched symmetry leading to differing stepping angles (the F_O complex has 360° divided by the number of *c* subunits, F_1 has three 80° and 40° substeps), and may be provided by the *b* subunit (Junge *et al.*, 2001). The *E. coli* stator-stalk appears to have some flexibility because function is retained despite shortening, or lengthening of the *b* subunits or the incorporation of *b* subunits of unequal lengths (Grabar and Cain, 2003; Sorgen *et al.*, 1999; Sorgen *et al.*, 1998). The mitochondrial structure does not support the idea of the *b* subunit functioning like a "flexible rope" (Grabar and Cain, 2003), although the portion of the *E. coli b* subunit where the deletions and insertions were made, corresponds to the single helix portion of the mitochondrial stator, which may indeed have some flexibility and likewise function to store elastic energy (Weber, 2006). An additional structural feature which may be shared by both stator stalks is a twist. The mitochondrial structure shows a right-handed twist between the *b* subunit and *d* and F_6 (Dickson *et al.*, 2006), and recently the b_2 dimer of *E. coli* was analyzed and proposed to form a right handed coiled-coil which tightens upon rotation (Del Rizzo *et al.*, 2006), although more recent work suggests it forms a left-handed coiled-coil (Wise and Vogel, 2008). This could potentially function as the transient elastic energy storage capacity of the enzyme.

1.4 The Catalytic Domain: F_1-ATPase

1.4.1 Structure of the F_1 catalytic domain

When F_1 is decoupled from the driving force of the electrochemical gradient by detachment from F_O, it functions as an ATPase catalyzing ATP hydrolysis but not

synthesis. Reconstitution studies of subunits from the *E. coli* enzyme determined that the $\alpha_3\beta_3\gamma$ is the minimum complex necessary to achieve steady state ATPase activity (Dunn and Futai, 1980; Futai, 1977). In a landmark accomplishment, the high resolution crystal structure of the bovine heart mitochondrial enzyme was solved, showing most of the $\alpha_3\beta_3$ ring and less than half of the γ subunit, representing the catalytic domain of F_1 (Abrahams *et al.*, 1994). A subsequent structure resolved the rest of γ, and the ε subunit, which in mitochondria, for historical reasons, is called δ (Gibbons *et al.*, 2000). The homologous α and β subunits share 24% identity and 51% similarity and have nearly identical folds. They are arranged alternately around the γ subunit N- and C-terminal α-helices, which form a long coiled-coil and fill the central cavity of the $\alpha_3\beta_3$ pseudohexamer, shown in Fig. 1.4.1. The rest of the γ subunit extends below the αβ hexagon to connect with ε and the *c* subunits of the F_O portion, forming the central stalk between F_1 and F_O.

There are six nucleotide-binding sites which form small hydrophobic pockets located at the αβ interfaces. Three of these are non-catalytic sites, which reside mostly on the α subunits, bind nucleotide very tightly, do not hydrolyze it and exchange it slowly (Issartel *et al.*, 1986; Penefsky and Cross, 1991; Senior, 1990). They have no

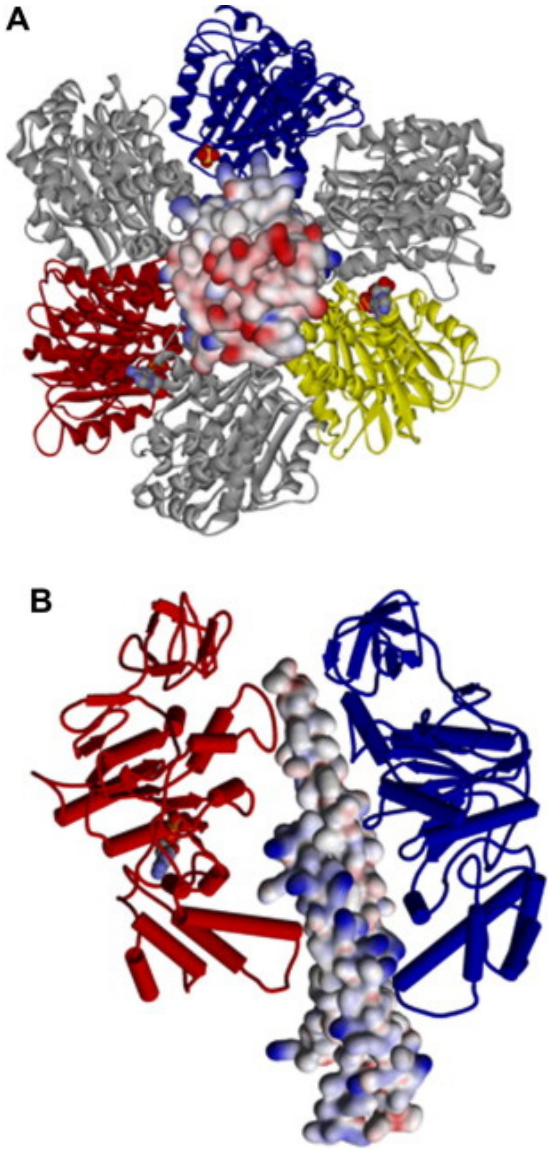

Figure 1.4.1. Ribbon diagram of the bovine heart mitochondrial F_1.

(A) From the "bottom", or membrane facing side, of the F_1 complex. α subunits are in gray, β_{TP} in yellow, β_{DP} in red, β_E in blue, and γ in the surface model showing electrostatic potential (blue is negative, red is positive, and white is apolar). (B) From the "side" of the complex showing only the γ subunit in relationship to two of the β subunit conformers, β_{DP} (red) with bound ADP (in CPK colors), and β_E (blue). Note that the lower portion of the β_E subunit is swung outwards which results in an open conformation of the nucleotide binding catalytic site. Structure based on (Abrahams *et al.*, 1994). Figure and legend from (Nakamoto *et al.*, 2008).

direct involvement in catalysis since enzyme function is not affected by depleting them of nucleotide (Wise and Senior, 1985), or substitution of αAsp261 by Asn which prevents the non-catalytic sites from binding nucleotide (Weber *et al.*, 1995). Their role may be one of enhancing stability of the complex, and allowing for efficient transmission of conformational changes between the α and β subunits. The three catalytic sites carry out ATP synthesis and hydrolysis and are located primarily on the β subunit but with a few residues from the adjoining α subunit contributing to the site.

1.4.2 Asymmetry of the catalytic domain of F_1

Boyer's "binding change mechanism" proposed that the three catalytic sites utilize the proton motive force to cycle sequentially through three different conformational states in the production and subsequent release of ATP (Boyer, 1993). This cooperative sequential participation of the catalytic sites implies asymmetry in that they exist in different states at a given moment. The asymmetric structure of F_1 from Walker's group (Abrahams *et al.*, 1994) may be considered a snapshot of the rotary mechanism in accordance with Boyer's theory in that it shows the enzyme with non-hydrolyzable AMP-PNP·Mg bound to the first site (β_{TP}), ADP·Mg bound to the second site (β_{DP}) and the third site being empty (β_E), Fig. 1.4.1. The asymmetry of catalytic sites requires the central γ subunit in addition to the α–β interactions. The symmetrical structure of the $\alpha_3\beta_3$ complex (lacking γ) from the thermophilic Bacillus PS3 enzyme, illustrates the role of the γ subunit in conferring asymmetry to the F_1 complex

(Shirakihara *et al.*, 1997). In the Walker structure (Abrahams *et al.*, 1994), the highly asymmetric portion of the γ subunit presents a different face to each β subunit, imparting a different conformation to each catalytic subunit (Al-Shawi *et al.*, 1997a).

Conclusive evidence for asymmetry has come from kinetic and biochemical analysis of enzyme function where behavior of the three sites was shown to be different (reviewed in (Boyer, 1993; Nakamoto, 1996; Weber and Senior, 1997). The binding affinities for nucleotide were determined using a fluorescent probe consisting of a tryptophan introduced into the adenine-binding pocket of the catalytic site, βY331W (reviewed in (Weber and Senior, 2004). Nucleotide binding was followed by monitoring fluorescence quenching of the βY331W. The affinity of Mg·ATP binding to the first site in *E. coli* is extremely high (K_{d1}= 0.2 nM) (Weber and Senior, 1997), whereas Mg·ATP binds to the second and third sites with lower affinity (K_{d2}=0.5 μM, K_{d3}=100 μM). The binding affinity for Mg·ATP is lower and the same for all three sites in isolated β subunits or in $\alpha_3\beta_3$ without γ (Al-Shawi *et al.*, 1990a; Kaibara *et al.*, 1996). Coordination of Mg^{2+} is also required for asymmetry of the sites (Weber and Senior, 1997), and in its absence, ATP affinity is the same for each site (Senior *et al.*, 1995; Weber and Senior, 1996).

The high resolution structure of F_1 revolutionized the study of the ATP synthase, and has provided critical information on subunit interactions and allowing insight into understanding of the enzyme function. However the structure gives only a snapshot in time at a particular point along the reaction pathway. The rotary mechanism of the F_OF_1 means it is dynamic, undergoing multiple conformational changes throughout the

catalytic cycle. There is no high resolution structure for the F_O portion of the enzyme, and the structures solved for the F_1 portion (Abrahams *et al.*, 1994; Braig *et al.*, 2000; Gibbons *et al.*, 2000; Menz *et al.*, 2001) do not seem to seem to show much variety in the conformational state of the enzyme, suggesting that accurate representations of high energy conformations, especially transition states, in conditions allowing crystallization have not been fully achieved. In addition the bulk of mutagenic, biochemical, kinetic and single molecule rotation studies on the enzyme have been performed on the *E. coli* and Bacillus PS3 enzymes, for which there is very little structural information. Therefore necessarily kinetics in combination with further structural studies will be invaluable for understanding enzyme function.

1.5 Role of F_1 in Catalysis

1.5.1 Unisite catalysis

The three catalytic sites are highly cooperative, exhibiting strong positive cooperativity for catalysis and negative cooperativity in Mg^{2+}-nucleotide binding. Rate constants for most elementary reaction steps have been determined under substochiometric Mg·ATP concentrations, where F_1 is present in 10-fold excess of Mg·ATP and it can be assumed the Mg·ATP binds to a single site, termed unisite (Al-Shawi and Senior, 1992; Grubmeyer *et al.*, 1982). Considering the concentrations of Mg·ATP in the cell, unisite hydrolysis is not a physiological mode of catalysis, but it

avoids some of the complications in the analysis of catalytic cooperativity between the sites. The scheme for the unisite reaction is as follows:

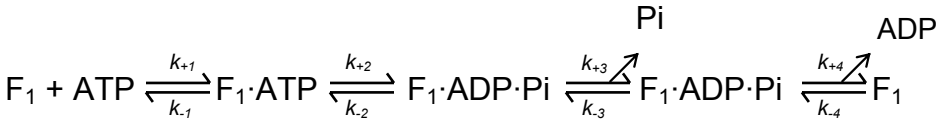

[Reaction Scheme 1]

Rate constants for the partial reactions have been determined under unisite conditions and characteristics of unisite activity are as follows: ATP binds to the first site with very high affinity (in *E. coli* K_{d1} = 0.2 nM (Weber and Senior, 1997)), reversible hydrolysis/synthesis is slow and occurs at an equilibrium constant close to unity, and release of products Pi and ADP is very slow (k_{+3}, $k_{+4} \leq 10^{-3}$ s^{-1}), and there is essentially no binding of Pi ($k_d > 2M$) to soluble F_1 or to F_OF_1 in the absence of proton motive force (Al-Shawi *et al.*, 1990b; Grubmeyer *et al.*, 1982).

1.5.2 Reaction chemistry and essential residues

Binding energy gained by the F_1-ATPase from the tight sequestration and coordination of substrate through multiple substrate-protein interactions (*e.g.* hydrogen bonds, hydrophobic interactions, salt bridges) was shown to be the main driving force for catalysis (Al-Shawi *et al.*, 1989; Al-Shawi *et al.*, 1990b; Al-Shawi and Senior, 1988). This was determined through deriving linear free energy relationship from thermodynamic and kinetic analyses of mutant F_1 enzymes. K_2 is independent of pH demonstrating that catalysis occurs in a sequestered environment (Al-Shawi and Senior, 1992). The fact that the hydrolysis/synthesis ratio, K_2, is close to one shows that there is

little free energy change in this step (Al-Shawi and Senior, 1988; Grubmeyer *et al.*, 1982), Boyer and co-workers used water-O^{18} phosphate exchange experiments to demonstrate that the hydrolysis/resynthesis of ATP occurs multiple times at the catalytic site, depending on the enzyme turnover rate (Boyer, 1993). The reaction chemistry of ATP hydrolysis does not involve covalent interactions with substrate or product by F_1-ATPase. Hydrolysis was thought to occur by nucleophilic attack by a single water molecule on the terminal phosphate of ATP, involving a pentacoordinate transition state with βGlu181 as the catalytic base activating the water molecule (Boyer, 1989; Webb *et al.*, 1980). Computational simulations using a quantum mechanical/molecular mechanical approach revealed nucleophilic attack involves the concerted involvement of two water molecules (Dittrich *et al.*, 2003; Dittrich *et al.*, 2004). This was termed a multicenter protein-relay mechanism and determined to be a more energetically favorable reaction (Dittrich *et al.*, 2004). The second water molecule efficiently polarized the nucleophilic water, by abstracting a proton, forming a transition state hydronium ion-like construct, stabilized by residues of the catalytic site, especially βGlu181. The nucleophilic water forms an in-line attack on the terminal phosphate forming the pentacovalent arrangement of P_γ, after which the transferred electron density of this phosphate helps to protonate the O_γ, Fig.1.5.1. This proton-relay mechanism is possible only in a protein environment, and is therefore a true enzymatic reaction pathway.

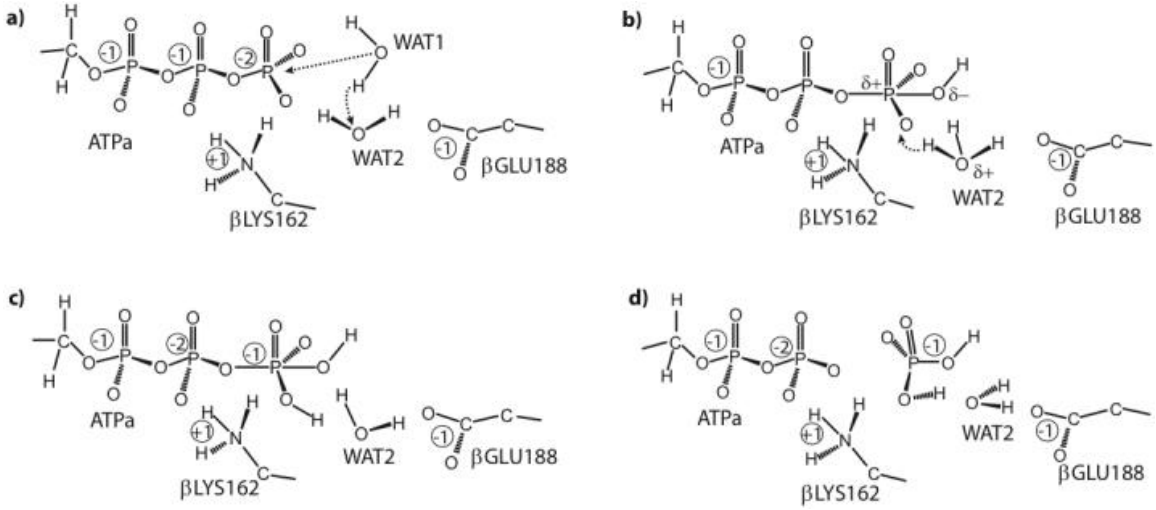

Figure 1.5.1. Schematic representation of ATP hydrolysis by the multi-center reaction.

Shown are the a) reactant, b) transition, c) intermediate and d) product state of the QM segment of the model. b) shows the involvement of two water molecules, and the formation of an H_3O^+-like intermediate. (Dittrich *et al.*, 2003).

The roles of residues in the catalytic site were determined through a vast amount of kinetic analysis on the effects of mutations on the catalytic mechanism, and also on substrate binding through use of βY331W as a fluorescent probe (see (Weber and Senior, 1997; Weber and Senior, 2004) for reviews). The P-loop residues βGly149-GAGVGK-βThr156, and several charged residues (βGlu181, βGlu185, βAsp242, βArg182, βArg246, αArg376) are in close proximity to the nucleotide phosphoryl groups (Fig. 1.5.2 and (Abrahams *et al.*, 1994)) and are important or essential for catalysis. Consistent with its role described above, replacement of βGlu181 strongly perturbs the transition state (Senior and Al-Shawi, 1992) βLys155 and βThr156, in the P-loop, are involved directly in nucleotide binding and catalysis. The essential βLys155 hydrogen bonds with P_γ and contributes significantly to binding energy (Ahmad and Senior, 2005b; Senior *et al.*, 1993). βArg182 and βArg246 are required for the initial binding of Pi (Ahmad and Senior, 2005a). βTh156, βGlu185 and βAsp242 participate in binding and/or coordination of Mg^{2+}, emphasizing its role as a cofactor in catalysis (Omote *et al.*, 1995; Omote *et al.*, 1992; Senior and Al-Shawi, 1992). Mutations of the αArg376, contributed from the adjacent α subunit, have little effect on unisite catalysis but abrogate cooperative catalysis (Le *et al.*, 2000). It is also believed to stabilize the transition state (Nadanaciva *et al.*, 1999), and has been identified as a residue required for Pi binding (Ahmad and Senior, 2005b). Based on this evidence its role as a Pi sensor in ATP catalysis has been suggested, as the conformational position also changes significantly between the β_{TP}/β_{DP} and β_E sites, as described in (Nakamoto *et al.*, 2008).

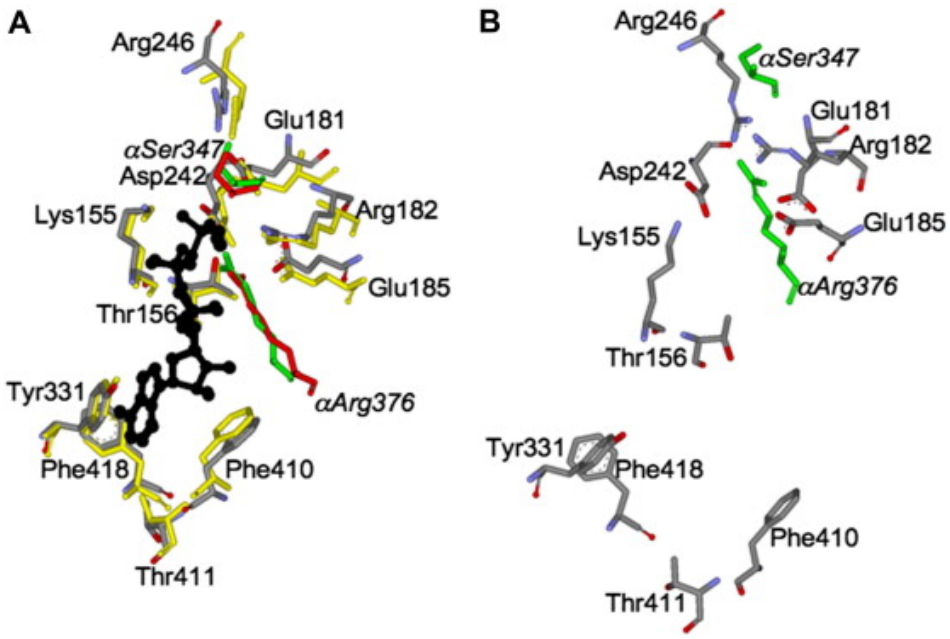

Figure 1.5.2. Key residues contributing to the three catalytic sites.

(A) Overlay of the residues in β_{TP} (in CPK colors) and β_{DP} sites (in yellow). Bound ATP or ADP and Mg^{2+} are in black. (B) The same amino acids in β_E. Note the difference in positions of certain amino acids, in particular αArg376 (*E. coli* numbering) and αSer347 (red in β_{TP}, green in β_{DP} and β_E), which indicate the more open β_E conformation (Abrahams *et al.*, 1994). (Nakamoto *et al.*, 2008).

1.5.3 Mulitsite catalysis

Promotion of maximal turnover rates requires occupation of all three catalytic sites with nucleotide and cooperative interactions among them (Weber *et al.*, 1993). The α and β subunits have considerable contact, which is critical for the cooperative communication between the sites. Modifications of residues in the α–β interface close to the catalytic site have little effect on unisite catalysis, but perturb cooperativity between sites (Le *et al.*, 2000; Maggio *et al.*, 1987; Turina *et al.*, 1993). The three sites show positive cooperativity since the unisite Mg·ATP hydrolysis rate is $\leq 10^{-3}$ s^{-1} and increases by ~10^6-fold to 100 s^{-1} when all three sites bind Mg·ATP (Grubmeyer *et al.*, 1982). The γ subunit is required for the cooperative behavior of the enzyme since the activity of the $\alpha_3\beta_3\gamma$ complex is capable of both unisite and multisite catalysis and is inhibited by azide, which affects the cooperative mechanism (Al-Shawi *et al.*, 1997a; Al-Shawi *et al.*, 1990b; Noumi *et al.*, 1987; Noumi *et al.*, 1988), yet the complex without γ displays no unisite activity, following Michaelis-Menten kinetics for Mg·ATP hydrolysis, with a single K_m for Mg·ATP, and activity is not inhibited by azide (Miwa and Yoshida, 1989). Mutational analyses support this since altered residues, which perturb catalytic cooperativity and coupling are located in the three regions of γ interact with the α and β subunits (Iwamoto *et al.*, 1990; Nakamoto *et al.*, 1995; Nakamoto *et al.*, 1993; Shin *et al.*, 1992). The three sites are strongly coupled since they also show negative cooperativity in binding Mg·ATP (Weber *et al.*, 1996).

The "binding change mechanism" was first proposed by Boyer to described the mechanism by which cooperativity promotes catalysis (Boyer, 1979). In conditions of

MgATP which allow binding to the third, low affinity catalytic site, the conformation of the other sites is changed resulting in enhanced hydrolysis rates, and especially increased rates of product release. The binding change mechanism proposed that each site occupies a different conformation at any one time and sequentially converts between the different conformations. In this manner each site would go through the three conformations to make or hydrolyze one ATP (Boyer, 1989; Boyer, 1993). While the partial reaction rates of the steps of the unisite reaction are known, the complication due to the cooperative nature of the enzyme made resolving the partial reactions of multisite catalysis difficult.

1.5.4 Structure and function of ε, an regulatory subunit of catalysis

ε is the smallest of the subunits of F_1 with molecular mass of 14,920 Da for the *E. coli* subunit. The ε subunit is tightly associated with the γ subunit (Dunn, 1982) and forms part of the rotor (Kato-Yamada *et al.*, 1998). Structurally the isolated *E. coli* subunit ε was determined by X-ray diffraction and multidimensional NMR to consist of two domains, a 10-stranded β barrel at the N-terminus, and a helix-loop-helix motif at the C-terminus (Uhlin *et al.*, 1997; Wilkens and Capaldi, 1998b; Wilkens *et al.*, 1995), shown in Fig. 1.5.3A. In addition, the mitochondrial δ subunit (equivalent subunit to ε in the bacterial F_1, termed δ in mitochondria for historical reasons) in the F_1 structure (Gibbons *et al.*, 2000), and the structure of ε from the thermophilic Bacillus PS3 enzyme

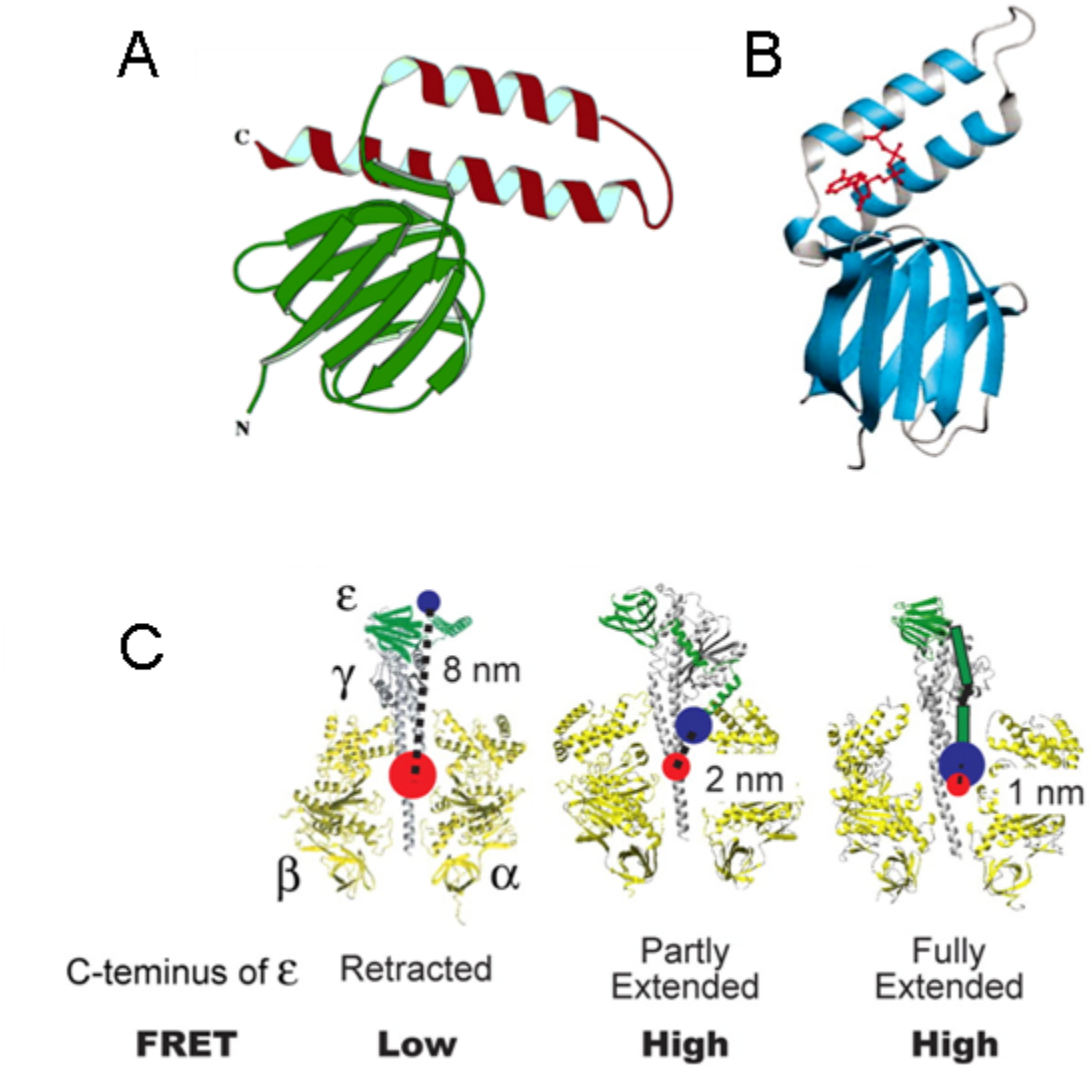

Figure 1.5.3 The F_1-ATPase ε subunit.

(A) Solution structure for *E. coli* ε subunit (Wilkens and Capaldi, 1998). (B) Crystal structure of the thermophilic *Bacillus* PS3 ε subunit, the bound ATP is depicted in *red* (Yagi *et al.*, 2007). (C) Depiction conformational dynamics of the ε subunit measured by FRET (Iino *et al.*, 2005). The structure of the bovine mitochondrial F_1 with one α and β, shown in *yellow*, γ depicted in *gray*, and the ε in *green* (δ from mitochondria is equivalent to ε and is termed ε here). The Cy3 (donor, *red circle*) and the Cy5 (acceptor, *blue circle*) were reacted with introduced cysteines, one at the top of γ (γS3C), and one at the end of the thermophilic *Bacillus* PS3 ε (ε134C), allowing distance between the probes and to be determined and hence position of the end of the ε C-terminal α-helix.

(shown in Fig. 1.5.3B (Yagi *et al.*, 2007)), demonstrated the high structural similarity of the ε from these disparate sources. These structures were all agreement with cross-linking data showing interaction of ε with γ and c subunits (Schulenberg *et al.*, 1999; Tang and Capaldi, 1996; Watts *et al.*, 1996; Zhang and Fillingame, 1994). This is consistent with a functional role of ε which is essential for binding of F_1 to F_O in the bacterial enzyme (Sternweis, 1978; Yoshida *et al.*, 1977). In particular it is the N-terminal domain that is critical for complex assembly (Cruz *et al.*, 1997; Kuki *et al.*, 1988).

ε exerts a large inhibitory effect on F_1 ATPase activity (Richter and Gao, 1996; Smith and Sternweis, 1977), which is somewhat relieved upon F_1 binding to F_O, although ε also inhibits the whole F_OF_1 enzyme (Kato-Yamada *et al.*, 1999; Ketchum and Nakamoto, 1998; Peskova and Nakamoto, 2000; Schulenberg and Capaldi, 1999). The C-terminal helix domain of ε is thought to mediate this inhibitory function which may be a regulatory mechanism for enzyme activity (Tsunoda *et al.*, 2001b) as there is large variability in sequence identity of the second C-terminal α helix (Feniouk *et al.*, 2006). Pronounced reduction of inhibition occurs in *E. coli* upon deletion of both helices (Cipriano and Dunn, 2006; Kuki *et al.*, 1988; Xiong *et al.*, 1998). The structure of *E. coli* ε complexed with a truncated γ subunit (γ'-ε) revealed a large conformational change in the ε subunit C-terminal domain which extended along the γ subunit shaft (Rodgers and Wilce, 2000). Such a structure reconciled results of cross-linking between ε and α or β subunits (Aggeler and Capaldi, 1996; Mendel-Hartvig and Capaldi, 1991a; Mendel-Hartvig and Capaldi, 1991b). It was shown that the interaction between the positively

charged residues on the second C-terminal helix of ε and the negatively charged residues of the βD380-ELSEE-D386 motif was important for the inhibitory effect in the Bacillus PS3 F_1 (Hara *et al.*, 2001). Fluorescence resonance energy transfer (FRET) was used to monitor the conformational transitions of the C-terminal helix of ε, in an effort to understand the functional role of this major conformational switch (Iino *et al.*, 2005), illustrated in Fig. 1.5.3C. In the presence of ADP, the non-hydrolyzable ATP analog AMP-PNP, or ADP with inhibitors azide and aluminum fluoride, the folded state was favored, while in the presence of ATP the extended form was induced, confirming results of cross-linking experiments which additionally showed $\Delta\mu_{H+}$ promoted the extended conformation (Suzuki *et al.*, 2003). The kinetics of ε conformational transitions from extended to contracted or *vice versa* upon ATP or ADP addition were relatively slow ($t_{½}$ = 100 s and 1300 s at 30 ºC, respectively) revealing they do not occur during each catalytic cycle (Iino *et al.*, 2005).

A role of ε as a sensor for ATP has also been proposed, since ε of the thermophilic Bacillus PS3 enzyme binds ATP (Fig 1.5.3B (Kato-Yamada, 2005)), as does ε from *E. coli* (Yagi *et al.*, 2007), although with much lower affinity. Binding of ATP to ε, in the thermophilic Bacillus PS3, changes the conformation to the folded state and relieves the inhibitory effect of ε ((Kato *et al.*, 2007) and other studies reviewd in (Feniouk *et al.*, 2006)).

The ε subunit also plays an important role in coupling catalysis and transport, which will be discussed in *Section 1.6.1.1.*

1.5.5 Rotational catalysis

Boyer first proposed a rotary motion as a cause for sequential change in the nucleotide binding affinities of the three catalytic β subunits (Gresser *et al.*, 1982). Later, the crystallographic structure of Abrahams *et al*. implicated γ for this role (Abrahams *et al.*, 1994). Cross-linking approaches were used by Cross and co-workers to show the γ subunit interacted with all three β subunits during catalysis (Duncan *et al.*, 1995a; Zhou *et al.*, 1997). Direct visualization of the rotation of the F_1 enzyme was reported in 1997 by the Yoshida group (Noji *et al.*, 1997). In these experiments the $\alpha_3\beta_3\gamma$ complex from the thermophilic Bacillus PS3 was immobilized through polyhistidine affinity tags at the N-termini of β, the side of the $\alpha_3\beta_3$ hexamer furthest from the membrane, and a fluorescent actin filament was attached via a cysteine introduced into the region of γ that faces the membrane. Rotation, observed in a small fraction of actin filaments, was dependent on ATP and stopped by inhibitors of ATPase activity. The direction of rotation with saturating ATP was always counterclockwise (observed from the membrane side), with rare reversals. Subsequent experiments have utilized the essential features of this single molecule set-up and determined that the *E. coli* enzyme functions in a like manner (Omote *et al.*, 1999). Furthermore, the ε subunit (Kato-Yamada *et al.*, 1998) and the *c*-ring are part of the rotor (Aggeler *et al.*, 1997; Kato-Yamada *et al.*, 1999; Pänke *et al.*, 2000; Sambongi *et al.*, 1999).

The presence of three catalytic sites on the enzyme implied that each site would transition through the reaction cycle during a 360º revolution, offset from each other by 120º, and three ATP are hydrolyzed/synthesized during each 360º rotation. γ subunit

rotation was observed to pause at 120º intervals under low ATP concentrations, and calculations of the free energy of ATP hydrolyzed and torque generated revealed the efficiency of energy conversion by F_1-ATPase close to 100% (Yasuda *et al.*, 1998). High-speed imaging and laser dark-field microscopy allowed use of a small non-impeding probe, a 40 nm gold bead, which allowed measurements of maximal rotation (130 s^{-1}) at saturating ATP (Yasuda *et al.*, 2001). These rates corresponded to the k_{cat} of ATP hydolysis divided by three, confirming that three ATP are consumed in one complete 360º rotation. The 120º steps were also resolved in this study into two partial steps, 90º and 30º (Yasuda *et al.*, 2001) (later refined to 80º and 40º (Shimabukuro *et al.*, 2003)). The rotational movement of each step was fast, constant and ATP-independent. Therefore the overall rate of rotation and ATP activities were determined by the length of the dwell before the 80º rotation. The length of the dwell before the 80º rotation step was dependent on the ATP concentration, suggesting it was the ATP binding step, and allowed calculation of the binding constant for ATP, k_{on}=2.6x10^7 $M^{-1}s^{-1}$. The 120º reaction cycle begins with a pause (termed the ATP-binding dwell) where the angular position of γ is defined as 0º, then a rapid 80º rotation step occurs, followed by another pause (termed the interim dwell), and finally a 40º rapid rotation step (Shimabukuro *et al.*, 2003) (Fig 1.5.4). The dwell before the 40º step was ATP-independent and further investigation determined that ATP cleavage occurs during this interim dwell based on analysis of the effects of the slowly hydrolysable substrate, ATPγS, and a catalytic site mutant, βE190D (*E. coli* numbering) (Shimabukuro *et al.*, 2003). Attempts to correlate

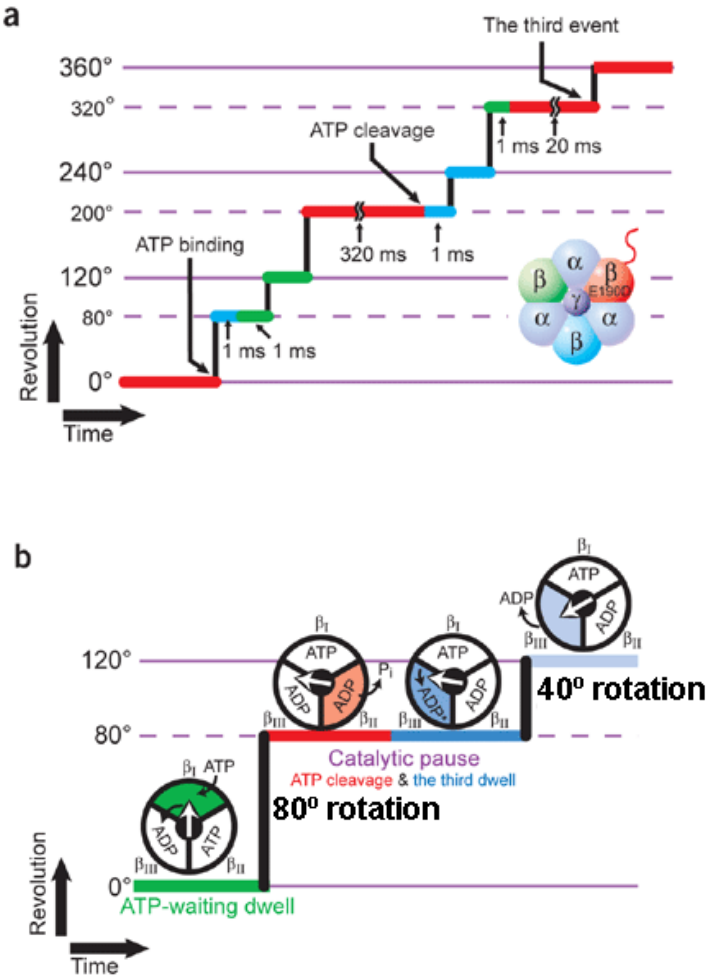

Figure 1.5.4. Illustration of the rotational stusteps of the γ subunit.

Observed for chimeric F_1 molecules containing one mutated βE190D subunit, and two wild-type β subunits. (**a**) The mutant βE190D subunit (*red)*, binds ATP at 0°, hydrolyzes ATP at 200° and regulates the third event at 320°. One of the wild-type β subunits (*green*) binds ATP at 120°, hydrolyzes it at 320° and regulates the third catalytic event at 440° (equivalent to 80° in the next 360º cycle). The second wild-type β subunit binds ATP at 240°, hydrolyzes it at 440° (equivalent to 80°) and regulates the third catalytic event at 560° (equivalent 200°). The three β subunits catalyze the same reactions in the same sequence but with a 120° phase difference, a sequential three-site mechanism. (**b**) Model illustration depicting the rotation substeps of γ doe a single 120° catalytic cycle. Figure from (Ariga *et al.*, 2007).

the catalytic reaction with rotation used the high-speed imaging of rotation concurrently with the fluorescent ATP analog 2'-O-Cy3-EDA-ATP (Cy3-ATP) (Adachi *et al.*, 2007; Nishizaka *et al.*, 2004). By this technique Cy3-ATP that bound at 0º (see Fig. 1.5.4 for clarification of γ rotation angle) was not immediately hydrolyzed, but was cleaved during the dwell at 200º, *i.e.* during the second 120º cycle, and release of the Cy3-nucleotide (presumably in the form of Cy3-ADP) occurred at 240º. The release of nucleotide at this point in the cycle, before going through the entire 360º, may indicate a "bisite" mechanism (ATP hydrolysis by an enzyme with only two sites filled with nucleotide) because the concentration of nucleotide was well below the K_M for Mg·ATP binding. Non fluorescent nucleotides are not visible and therefore not detectable, so occupancy of other sites was not known. Most of the single molecule work at the present time is an effort to understand how the partial rotations are coupled to the enzymatic reaction steps. While these experiments have provided a wealth of information about the rotational behavior of the enzyme, they are limited due to the inability to measure the steps of the enzymatic reaction, particularly hydrolysis/synthesis and product release. The question of how the enzyme couples chemical energy from ATP hydrolysis to rotation, termed chemomechanical coupling, is a fundamental unresolved question in the field.

As stated above, the ε, γ and *c*-ring were all demonstrated to rotate, which was verified by showing that the cross-linked γ and ε connection with the *c*-ring remained fixed during enzyme function (Jones *et al.*, 2000; Schulenberg *et al.*, 1999; Tsunoda *et al.*, 2001a). Structurally, the extensive contact between the *c*-ring and the γ-ε stalk

suggests that they may rotate as an ensemble during catalysis (Stock *et al.*, 1999). Not easily reconciled with this functional cross-linked γ-ε-*c* rotating ensemble, is the unresolved issue of the mismatch between the most recent *c* subunit stoichiometry of 10 (Jiang *et al.*, 2001), and the three 120° rotation steps of γ. The mechanism by which energy is stored in the enzyme during the stepwise transport of three to four protons across the membrane (which takes place between each step of ATP release) needs further investigation.

1.5.6 Rotation in ATP synthesis

ATP synthesis kinetic and thermodynamic analysis has shown that the energy requiring steps are ATP release and P_i binding (Al-Shawi *et al.*, 1990b). In the absence of a protonmotive force (PMF) Pi binding (k_{-3}) is essentially non-existent, with an estimated K_D of >10 M, but in the presence of $\Delta\mu_{H+}$ in ATP synthesis the Pi on-rate constant (k_{-3}) is greatly enhanced (Al-Shawi and Nakamoto, 1997; Wise and Senior, 1985). In a similar manner ATP affinity in *E. coli* is decreased by ~10^7 with a $\Delta\mu_{H+}$, by enhancement of k_{-1}, the ATP off-rate constant (Al-Shawi *et al.*, 1990b). Synthesis is also a cooperative process although the affinity for ADP is not affected by the presence of $\Delta\mu_{H+}$, its binding to other sites enhances the ATP off-rate (Souid and Penefsky, 1995; Weber *et al.*, 1993). Importantly, the uncoupling mutation, γM23K (discussed in section 1.6.1.2), was shown to perturb these two major energy-requiring steps of synthesis (Al-Shawi *et al.*, 1997b).

Previously it was assumed that ATP synthesis and hydrolysis followed the same pathway in reverse directions of each other, since both use an alternate site, cooperative

mechanism, and K_2, the equilibrium constant between synthesis and hydrolysis, remains near unity (Al-Shawi *et al.*, 1990a). Further evidence supporting this has come from isokinetic analysis of steady state hydrolysis and synthesis of F_OF_1 enzymes, which fell on the same regression line indicating they shared the same transition state structure, and hence utilized the same pathway (Al-Shawi *et al.*, 1997b). Different transition states may exist for the two pathways, but the rate-limiting transition state is the same for both, therefore the direction of rotation must be opposite for the two reactions. Single molecule experiments confirmed this to be the case. Magnetic beads attached to F_1 were forced (by electro magnets) to rotate in the direction of ATP synthesis, and the resulting ATP production was detected by a luciferin-luciferase reaction (Itoh *et al.*, 2004). In an approach using FRET to measure the position of γ and ε in F_OF_1, rotation was determined to proceed in the direction opposite to hydrolysis when the membrane was energized with a $\Delta\mu_{H+}$ (Zimmermann *et al.*, 2006; Zimmermann *et al.*, 2005). Additionally there is some evidence that ε is required for efficiently coupling rotation driven ATP synthesis (Rondelez *et al.*, 2005), consistent with the suppression of ATP synthesis, but not hydrolysis in the chloroplast F_OF_1 without ε (Nowak *et al.*, 2002).

1.6 Coupling Between Transport and Catalysis

1.6.1 Altered interactions affecting coupling efficiency

1.6.1.1 γ-ε-c interface

Energy coupling involves the transmission of conformational information through the three rotor subunits making the interface of the F_1-γε and F_O-c subunits a critical

region in ensuring the efficiency of the mechanism (reviewed in (Nakamoto, 1999; Nakamoto *et al.*, 2000)). The close association and interaction of several ε residues, γTyr205, γTyr207, and the polar loop region of the *c* subunits have been shown extensively through cross-linking studies (Schulenberg *et al.*, 1999; Tang and Capaldi, 1996; Watts *et al.*, 1996; Zhang and Fillingame, 1994). Mutational analysis has been used to show the importance of the *c* subunit polar loop region in binding of F_1 to F_O, which results in activation of the enzyme (Dunn *et al.*, 1987; Fraga and Fillingame, 1989; Miller *et al.*, 1989). Mutations that cause disruptions in coupling have been identified in this region, and genetic analysis revealed several second-site suppressor mutations which restored efficient function of the enzyme (Ketchum and Nakamoto, 1998; Zhang and Fillingame, 1994). When ε interacts with the F_1 complex it has an inhibitory effect on catalysis (Dunn *et al.*, 1987), which is partially relieved upon binding to F_O. Mutant enzymes and detergent which perturb this ε inhibition were used to study the coupling function of this region. The γ-ε-c coupling domain modulates catalysis indirectly through conformational effects of the γ subunit, yet from Arrhenius and isokinetic analyses it was proposed that this portion of the enzyme (and particularly the ε subunit) plays an integral role in determining the proper transition-state of the catalytic mechanism and therefore is critical in achieving maximum coupling efficiency of the enzyme (Peskova and Nakamoto, 2000). Cross-linking studies have also shown that the carboxyl-terminus of ε interacts with the α and β subunits, so it may also affect coupling through this direct interaction (Aggeler and Capaldi, 1996; Aggeler *et al.*, 1995a; Aggeler *et al.*, 1995b; Bulygin *et al.*, 1998).

Two structures of this portion of the enzyme have been published (though not including the *c* subunits) showing the interactions between γ, δ_{mito} and ε_{mito} from the bovine mitochondrial enzyme (Gibbons *et al.*, 2000) and a truncated form of γ (γ') and ε from *E. coli* (Rodgers and Wilce, 2000). From this structural information and electron paramagnetic resonance using site directed spin labeling (EPR-SDSL) experiments allowing functional analysis of each residue, a model for the γ-ε-c interface was proposed where the acidic residues γAsp204, γGlu208 and γAsp210 interact with the c-subunits and the odd numbered residues of the γLys-201→γTyr207 β-strand interact with the ε-subunit (Andrews *et al.*, 2001).

1.6.1.2 β-γ interactions

The γ–β interactions were observed in the crystal structure to be located in two regions. The first consisted of hydrophobic interactions near the 'top' of the γ subunit, referred to as a "greased bearing," which was thought to offer little resistance to rotation (Abrahams *et al.*, 1994). The second region is at the 'bottom' of the hexamer at the highly asymmetric portion of γ discussed above. Much evidence for the role of the γ subunit in the regulation of ATPase activity and in coupling catalysis with proton translocation has been accumulated through extensive random and site-directed mutagenesis. An early indication for this role for the γ subunit was suggested by mutants in the C-terminal region (γGln269→Leu, γGlu275→Lys, γThr277→end), which exhibited varying degrees of ATP-dependent proton gradients, yet all had ATPase activities similar to that of the wild-type enzyme (Iwamoto *et al.*, 1990). These proton

gradient deficiencies were caused neither by non-specific proton leakage, nor by defective F_O sectors. Since the carboxy terminal mutations mainly affected catalysis, the other highly conserved amino terminal region was investigated in the same manner (Shin *et al.*, 1992). Mutants were generated in the highly conserved amino terminal region where surprisingly only the Met23→Lys/Arg (γM23K/R) significantly affected enzyme function: very low levels of ATP-dependent H^+ pumping and $\Delta\mu_{H^+}$-driven ATP synthesis, yet with catalytic and transport functions of the enzyme appearing intact (Shin *et al.*, 1992). Interestingly, this deleterious effect exhibited strong temperature dependence, being more severe at higher temperatures. Second-site suppressor mutations, which restored efficient coupling in the γM23K enzyme, were identified in the carboxyl-terminus of the γ subunit including γArg242 and seven different residues between γGln269 and γAla280 (Nakamoto *et al.*, 1993). In particular, strains with the single mutations γGln269→Arg and γThr273→Ser exhibited the same temperature sensitivity as γM23K whereas the double mutants were thermally stable. The same method of suppressor mutagenesis was used to identify three regions of the γ subunit (γ18-35, γ236-246 and γ269-280), which form a domain critical for efficient coupling and catalytic function (Nakamoto *et al.*, 1995). Surprisingly, these suppressor mutations mapped onto the crystallographic structure show that they do not interact directly. This, in addition to the fact that multiple and diverse amino acid replacements relieve a particular perturbation, indicates subtle dynamic conformational communication between the transport and catalytic functions. Several γ–β interactions important in efficient coupling are illustrated in Fig. 1.6.1.

Temperature dependence of steady state catalysis revealed the γM23K mutation to have increased enthalpic and entropic parameters for the catalytic transition state (Al-Shawi and Nakamoto, 1997). According to transition state theory the higher activation energy indicates the existence of additional bonds within the enzyme (between rotor and stator) that must be broken to achieve the transition state. The positive charge of Lys or Arg at position 23 allows the formation of an ionized hydrogen bond with one of the βGlu-381, located in the conserved β^{380}DELSEED^{386} segment, thereby increasing the energy of interaction between γ and β (Al-Shawi *et al.*, 1997a).

Further analysis of fundamental reaction steps indicate that the mutation traps the enzyme in a P_i release mode preventing proper use of binding energy to drive catalysis and supporting the γ–β interface as important in the transmission of coupling information (Al-Shawi *et al.*, 1997b). Several second site mutations within the γ–β region of interaction strengthened this hypothesis of rotor-stator perturbations (Ketchum and Nakamoto, 1998). Since the amino acid substitutions alter the activation energy for the rate-limiting transition state for both hydrolysis and catalysis and affect rotor-stator interactions it was hypothesized that the rate-limiting transition state involves rotation of γ relative to the $\alpha_3\beta_3$ stator. The extra interaction, and higher energy transition state caused by the γM23K mutation is hypothesized to create an alternative lower energy kinetic pathway which allows product release from the enzyme without rotation of the γ subunit, thus uncoupling catalysis from transport (Nakamoto *et al.*, 2000).

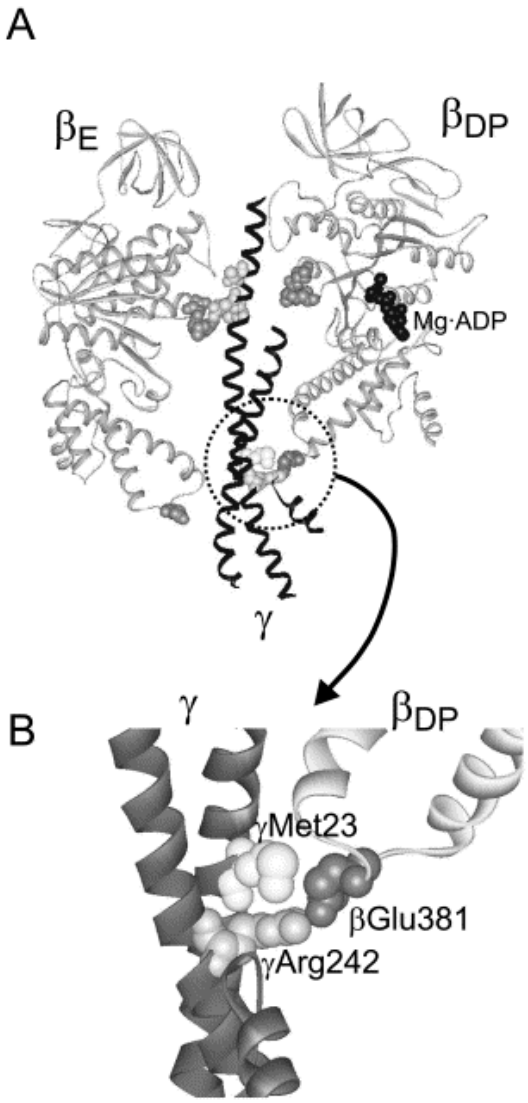

Figure 1.6.1. Regions of interaction between γ and β subunits.
Ribbon diagrams based on structure of bovine F_1 (Abrahams *et al.*, 1994). The coiled coil γ termini are illustrated in *black*, with two β subunit conformers β_{DP}, and β_E. (A) The regions of interaction between the γ subunit helices and the β subunit conformers, with specific residues shown in space-filling models. The interaction between γ and β_E near the catalytic site involves γArg268, Gln269 and Thr273, and βAsp302, Thr304 and Asp305 (*E. coli* numbering). The circled γ-β_{DP} interaction includes γMet23 and γArg242 with βGlu381 of the β^{380}DELSEED^{386} sequence. (B) Details of the γ - β_{DP} interaction. Figure from (Nakamoto *et al.*, 2000).

The comparison of the rotation and torque generation of the *E. coli* γM23K mutant with wild-type F_1 showed that both enzymes rotated at the same rate, thus producing the same frictional torque (Omote *et al.*, 1999). This in addition to the study by Hara et al. which showed that substitution of each β^{380}DELSEED^{386} by Ala created the same torque regardless of the substitution (Hara *et al.*, 2000) illustrates that torque generation alone does not efficiently convey energy to the transport mechanism. Many inter- and intra-subunit interactions and the coordination of these throughout the entire complex affect the transmission of information between catalytic substeps and transport.

1.7 Significance and Applications

The most prevalent synthetic chemical reaction in the biological world is the synthesis of ATP. The ATP synthase is one of the most ubiquitous and abundant proteins on earth. Greater than 60% of the amino acid residues of the β subunit are conserved through evolution from *E. coli* to plants to mammals. This is rather surprising given the early evolutionary divergence and the protein's complexity (Nelson, 1992) and clearly emphasizes the central role it plays in energy metabolism. In fact, a valid argument could be made that the F_OF_1 ATP synthase is the most important protein for multicellular life.

However not only is the F_OF_1 ATP synthase of particular importance due to its central role in metabolism but also because of its unique rotational mechanism. Apart from the bacterial flagellar the ATPase is the only known molecular rotary motor, and is remarkably reminiscent of man-made motors leading to the intriguing notion of using this nano-motor to do work at the molecular level. One of the most interesting probes used in

the single molecule rotation experiments was a manufactured nickel rod illustrating the usefulness of the F_1-ATPase as a biological nanomotor (Soong *et al.*, 2000).

In addition, the integral role of the ATP synthase in cellular respiration has important medical implications. This is particularly evident in organs and/or cells with high metabolic rates such as cardiac muscle cells and neurons. Mutations or perturbations, so called primary defects in function of the ATP synthase, can have profound effects on the efficiency of oxidative phosphorylation (Carelli *et al.*, 2002; Schon *et al.*, 2001). It was shown that ATP6 missense mutations perturb enzyme coupling so that synthesis of ATP is decreased leading to neuropathy, ataxia or Leigh syndrome, a fatal encephalopathy (Sgarbi *et al.*, 2006). In addition, abnormalities in function of respiratory chain enzyme cause secondary inhibition of the ATP synthase (for reviews see (Das, 2003; Houstek *et al.*, 2006). Complex V of oxidative phosphorylation, which is the F_OF_1 ATP synthase, is implicated in some neurodegenerative disorders/syndromes (Garcia *et al.*, 2000; Kim *et al.*, 2000; McGeoch and Guidotti, 2001; Nijtmans *et al.*, 2001). The F_OF_1-ATP synthase plays a critical role in efficient execution of apoptosis *via* caspase activation through alkalinizaton of the mitochondrial matrix (Matsuyama *et al.*, 2000). In addition F_OF_1 has been identified on the surface of endothelial cells as the major binding site for angiostatin, a naturally occurring tumor angiogenesis inhibitor (Moser *et al.*, 1999). Antibodies against α and β subunits mimicked angiostatin activity (Moser *et al.*, 2001), which was shown to inhibit both ATP hydrolysis and ATP synthesis in isolated mitochondria and intact endothelial cells (Burwick *et al.*, 2005).

Perturbations of the ability of F_OF_1 to produce ATP, or pump H^+, have profound effects on cellular bioenergetics. Therefore understanding the mechanism, and the role of rotation in coordinating the catalytic mechanism, which determine the efficiency of metabolism at the molecular level is important for a great number and diversity of diseases. In addition, research on the mechanism and coupling of F_OF_1 has broad implications for the enzymes involved in active transport, and in understanding the fundamental question of how chemical energy is converted into mechanical energy at the molecular level.

1.8 Complexity of the System

The F_OF_1 ATP synthase has been studied for several decades, and great advances have been made in understanding its structure and function. However the complexity of the enzyme and the mechanism by which it synthesizes or hydrolyzes ATP is such that catalytic events even on the F_1 sector of the enzyme are not yet understood despite a substantial amount of structural and functional data.

1.8.1 Structural complexity

The structural complexity of the F_OF_1-ATP synthase is significant. It is a large, complex, dynamic, multisubunit protein. It has a molecular weight of over 500,000 Daltons with each sector of the protein, F_O and F_1, composed of multiple subunits. The *E. coli* enzyme has the simplest composition, with a total of 22 subunits (Senior *et al.*, 2002), and of these, more than half are membraneous. These multiple subunits are held

together completely through non-covalent bonds as there are no disulfide bonds in the complex. In addition the function of F_OF_1 as a true rotary motor means that it is composed of counter rotating assemblies of subunits, in the *E. coli* enzyme there are roughly an equal number each in the stator and rotor. The interactions between the stator and rotor allowing rotation of one with respect to each other are complex. Little is known about the physical properties or the conformational dynamics of the γ and ε subunits which allow them to behave as polypeptide rotors in the molecular motor.

There are multiple copies of several of the subunits, including the homologous α and β subunits, a structural feature which on a practical level presents a challenge to experimental design. There are multiple nucleotide binding sites on the enzyme: six nucleotide binding sites, three catalytic sties on β subunits and three non-catalytic sites on α subunits, and in addition the ε subunit has been shown to bind ATP in at least two bacterial species (Kato-Yamada, 2005; Yagi *et al.*, 2007).

Finally, F_1 can be reversibly stripped off the F_O and functions as a soluble ATPase (whether this has a functional role in the cell is not known), however the F_OF_1 is membrane embedded, and to truly understand ATP synthesis and proton pumping, the holoenzyme must be studied.

1.8.2 Thermodynamic and Kinetic Complexity

The F_OF_1 ATP synthase is an incredibly dynamic molecule with three sites working in concert, each at a different point along the catalytic pathway. It is a remarkable enzyme and is kinetically complex exhibiting both negative and positive cooperativity between sites. It displays negative cooperativity in binding of substrate

where affinity for substrate of the first catalytic site is three orders of magnitude higher than affinity of the second site, and six orders of magnitude higher than the affinity of the third site (Weber *et al.*, 1993). The ATP synthase shows positive cooperativity in the promotion of catalysis such that the enzyme hydrolyzes substrate slowly at a single site, but binding of substrate to the second and third sites promotes catalysis by six-orders of magnitude, by accelerating product release (Cross *et al.*, 1982). The molecular terms of positive catalytic cooperativity are not yet understood. The negative cooperativity of binding and positive catalytic cooperativity are evident in the synthesis direction as well as the hydrolysis direction (Tomashek *et al.*, 2004). The unisite mode of catalysis has been studied extensively, as have maximal steady state rates, but kinetic analysis of the partial reaction steps of the steady state, physiological operating mode of the enzyme, was difficult due to the complicated site-site interactions in multisite catalysis.

The activity of F_OF_1 is subject to complex regulation by the endogenous epsilon subunit that is not fully understood. This regulation is mediated at least partly through the electrostatic interactions between the acidic residues of the highly conserved β^{380}DELSEED^{386} motif and the basic residues of the C-terminal α-helix of ε (Hara *et al.*, 2001). The chloroplast enzyme has an additional regulatory feature where formation or reduction of a disulfide bond between two cysteine residues in the γ subunit inhibits or activates the enzyme. The mitochondrial enzyme has at least one extra subunit, the inhibitory F_1 protein (or IF1), that regulates enzyme activity. The extraordinary feature of this regulation is that enzyme efficiency is maintained at almost 100%.

The F_O and F_1 sectors each function as a motor. Their step sizes are clearly different. The F_1 enzyme rotates in three 120º steps, with each step further divided into 80º and 40º substeps (Shimabukuro *et al.*, 2003). The size of the F_O motor steps is inversely proportional to the number of *c* subunits, (360º divided by the number of *c* subunits). The mechanism by which the two motors are synchronized to efficiently couple energy despite, or perhaps because of, their step-size mismatch is another complicated aspect of enzyme function. This step-size difference is an aspect of the mechanism by which the enzyme transmits coupling energy to effectively link the two disparate functions of proton transport and ATP synthesis/hydrolysis. Several specific residues and regions of various subunits (reviewed in section *1.6.1*) critical to efficient coupling between F_O and F_1 have been identified. It is clear from this body of work that the mechanism involves many coordinated interactions between multiple subunits, yet the energy transmission is incredibly efficient. Thermodynamically the prevention of energy dissipation through alternate pathways is a complex feat for such a large protein.

On a more fundamental level, the most remarkable feature of F_OF_1 ATP synthase function is that it couples multiple different types of energy with virtually no energy loss. The three types of mechanisms coordinated by the enzyme are: (1) chemical, (2) electro-chemo-mechanical, and (3) chemo-mechanical. (1) The chemical mechanism is the hydrolysis/synthesis of ATP, a non-equilibrium reaction in solution, which is catalyzed effectively by the enzyme to release the energy stored in the phosphoanhydride bond of ATP. (2) The mechanism of the F_O portion of the enzyme involves electro-chemo-mechanical coupling through the conversion of energy stored in the electrochemical

potential gradient (which includes both the membrane potential, the electrical component, $\Delta\Psi$, and the ion gradient, the chemical component, ΔpH) to mechanical energy in rotation of the *c*-ring. An added complication in this area is the finding that the two components of the ionmotive force ($\Delta\Psi$ and ΔpH) while thermodynamically equivalent, are not kinetically equivalent (Kaim and Dimroth, 1999). Integrally related, is the fact that it appears that in a given species, the number of *c* subunits in the ATP synthase seems to be correlated with the size of the membrane potential ($\Delta\mu_{H+}$) of that a species. In addition the membrane potential, $\Delta\mu_{H+}$. (3) The F_1 portion interconverts chemical energy with mechanical energy by coupling rotation to hydrolysis or synthesis of ATP. A great deal of work, using many varied techniques, has focused on understanding how the enzyme accomplishes this rotational coupling. It is this chemomechanical feature of F_1 function that the present study addresses.

2. Setting the chemical framework: Pre steady state kinetics of wild-type E. coli F_1-ATPase.

Adapted from:

Determination of the partial reactions of rotational catalysis in the F_1-ATPase

Joanne A. Baylis Scanlon, Marwan K. Al-Shawi, Nga Phi Le, Robert K. Nakamoto (2007) *Biochemistry* **46**: 8785-97.

2.1 Abstract

Steady state ATP hydrolysis in the F_1-ATPase of the F_OF_1 ATP synthase complex involves rotation of the central γ subunit relative to the catalytic sites in the $\alpha_3\beta_3$ pseudo hexamer. To understand the relationship between the catalytic mechanism and γ subunit rotation, the pre-steady state kinetics of Mg·ATP hydrolysis in the soluble F_1-ATPase upon rapid filling of all three catalytic sites was determined. The experimentally accessible partial reactions leading up to the rate limiting step and continuing through to the steady state mode were obtained for the first time. The burst kinetics and steady state hydrolysis for a range of Mg·ATP concentrations provide adequate constraints for a unique minimal kinetic model which can fit all the data and satisfies extensive sensitivity tests. Significantly, the fits show that the ratio of the rates of ATP hydrolysis and synthesis is close to unity even in the steady state mode of hydrolysis. Furthermore, the

rate of Pi binding in the absence of the membranous F_O sector is insignificant thus productive Pi binding does not occur without the influence of a proton motive force. In addition to the minimal steps of ATP binding, reversible ATP hydrolysis/synthesis and the release of product Pi and ADP, one additional rate-limiting step is required to fit the burst kinetics. Based on testing of all possible minimal kinetic models, this step must follow hydrolysis and precede Pi release in order to explain the burst kinetics. Consistent with the single molecule analysis of Yasuda *et al.* [Yasuda, R., Noji, H., Yoshida, M., Kinosita, K., and Itoh, H. (2001) *Nature* 410, 898-904], we propose that the rate-limiting step involves a partial rotation of the γ subunit; hence we name this step k_γ. Moreover, the only model that is consistent with our data and many other observations in the literature suggests that reversible hydrolysis/synthesis can only occur in the active site of the β_{TP} conformer [Abrahams, J. P., Leslie, A. G. W., Lutter, R., and Walker, J. E. (1994) *Nature 370*, 621-628].

2.2 Introduction

Steady state ATP hydrolysis in the F_1-ATPase involves rotation of the central γ subunit relative to the catalytic sites in the $\alpha_3\beta_3$ pseudo hexamer (see Ref. (Boyer, 2002; Dittrich and Schulten, 2005; Kinosita *et al.*, 2004; Nakamoto, 1999; Nakamoto *et al.*, 1999; Ren and Allison, 2000; Senior *et al.*, 2002) for reviews). At any point in time the three catalytic sites, which are predominantly within the β subunits, are in different conformations depending on the specific interactions with the γ subunit. The x-ray

crystal structure of bovine F_1 (Abrahams *et al.*, 1994) shows that two of the catalytic sites are in "closed" conformations with the bound nucleotides confined in a cleft inaccessible to solvent, and the third site is "open" to solvent. In addition, there are three non-catalytic nucleotide sites predominantly in the α subunits. During ATP hydrolysis, the catalytic reaction forces the rotation of the γ subunit and the rotation invokes conformational changes in all three catalytic sites. Generally, chemical cross-links between rotor and stator subunits (Aggeler *et al.*, 1993; Aggeler and Capaldi, 1996; Aggeler *et al.*, 1995a; Duncan *et al.*, 1995a) or between stator subunits (Aggeler *et al.*, 1998; Tsunoda *et al.*, 1999) impede rotation and catalysis. Perturbation of some specific interactions between the rotor γ subunit and the stator β subunits cause inefficient coupling between catalysis and rotation which indicate the critical role of the rotor in coordinating the catalytic mechanism (Al-Shawi *et al.*, 1997a; Nakamoto *et al.*, 1995; Nakamoto *et al.*, 1993). Furthermore, interactions among the sites that are mediated in part through the α subunits are also important in defining the conformation of each site and the interactions with substrates and products. Several mutations in the α subunit have been characterized that block transmission of information between sites (Le *et al.*, 2000; Maggio *et al.*, 1987; Nadanaciva *et al.*, 1999; Rao *et al.*, 1987; Weber *et al.*, 1995).

Despite the considerable information from high resolution structures and other types of analyses, coordination of the catalytic mechanism and rotation is not well understood. The rotational mechanism carries out energy coupling between the chemistry of ATP hydrolysis or synthesis, and the mechanical and conformational coupling to direct H^+ transport across the membrane through the F_O sector of the

complex. Several lines of evidence indicate that catalysis of ATP hydrolysis that is efficiently coupled to γ subunit rotation only occurs during steady state turnover when all three catalytic sites are involved. Even though two of the catalytic sites bind ATP with high affinity (<1x10^{-8} M and 8x10^{-7} M), Weber *et al*. (Weber *et al.*, 1993) demonstrated that rate enhancement of ATP hydrolysis coincides with occupancy of the third catalytic site, which has a K_d for Mg·ATP of 2-5x10^{-5} M. The very similar values for the steady state K_M for Mg·ATP hydrolysis and the K_M for activating rotation of the γ subunit (Yasuda *et al.*, 2001) indicate that rotation is an integral part of the three site catalytic mechanism. In contrast, at very low [Mg·ATP] where substrate is sub-stoichiometric, ATP binds only in the first high affinity site and is hydrolyzed with slow kinetics (Al-Shawi and Senior, 1988; Cross *et al.*, 1982; Duncan and Senior, 1985; Grubmeyer *et al.*, 1982). Significantly, such "unisite" catalysis is not associated with rotation (García and Capaldi, 1998).

To gain a mechanistic understanding of the coupling between catalysis and rotation, we have dissected the elementary rate constants of experimentally accessible reactions leading up to the rate limiting step and the onset of steady state hydrolysis. We fit and simulated the pre-steady state and steady state kinetics for a wide range of substrate concentrations using a minimal kinetic model. Through these studies, we find that the pre-steady state kinetics of ATP hydrolysis upon rapid filling of all three catalytic sites indicates that ATP undergoes reversible hydrolysis and synthesis with ADP and Pi at one site and that a rate limiting conformation change occurs kinetically before release of Pi. The results fit uniquely to a rotational catalytic scheme involving all three catalytic

sites in the following order: (1) Mg·ATP binds to the low affinity site (β_E, (Abrahams *et al.*, 1994)), (2) nucleotide bound at the high affinity site (β_{TP}) undergoes reversible hydrolysis/synthesis, (3) a rate limiting step occurs which likely involves partial rotation of the γ subunit that drives changes of the catalytic sites into the next conformational states, and (4) products Pi and ADP generated in the previous cycle are released from the site switching from the intermediate affinity (β_{DP}) site to the low affinity open site (β_E).

2.3 Experimental Procedures

2.3.1 Enzyme preparations.

E. coli F_1 complex was purified as previously described (Al-Shawi and Senior, 1992) from the *unc* operon deleted strain DK8 (Klionsky *et al.*, 1984) harboring the high copy number plasmid pBWU13 (Moriyama *et al.*, 1991). F_1 preparations were replete with δ and ε subunits as verified by SDS-PAGE analysis and the expected k_{cat} for steady state ATP hydrolysis rates as reported by Al-Shawi and Senior (Al-Shawi and Senior, 1992). The βY331W mutant was expressed from the same plasmid except for the introduction of the tryptophan codon (from TAC to TGG) as previously described (Le *et al.*, 2000). The ε subunit was expressed with an amino terminal polyhistidine tag (His-ε) in strain BL21(DE3)*pLysS* cells as described by Andrews *et al.* (Andrews *et al.*, 2001). His-ε was purified in a similar manner as previously described (Andrews *et al.*, 2001) except cell lysate was applied to a Ni-NTA resin column (Qiagen Inc., Valencia, CA) and washed initially using buffer with no imidazole, then using an imidazole gradient of 0-40 mM over four column volumes. Elution of His-ε was achieved using another gradient

(40-250 mM imidazole) over four additional column volumes. Incubation with rTEV protease (Life Technologies, Gaithersburg, MD) cleaved the polyhistidine tag. The free His-tags, the His-tagged rTEV protease and uncleaved ε subunit were separated from purified ε by passage over a Talon affinity column (Clontech, Palo Alto, CA). A greater yield of ε is achieved with the use of Talon resin at this stage rather than Ni-NTA resin because there is less non-specific binding of cleaved ε to the Talon column.

The F_1 enzyme was prepared for kinetic experiments by dilution to ~2 mg/ml in 25 mM TES[1]-KOH, 0.244 mM $MgSO_4$, 0.2 mM EDTA, pH 7.5 at 25 °C, and passage through two Sephadex G50 centrifuge columns (Penefsky, 1979) equilibrated with the same buffer. The protein concentration was determined by the method of Lowry *et al.* (1951). Passing the multisubunit enzyme over centrifuge columns results in the loss of a small portion of the ε subunit from F_1. To compensate, 2-3 μM (approximately one-half the molar concentration of F_1) of ε was added to the F_1 after each passage over the centrifuge columns. The F_1 was then diluted to 1 μM in the same buffer as above and used within two hours.

2.3.2 Determination of bound nucleotide.

A known amount of F_1 enzyme was precipitated by addition of 0.12 M perchloric acid and allowed to incubate on ice for 10 min. The protein was subsequently removed by centrifugation, and the supernatant neutralized by addition of Trizma base (Sigma-Aldrich) to a final concentration of 107 mM. An aliquot of the sample was subjected to ion exchange HPLC using a Titansphere TiO_2 column (Alltech Assoc., Deerfield, IL).

The chromatographic assay was performed in a similar manner to Kimura *et al.* (Kimura *et al.*, 2004), using a mobile phase composed of 50 mM NaH_2PO_4 buffer, pH 8.0 in 50 % v/v acetonitrile with a flow rate of 1 mL/min at 40 °C. The ADP and ATP-associated absorbance at 259 nm was integrated and the amount of nucleotide determined against standard amounts of ADP or ATP chromatographed over the same matrix.

2.3.3 Calibration of the rapid quench-flow apparatus

The millisecond time courses of [γ-^{32}P]ATP hydrolysis were generated using a Kintek (Austin, TX) RQF-3 rapid quench-flow apparatus with circulating water temperature control. Mixing and quenching times were verified by performing the following calibration reactions: (1) for times less than 40 ms, hydrolysis of benzylidene malononitrile (BMN) by 2M NaOH at 20 °C was followed according to the Kintek instruction manual. The reaction was quenched by 4 N HCl, and an equal volume of 4M potassium acetate, pH 6.5, was added to each sample to adjust the pH to ~4.5 before reading the absorbance at 310 nm. (2) For times longer than 25 ms, we followed the hydrolysis of 2,4-dinitrophenylacetate by NaOH to produce 2,4-dinitrophenol and acetate at 25 °C. Variations of the latter reaction over different time domains, was critical to avoid instrument artifacts that frequently appear in the intermediate times. We found that a thorough calibration of the instrument required that these reactions cover all time phases. Therefore different concentrations of NaOH were used to give the appropriate rate for the desired time range.

Artifacts may arise from volume or timing errors due to the design of the Kintek chemical quench-flow instrument which uses seven different delay loops to achieve

mixing times in the range from millisecond to second times. In order to examine and correct such errors, an Applied Photophysics (Surrey, UK) SX.18MV-R stopped-flow spectrometer was used to verify the rate constant of the base hydrolyzed reaction of 0.5 mM 4-nitrophenyl acetate by 0.1 M NaOH (final concentrations) measured in the quench-flow device. The rationale and results of the calibrations are presented in the *Results,* section *2.4.1* and shown in Fig. 2.4.1 and 2.4.2.

2.3.4 Pre-steady state hydrolysis of [γ-^{32}P]ATP.

The components of each syringe in the Kintek RQF-3 rapid quench-flow device (1:1 mixing volume ratio) were as follows: syringe A contained purified F_1 (with an additional equimolar concentration of ε subunit), prepared as described above, and syringe B contained 25 mM TES-KOH, 0.2 mM EDTA, pH 7.5 at 25 °C and varying concentrations of [γ-^{32}P]ATP and $MgSO_4$. The following Mg·ATP concentrations were obtained with the indicated [γ-^{32}P]ATP and $MgSO_4$ concentrations after mixing in the chemical quench instrument: 260 μM Mg·ATP final, 1.266 mM [γ-^{32}P]ATP and 0.764 mM $MgSO_4$; 106 μM Mg·ATP final, 1 mM [γ-^{32}P]ATP and 0.46 mM $MgSO_4$; 62 μM Mg·ATP final, 0.245 mM [γ-^{32}P]ATP and 0.33 mM $MgSO_4$; 29.2 μM Mg·ATP final, 0.267 mM [γ-^{32}P]ATP and 0.23 mM $MgSO_4$; 17.8 μM Mg·ATP, 0.087 mM [γ-^{32}P]ATP and 0.278 mM $MgSO_4$; and 4.8 μM Mg·ATP, 0.011 mM [γ-^{32}P]ATP and 0.252 mM $MgSO_4$. Reactions, which were run at 25 °C, were quenched by rapid addition of 1 mM KH_2PO_4 in 0.033 N perchloric acid (final concentration). A two step procedure was developed to minimize problems with the high background due to the high concentration

of [γ-^{32}P]ATP used in these experiments. First, an equal volume of ice cold acid-activated charcoal suspension, 1 % (w/v) (Norit, Sigma Chemicals, St. Louis, MO) was added to the quenched sample and incubated on ice for 10 minutes. The charcoal was removed by centrifugation at 22,000 g for 10 min, and 400 µl of the cleared supernatant was centrifuged at 426,000 g for a further 7 min to remove any finer particles. This treatment removed 96% of the un-reacted ATP. 300 µl of the final supernatant was diluted with 300 µl of 0.6 N perchloric acid plus 1 mM KH_2PO_4. The second step was the precipitation of inorganic phosphate by addition of 600 µl of acid molybdate solution (Sugino and Miyoshi, 1964). After incubating on ice for 20 min, the precipitate was centrifuged at 22,000 g and the supernatant removed. The pellet was washed once with 1 mL of 0.16 N perchloric acid. The final pellet was dissolved by addition of 1 M NaOH and the radioactivity determined by Cherenkov counting in 15 mL of 0.2 M Trizma base. Background samples were prepared by adding quench solution to the protein before addition of substrate and radioactivity. These samples were processed in the same manner and subtracted from the time point samples.

2.3.5 Determination of Kinetic Constants for ATP Hydrolysis.

Steady state ATP hydrolysis was measured in essentially the same conditions as the pre-steady state experiments described above, using [γ-^{32}P]ATP and measuring Pi production. All buffers were designed so that the concentration of free Mg^{2+} was constant at approximately 50 µM. A bent-tipped syringe was used for rapid mixing of 15 µL of substrate (Ray *et al.*, 1988) with an equal volume of 1 µM F_1 in a vortexed tube.

The reaction was quenched at various time points with 1 mM KH_2PO_4 in 0.03 N perchloric acid (final concentrations). Samples were processed following the same two step protocol developed for samples in the pre-steady state experiments for the removal of excess background [γ-^{32}P]ATP. Zero time points were acquired by mixing quench solution and protein before addition of substrate. Reaction medium for the determination of kinetic constants as a function of Mg·ATP contained 25 mM TES, 0.2 mM EDTA, and varying concentrations of ATP (0-1.26 mM ATP) and $MgSO_4$ (0.245-0.764 mM) to ensure a final low free Mg^{2+} concentration of approximately 50 μM at pH 7.5 at 25 °C. ATP hydrolysis rates were determined from time points measured from 1–10 seconds.

The inhibitory constant of ADP (K_I^{ADP}) was determined in buffer where Mg·ATP was held constant at 105 μM and ADP was increased from 0-1 mM. The buffer contained 25 mM TES, 0.2 mM EDTA, 0.35 mM $MgSO_4$, 0.25 mM ATP and to keep the free Mg^{2+} constant, additional $MgSO_4$ was supplemented with the ADP in a constant molar ratio. ATP hydrolysis rates were determined for a time course in each reaction condition of 1-10 s.

2.3.6 Pre-Steady State Nucleotide Binding.

Nucleotide binding to the catalytic sites was monitored by the decrease in tryptophan fluorescence intensity of the βY331W mutant F_1 as previously described (Weber *et al.*, 1993). The kinetics of fluorescence quenching were followed in an Applied Photophysics SX.18MV-R stopped-flow spectrometer. The excitation wavelength was 295 nm and emission was monitored through a 320 nm cutoff filter in the stopped-flow apparatus (or at 360 nm in the steady state fluorimeter). The syringe

contents were essentially the same as for the rapid quench flow experiments except for the lack of radioactivity. The conditions for the Mg·ATP titration were as follows: syringe A contained 1 μM of purified F_1 prepared as described above, and syringe B contained 25 mM TES-KOH, 0.2mM EDTA, pH 7.5 at 25 °C and ATP and $MgSO_4$ concentrations that resulted in a final free Mg^{2+} concentration of 50 μM and the following Mg·ATP concentrations: 519 μM Mg·ATP, 1.26 mM ATP and 0.764 mM $MgSO_4$; 260 μM Mg·ATP, 0.63 mM ATP and 0.504 mM $MgSO_4$; 104 μM Mg·ATP, 0.252 mM ATP and 0.348 mM $MgSO_4$; 40 μM Mg·ATP, 0.097 mM ATP and 0.284 mM $MgSO_4$; 17.3 μM Mg·ATP, 0.042 mM ATP and 0.261 mM $MgSO_4$; 10.4 μM Mg·ATP, 0.025 mM ATP and 0.254 mM $MgSO_4$; 4 μM Mg·ATP, 0.0097 mM ATP and 0.248 mM $MgSO_4$; 1 μM Mg·ATP, 0.0025 mM ATP and 0.245 mM $MgSO_4$. The ADP titration conditions were the same for syringe A, and syringe B contained 25 mM TES-KOH, 0.2 mM EDTA, pH 7.5 at 25 °C, and varying concentrations of ADP and $MgSO_4$. The following combinations resulted in the indicated ADP concentration and a final free Mg^{2+} of 50 μM: 2000 μM ADP and 0.326 mM $MgSO_4$; 1000 μM ADP and 0.285 mM $MgSO_4$; 500 μM ADP and 0.264 mM $MgSO_4$; 250 μM ADP and 0.254 mM $MgSO_4$; 250 μM ADP and 0.254 mM $MgSO_4$; 100 μM ADP and 0.248 mM $MgSO_4$; 50 μM ADP and 0.246 mM $MgSO_4$; 20 μM ADP and 0.245 mM $MgSO_4$; 10 μM ADP and 0.2444 mM $MgSO_4$; 5 μM ADP and 0.2442 mM $MgSO_4$. The kinetic fluorescence curves shown in Fig. 2.4.6 and 2.4.7 were generated from 2-4 stopped-flow mixing experiments. Nucleotide occupancy was determined based on the affinity constants for βY331W as described by the Senior laboratory (Weber *et al.*, 1993).

2.3.7 Model fitting and sensitivity analysis.

Differential equation integration, location of the region of the minimum, fitting of experimental data, model simulations and statistical analyses were performed using the experimental data fitting program Scientist Version 2.0 (Micromath Research, Inc., St Louis, Missouri). The Scientist program solves systems of model equations, generates fits to the data and simulates all other parameters, yielding progress curves for all species.

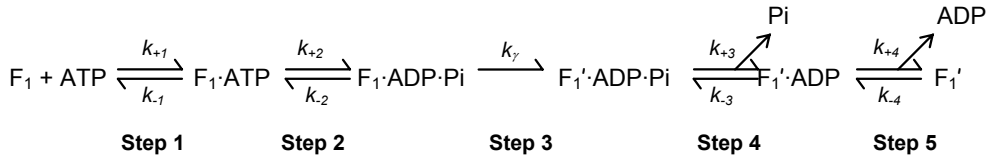

[Reaction Scheme 2]

Differential equations for the whole reaction scheme (Reaction Scheme 2) were set up as follows:

$d[F_1]/dt = -k_{+1}[F_1][ATP] + k_{-1}[F_1{\cdot}ATP] + k_{+4}[F_1''{\cdot}ADP] - k_{-4}[F_1][ADP]$

$d[ATP]/dt = -k_{+1}[F_1][ATP] + k_{-1}[F_1{\cdot}ATP]$

$d[F_1{\cdot}ATP]/dt = k_{+1}[F_1][ATP] - k_{-1}[F_1{\cdot}ATP] - k_{+2}[F_1{\cdot}ATP] + k_{-2}[F_1{\cdot}ADP{\cdot}Pi]$

$d[F_1{\cdot}ADP{\cdot}Pi]/dt = k_{+2}[F_1{\cdot}ATP] - k_{-2}[F_1{\cdot}ADP{\cdot}Pi]$

$d[F_1'{\cdot}ADP{\cdot}Pi]/dt = k_{\gamma}[F_1{\cdot}ADP{\cdot}Pi] - k_{+3}[F_1'{\cdot}ADP{\cdot}Pi] + k_{-3}[F_1'{\cdot}ADP][Pi]$

$d[F_1'{\cdot}ADP]/dt = k_{+3}[F_1'{\cdot}ADP{\cdot}Pi] - k_{-3}[F_1''{\cdot}ADP][Pi] - k_{+4}[F_1''{\cdot}ADP] + k_{-4}[F_1][ADP]$

$d[Pi]/dt = k_{+3}[F_1'{\cdot}ADP{\cdot}Pi] - k_{-3}[F_1'{\cdot}ADP][Pi]$

$d[ADP]/dt = k_{+4}[F_1'{\cdot}ADP] - k_{-4}[F_1][ADP]$

$Q = [F_1{\cdot}ADP{\cdot}Pi] + [F_1'{\cdot}ADP{\cdot}Pi] + [Pi]$

Where Q represents the quench-flow data, *i.e.* amount of Pi generated. F_1 and F_1' represent the enzyme in different conformational states, which is necessary to distinguish the concentrations of F_1·ADP·Pi, the state before the putative γ subunit rotation step, k_γ, and F_1"·ADP·Pi, the state after k_γ. The numerical integration of the differential equations was performed using the EPISODE integrator package for stiff systems (where there are large differences in the way two or more dependent variables depend on the independent variable, *e.g.* kinetic rate constants with large differences in rates). The analytic Jacobian matrix was used internally in the EPISODE integrator so that at each step of the corrector iteration it solves systems of nonlinear equations that arise. Parameters were initially estimated based on experimental evidence described in this paper and from previously published work. These initial parameters were refined using the simplex technique (Deming and Morgan, 1979) in Scientist v2.0 which searches the parameter space to locate the region of the local minima. A non-linear least squares fit was then performed using the refined parameters. The least squares minimization in Scientist v2.0 is based on the algorithm by Powell (Powell, 1970), but it is altered to include scaling of variables automatically, and also systems with more unknowns than equations. The two steps, simplex searching to improve parameter estimates followed by least squares minimization, were performed until the best fits were determined for each [Mg·ATP] condition.

The goodness-of-fit of the simulations to the data were determined partly by the R^2 parameter, but the more sensitive parameter used for most evaluations was the Model Selection Criterion (MSC, See Ref. (MicroMath_Research, 1995)). The MSC is a

modified Akaike Information Criterion (AIC) (Akaike, 1974; Akaike, 1976). The AIC is a statistical method that objectively distinguishes between different models, selecting the model that fits well, but with the fewest parameters, *i.e.* it selects for simplicity and parsimony. In this way it is an attempt to represent the "information content" of a set of parameter estimates (relating the fraction of variability to the number of parameters used to obtain the fit). The AIC and MSC give the same rankings between models, but the AIC is dependent on the number of observations and the magnitude of the data points. The MSC is a reciprocal form of the AIC and has been normalized so it is independent of the scaling of the data points (MicroMath_Research, 1995). Essentially the larger the MSC value, the more appropriate the model.

A sensitivity analysis of each parameter was performed. The data set for 62 μM Mg·ATP was used for the analysis because it gave an excellent fit to our model (MSC: 5.56), the partial rate constants represented those of the other conditions very well, and it was the highest [Mg·ATP] concentration with minimal scatter of the data points. The parameters for the best fit to this data set are listed in Table 2.4.1 and were used for the sensitivity analysis. Each rate constant was perturbed individually (10-fold or 2-fold) as listed in Table 2.4.2, while the other rate constants were not varied. These parameter sets were used as seed values for a minima-seeking simplex algorithm which improved initial parameter estimates for the subsequent non-linear least squares analysis which fit the parameter set to the experimental data. The simplex search and least-squares analysis could not be completed for the most sensitive parameters due to undefined numbers. In cases where the model fit was performed successfully the deviations of the model curves

from the data were assessed visually and by performing a statistical analysis to determine the MSC values of the fits.

2.3.8 Other procedures.

Except where [γ-^{32}P]ATP was used, steady state ATPase activities were determined colorimetrically as previously described (Al-Shawi *et al.*, 1997a). Concentrations of free Mg^{2+}, free ATP, Mg·ATP and Mg·ADP were calculated using the algorithm of Fabiato and Fabiato (Fabiato and Fabiato, 1979). All chemicals and reagents were of the highest quality available.

2.4 Results

2.4.1 Calibration of the Kintek quench-flow rapid mixing device

Elucidation of the multisite catalytic rates of the F_1-ATPase necessitates the use of rapid mixing devices, however due to the precise nature of the pre-steady state experiments the data are sensitive to artifacts that may arise because of the design of the rapid mixing machines. Accurate calibrations are absolutely critical when working at this time scale to ensure correction of data artifacts from the instruments that might otherwise affect the modeling and interpretation of the data. A reaction measured by use of the Kintek (Austin, TX) RQF-3 rapid quench-flow apparatus may be subject to volume or timing errors because each point is measured individually and the time of the reaction is determined indirectly based on the rate of flow and the reaction loop volume.

Mixing and quenching times for the Kintek chemical quench-flow machine were verified for times less than 40 ms, by determining the rate of hydrolysis of 1mM benzylidenemalononitrile by 2 M NaOH at 20 °C. We observed a k_{app} of 147 s^{-1} for the first-order reaction, which was quite close to the expected 140 s^{-1} from the Kintek manual. For times longer than 25 ms, we followed the hydrolysis of 2,4-dinitrophenylacetate by NaOH to produce 2,4-dinitrophenol and acetate at 25 °C. A second order rate constant of 57.6 $M^{-1}s^{-1}$ was obtained for this reaction, which was in good agreement with previously published values (Froehlich *et al.*, 1976).

The integrity of the Kintek Quench Flow machine was evaluated more rigorously at very short reaction times (<10 ms), through the first reaction loop (Loop 1), by measuring the hydrolysis of 4 mM BMN by 2 M NaOH at 25 ºC, shown in Fig. 2.4.1. This also allowed determination of instrument accuracy in measuring a reaction time of 1 ms (less than the specified dead time of 2 ms). Scatter of data in this single shot experiment was very small, and a single exponential function accurately fit the data (rate constant = 240 s^{-1}; R^2= 0.997). The Kintek quench flow instrument function was thus verified in this time range, and the instrument accurately measured the reaction at 1 ms.

An advantage to using the Kintek RQF-3 rapid quench-flow device is the small volumes of reactants, ~15 μL, however small errors in these volumes manifest in the data. In addition, the Kintek chemical quench-flow device has seven reaction loops with volumes ranging from approximately 16 μL to 200 μL, yielding seven different pathways through which the reaction mixture flows.

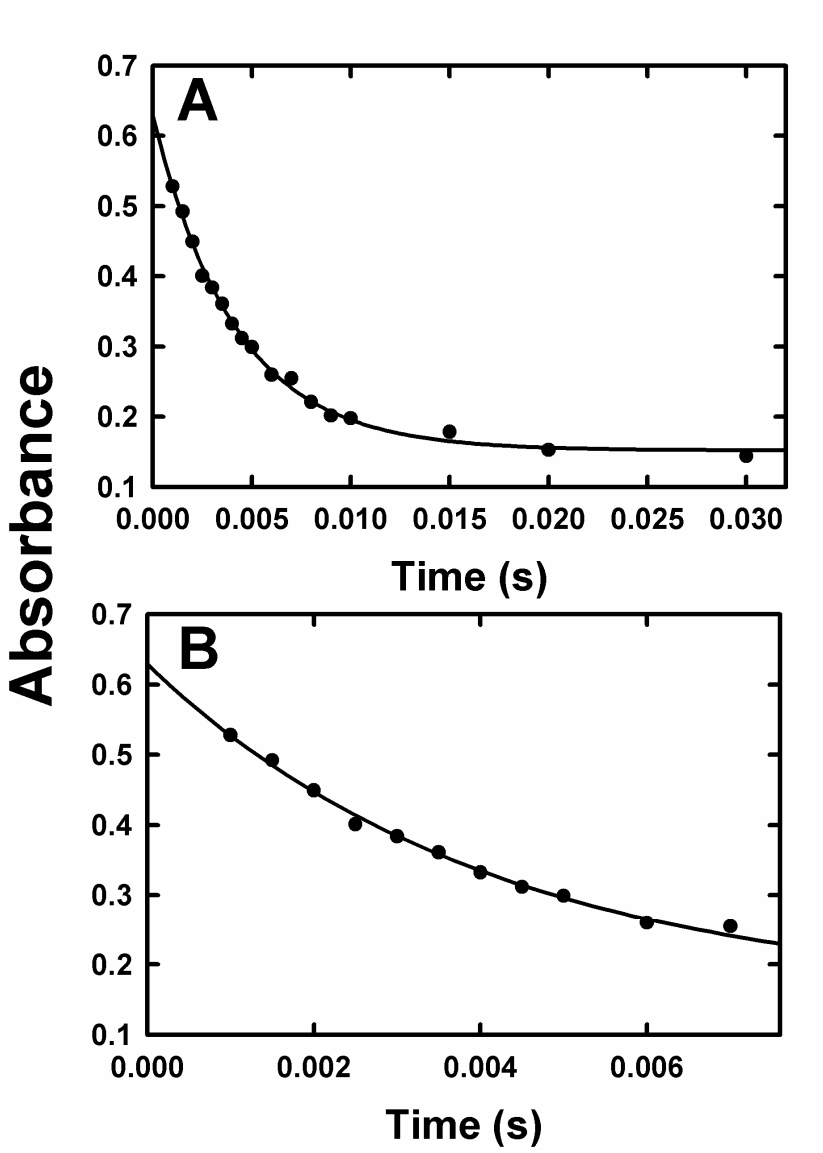

Figure 2.4.1. Verification of Kintek RQF-3 quench-flow machine function in the early time domain.

The hydrolysis reaction of 2 mM benzylidenemalononitrile with 1 M NaOH (final concentrations) was followed by measuring absorbance at 300nm. (A) The total time course of the reaction. (B) Time course of the reaction through the first delay loop. The line shown is the exponential decay nonlinear regression fit to the data R^2=0.997.

Because each time point of the reaction is measured individually, to correctly measure both the time course and amplitude of a reaction, the volume and flow rate through each reaction loop must be consistent and transitions between loops should be smooth. To correct any errors in volume or time measurement, the Kintek quench-flow machine was calibrated by parallel kinetic traces from an Applied Photophysics SX.18MV-R stopped-flow spectrometer (Surrey, UK), a more direct method for measuring a reaction. The results of the calibration are shown in Fig. 2.4.2 where the same test reaction of 4-nitrophenyl acetate hydrolyzed by NaOH was measured in each instrument. The Kintek quench-flow instrument clearly underestimates the reaction from 50 ms to 1 s. The cause of this difference was later determined to be due to an error in the sample volumes reacted by the device, which was determined by precise measurements of volume recovery (data not shown). The use of two rapid mixing devices allowed us to determine the extent of the artifact, and more importantly, to match the quench-flow device to the stopped-flow spectrometer and correct the error of the Kintek quench-flow instrument. Interestingly, data published from other laboratories using this same Kintek instrument frequently contains the same artifact (data not shown).

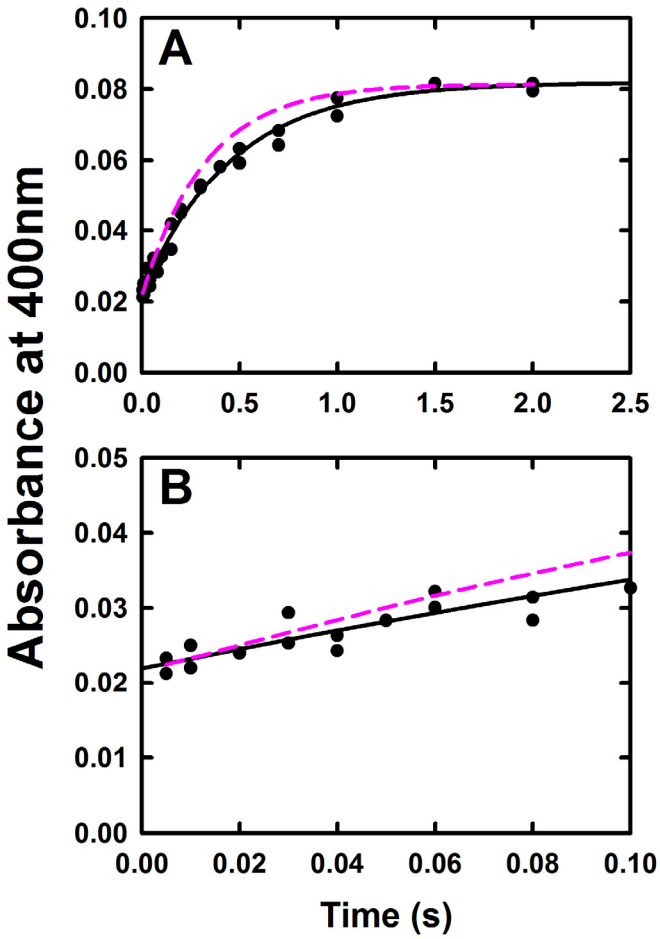

Figure 2.4.2. Calibration of the Kintek RQF-3 quench-flow machine by the Applied Photophysics SX.18MV-R stopped-flow spectrometer.

The hydrolysis reaction of 0.5 mM 4-nitrophenyl acetate reacted with 0.1 M NaOH (final concentrations) at 25 °C was followed by measuring absorbance at 400 nm. (A) Total time course for the reaction to 2.5 s. (B) Early time course of the reaction to 0.1s. The reaction in the Kintek quench-flow device was quenched with 0.67 N HCl (final concentration), depicted by (●). The stopped flow rate constant was determined from the average of 3 experiments. Data were fit by nonlinear regression to the equation for an exponential rise to a maximum. The *black solid line* is the fit to the quench flow data, and the *pink dashed line* is the fit to the stopped-flow data. The rate constant for the reaction was determined in each instrument: the stopped-flow device gave 6.4 s^{-1}, the quench-flow device gave 4.5 s^{-1}.

2.4.2 Design of experimental conditions for pre-steady state ATP hydrolysis by F_1.

As discussed in the *Introduction*, experimental results from several laboratories contribute to the hypothesis that ATP hydrolysis is coupled to γ subunit rotation only at ATP concentrations high enough to occupy all three catalytic sites. Consequently, determination of pre-steady state kinetics of the rotational catalytic pathway must be initiated with Mg·ATP concentrations similar to the K_M for steady state ATPase activity, *i.e.* in the range of 10^{-5}-10^{-4} M. The true substrate of F_1 is Mg·ATP and excess free Mg^{2+} is well known to be inhibitory (Al-Shawi *et al.*, 1988). Conditions were therefore chosen with an excess of ATP over total Mg^{2+}, with free Mg^{2+} buffered at 50 μM. Furthermore, it was necessary to use radioactive [γ-^{32}P]ATP because we needed to be able to detect stoichiometric amounts of Pi in the first few turnovers of the enzyme. Reaction conditions used for the time course of ATP hydrolysis given in the legend to Fig. 2.4.3 and *Experimental Procedures* are a compromise to satisfy these requirements and to assure that the enzyme is working in a multisite catalytic mode maximally coupled to rotation.

The large background due to [γ-^{32}P]ATP levels compared to the small amounts of Pi produced, and the non-enzymatic hydrolysis of [γ-^{32}P]ATP during downstream sample processing, were reduced by developing a protocol for quantitative separation of Pi produced from the total background ATP. A two-step procedure was used to remove ATP from the acid quenched solution (see *Experimental Procedures*): first, treatment with acid-activated charcoal and its subsequent removal by centrifugation, and second, precipitation of Pi with acidic molybdate solution (Sugino and Miyoshi, 1964). This

allowed the effective separation of the Pi produced from the background ATP which was typically 100-1000 fold in excess.

Another consideration is the nucleotide occupancy of the enzyme at the beginning of the reaction. ADP bound to all three catalytic sites may slow the onset of catalysis (Wise *et al.*, 1981), while an enzyme completely devoid of nucleotide may behave differently as the non-catalytic sites will need to refill before the complex reacquires the normal steady state load of nucleotide. Purified F_1 was gently treated by passage through two centrifuge columns as described in the *Experimental Procedures* to remove nucleotide from two catalytic sites while leaving nucleotides in the non-catalytic sites. An ion exchange HPLC assay (see *Experimental Procedures*) was used to determine that the starting enzyme contained 4.1±0.1 bound nucleotides per F_1, of which 2.9±0.1 mol were ATP and 1.1±0.03 mol were ADP (from three independent determinations). Based on previous determinations we assumed that three ATP are in non-catalytic sites and one ADP is in a catalytic site (Cross and Nalin, 1982; Nalin and Cross, 1982).

2.4.3 Pre-steady state measurement of ATP hydrolysis at high [Mg·ATP]

The pre-steady state kinetics of ATP hydrolysis was analyzed to determine the rate constants of the partial reactions of the enzyme in a catalytic mode involving rotation of the γ subunit. The data sets and fits (Fig. 2.4.3, Table 2.4.1 and discussed in detail below) show the activation of steady state ATP hydrolysis rates for a range of Mg·ATP concentrations from 4.8-260 μM. These data sets are representative of several experiments repeated at all Mg·ATP concentrations and with several different enzyme

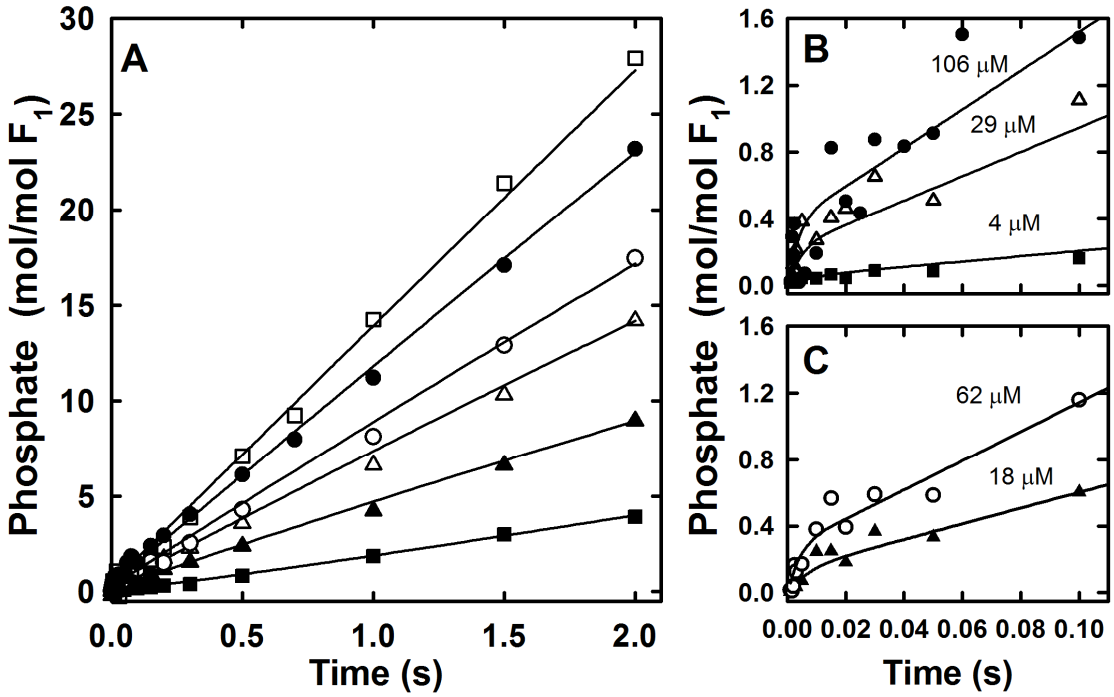

Figure 2.4.3. Pre-steady state hydrolysis by F_1 after fast addition of various concentrations of Mg·ATP.

A. The complete time course up to 2.0 s. Purified F_1 was prepared for each Mg·ATP condition as described in *Experimental Procedures* and diluted to 1 μM in 25 mM TES-KOH, 0.244 mM $MgSO_4$, 0.2 mM EDTA, pH 7.5 at 25 °C and loaded into Syringe A of the chemical quench instrument. The [γ-^{32}P]ATP and $MgSO_4$ concentrations in Syringe B resulted in the following final [Mg·ATP]: 260 μM Mg·ATP (□);106 μM Mg·ATP (●); 62 μM Mg·ATP (○); 29.2 μM Mg·ATP (△); 17.8 μM Mg·ATP (▲); and 4.8 μM Mg·ATP (■). The lines show the best fit to each condition based on Reaction Scheme 2 and constants in Table 2.4.1. *B*. The early time points up to 0.1 s for 106 μM Mg·ATP(●), 29.2 μM Mg·ATP (△) and 4.8 μM Mg·ATP (■). C. The early time points up to 0.1s for 62 μM Mg·ATP (○) and 17.8 μM Mg·ATP (▲). The early time course for the 260 μM Mg·ATP data set is omitted for clarity.

preparations. As can be clearly seen in the faster time frame (Fig. 2.4.3B and 2.4.3C, separated into two frames for clarity), ATP hydrolysis occurs with an initial burst within the first 10-20 ms then enters into the slower steady state phase, (the enzyme enters the steady state mode at ~50 ms under all conditions). The scatter in the data at the early time points of the higher concentrations (Fig 2.4.3B and 2.4.3C) was unavoidable due to the high background. Despite this limitation, the higher quality data for the lower concentrations and for the longer time points of the higher concentrations, allow us to obtain confident fits including the initial burst of hydrolysis of Mg·ATP.

The number of sites involved in the burst was determined using the individual fits for each condition, back extrapolating the steady state rates (from 50 ms onwards) to zero time, and fitting these values to the Michaelis-Menten equation to give an active site titration (Fig. 2.4.4). This analysis gave a stoichiometry of 0.5, indicating that one active site per F_1 molecule gives rise to the burst and additionally that the ATP and ADP + Pi bound to the enzyme are carrying out reversible hydrolysis/synthesis. An apparent K_M of 51 μM was calculated from the steady state rates in the quench flow instrument, which was essentially the same as the apparent K_M of 45 μM for the steady state hydrolysis of Mg·ATP determined in hand mixing measurements under the same conditions (Fig. 2.4.5A), and by Weber *et al.* using the βY331W F_1 (Weber and Senior, 2001; Weber *et al.*, 1993). These K_M values also match the K_d for the third low affinity site measured in Fig. 2.4.6A. The agreement of these values strongly suggests that the pre-steady state burst of hydrolysis is due to binding of Mg·ATP to the third catalytic site.

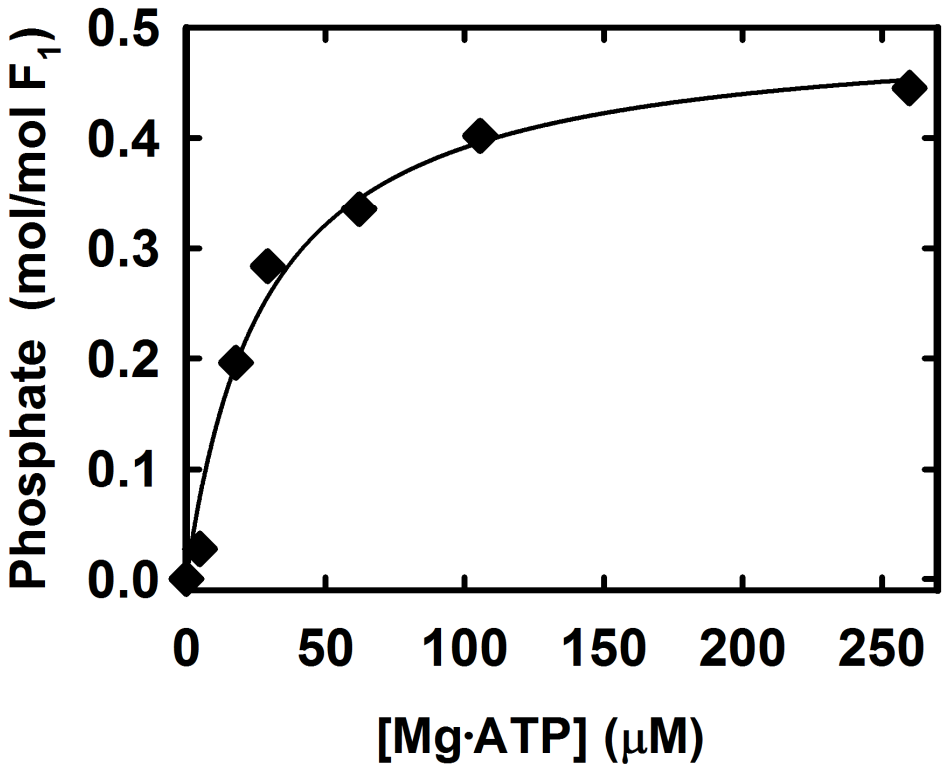

Figure 2.4.4. Analysis of the burst of hydrolysis.

The active site titration described in *Results* was a back extrapolation to zero time of the steady state rates for the individual fits to the pre-steady state data in Fig. 1. The solid line shows the fit to the data using the Michaelis-Menten equation and gives a stoichiometry of 0.5 sites per F_1 molecule.

2.4.4 Kinetic constants determined for Mg·ATP and ADP under conditions used for pre-steady state experiments

In order to ensure the veracity of pre-steady state experiments and to validate model fits to the pre-steady state rapid kinetic data it was important to determine the steady state kinetic constants of Mg·ATP hydrolysis and ADP inhibition under the same conditions. The K_M and V_{max} for Mg·ATP steady state hydrolysis were determined from the fit to the data in Fig. 2.4.5A. In Fig. 2.4.5B the K_I for ADP was determined by measuring the initial rates of Mg·ATP hydrolysis ([Mg·ATP]=105 μM) under conditions with increasing concentrations of ADP. The K_I for ADP was determined from the data fit to be 119 μM, which is in good agreement with K_d determined from experiments of ADP binding to the βY331W mutant, discussed later. The steady state kinetic constants measured under the conditions stated here are similar to published values, and the steady state parameters determined in the rapid quench flow experiments.

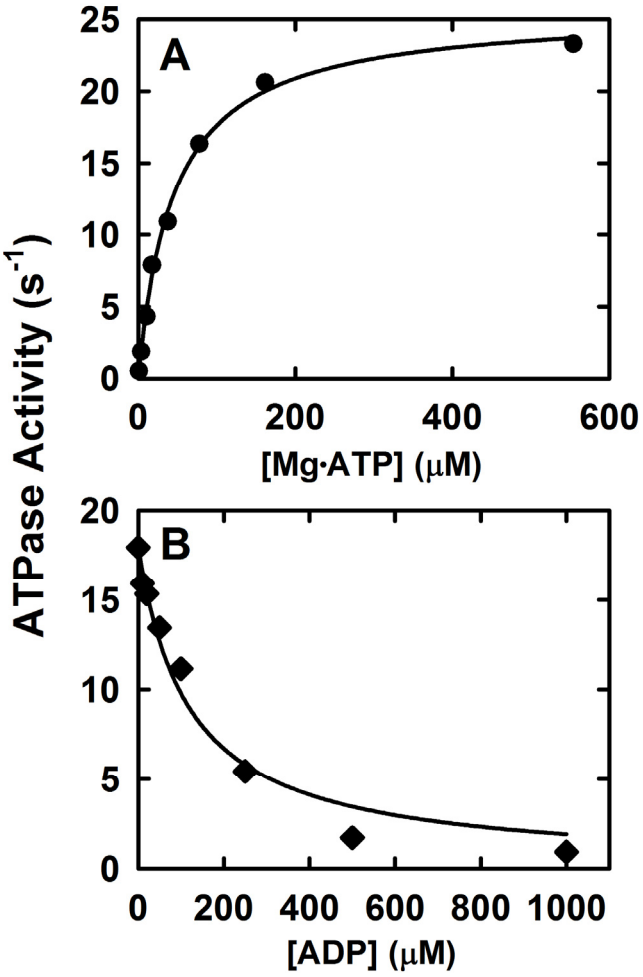

Figure 2.4.5. Titrations to determine the steady state kinetic constants of Mg·ATP hydrolysis.

F_1 was prepared in the same way as pre-steady state experiments described in *Experimental Procedures*. Initial steady state rates of hydrolysis of Mg·ATP were measured over a range of concentrations using [γ-^{32}P]ATP and measuring Pi production. All buffers contained 25 mM TES-KOH, 0.2 mM EDTA, 0.244 mM $MgSO_4$, pH 7.5 at 25 ºC. ATP, ADP and Pi were added in increasing concentrations with additional $MgSO_4$ to ensure a final free [Mg^{2+}] of approximately 50 μM for all conditions. Lines drawn are fits to the data using the Michaelis-Menten equation. (A) (●) ATP hydrolysis rates for varying concentrations of Mg·ATP (1 μM-519 μM). Parameters for the fit: apparent K_M for ATP=44.8μM, and V_{max}=25.6 s^{-1}. (B) (◆) ATP hydrolysis rates measured with increasing concentrations of ADP. The [Mg·ATP] was held constant at 105 μM, ADP was increased from 0-1 mM, and $MgSO_4$ was supplemented with ADP at a constant molar ratio. Parameters for the fit: K_I for ADP=119 μM, and k_{cat}=18 s^{-1}.

2.4.5 Pre-steady state binding of Mg·ATP and Mg·ADP monitored by fluorescence quenching of the βY331W mutant

In order to establish that binding of Mg·ATP to the three catalytic sites occurs with compatible kinetics to the rapid burst of Mg·ATP hydrolysis, the fluorescence quenching of the βY331W mutant F_1 (Weber *et al.*, 1993) was followed in the stopped-flow spectrometer. The experiments in Fig. 2.4.6 were performed under the same conditions as the quench flow experiments, and the βY331W mutant F_1 was prepared in the same way as wild-type F_1 described in the *Experimental Procedures*. Again the nucleotide occupancy of the enzyme at the beginning of the reaction was important to determine and was measured by the ion exchange HPLC assay to be 3.8±0.2 mol nucleotide bound per mol F_1 (similar to the wild-type enzyme).

The rate of binding of Mg·ATP to F_1 under the conditions used for the quench-flow experiments is very rapid, as can be seen from Fig. 2.4.6A. The fluorescence stopped-flow traces were used to calculate nucleotide occupancy as previously described by Weber *et al.* (Weber *et al.*, 1993). Second order fits of the data indicate that binding to all three catalytic sites is diffusion limited (~$1x10^9$ $M^{-1}s^{-1}$). Clearly the binding of Mg·ATP is not rate limiting to the rest of the reaction. Using the extent of sites filled at 5 ms, the $K_{1/2}$ for rapid binding of Mg·ATP to all three sites was approximately 13 μM in the same low free Mg^{2+} conditions used in the quench-flow experiments described above. The addition of higher Mg^{2+} (up to 0.89 mM free Mg^{2+}) did not strongly affect the binding affinity (Fig. 2.4.7). The binding stoichiometry was calculated from the extent of quenching of βY331W fluorescence and we note that for the 104 μM Mg·ATP

Figure 2.4.6. Pre-steady state association of Mg·ATP and ADP with the βY331W mutant F_1 under low Mg^{2+} conditions.

The binding of Mg·ATP or ADP to the βY331W mutant F_1 was followed by the decrease of tryptophan fluorescence as previously described (Le *et al.*, 2000; Weber *et al.*, 1993). Details are given in the *Experimental Procedures* for the stopped-flow set up. F_1 was prepared as described in the *Experimental Procedures*, and contained 3.8±0.2 mol nucleotide bound per mol F_1. Syringe A contained 1 μM F_1 in 25 mM TES-KOH, 0.2 mM EDTA and 0.244 mM $MgSO_4$, pH 7.5 at 25 °C. (A) The ATP and $MgSO_4$ concentrations in Syringe B resulted in a final free Mg^{2+} of 50 μM and the following [Mg·ATP]: 519 μM Mg·ATP; 260 μM Mg·ATP; 104 μM Mg·ATP; 40 μM Mg·ATP; 17.3 μM Mg·ATP; 10.4 μM Mg·ATP; 4 μM Mg·ATP; 1 μM Mg·ATP. (B) The ADP and $MgSO_4$ concentrations in Syringe B resulted in a final free Mg^{2+} of 49 μM and the following [ADP]: 2000 μM ADP; 1000 μM ADP; 250 μM ADP; 100 μM ADP; 20 μM ADP; 10 μM ADP; 5 μM ADP.

Fig. 2.4.6

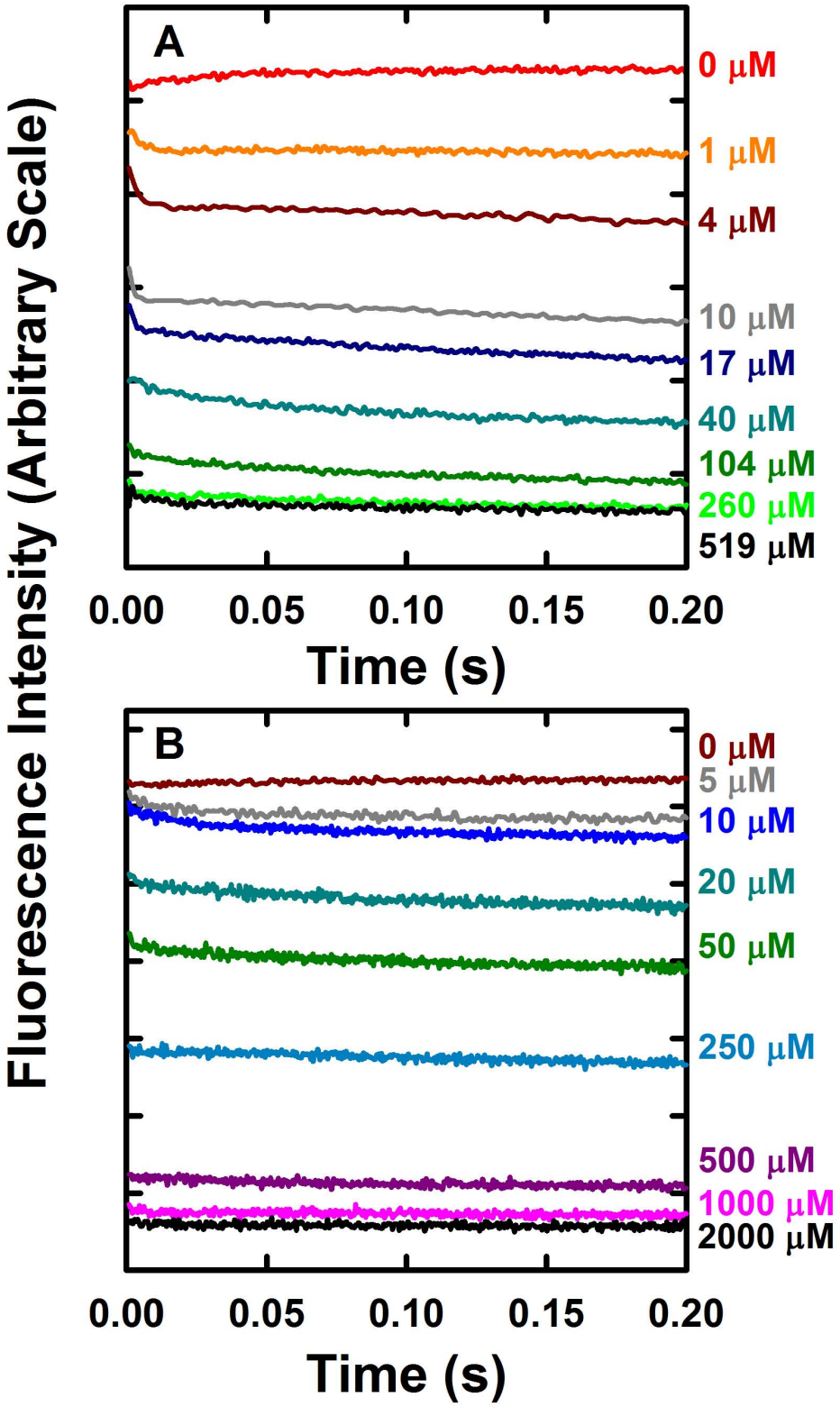
A
0 μM
1 μM
4 μM
10 μM
17 μM
40 μM
104 μM
260 μM
519 μM
0.00
0.05
0.10
0.15
0.20
Time (s)
B
0 μM
5 μM
10 μM
20 μM
50 μM
250 μM
500 μM
1000 μM
2000 μM
0.00
0.05
0.10
0.15
0.20
Time (s)
Fluorescence Intensity (Arbitrary Scale)

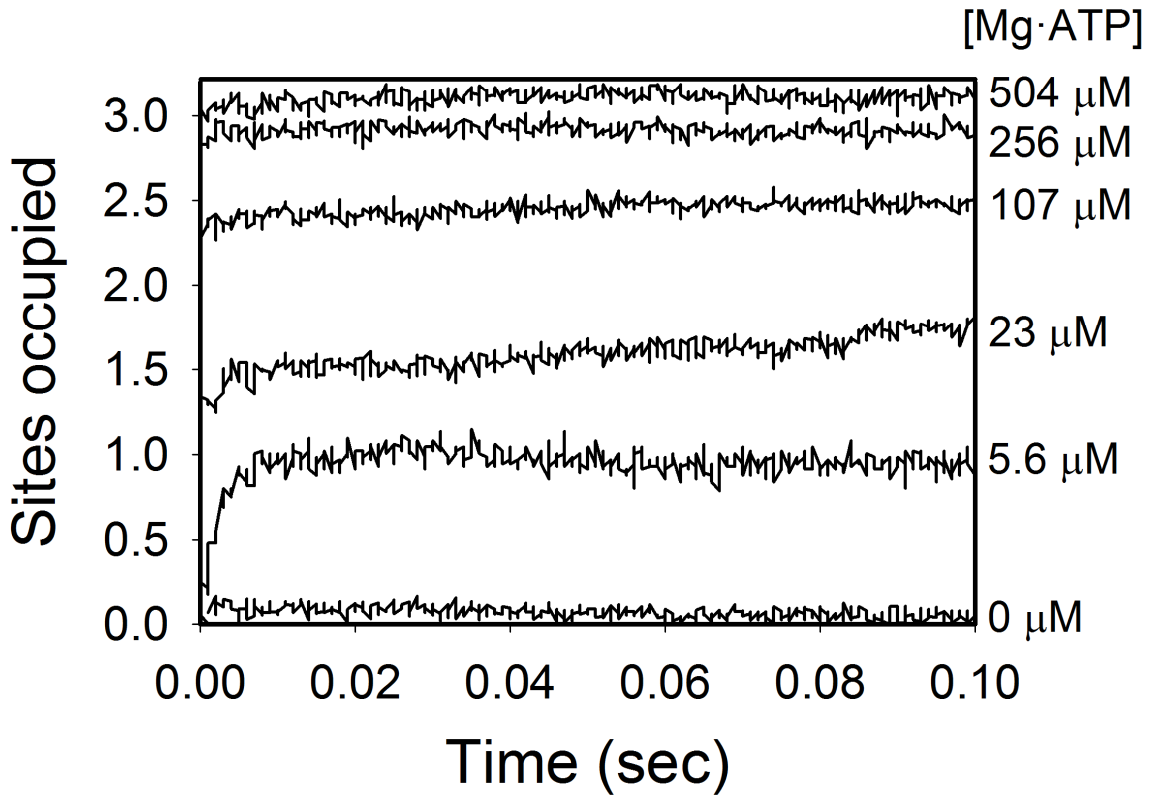

Figure 2.4.7. Pre-steady state association of Mg·ATP with the βY331W mutant F_1 under high Mg^{2+} conditions.

The binding of Mg·ATP to the βY331W mutant F_1 was followed by the decrease of tryptophan fluorescence as previously described (Le et al., 2000; Weber et al., 1993). Details are given in the *Experimental Procedures* for the stopped-flow set up. F_1 was prepared as described in the *Experimental Procedures* (3.4±0.1 mol nucleotide bound per mol F_1), equilibrated with 25 mM TES/KOH and 0.89 mM $MgCl_2$, diluted to 1 μM with the same buffer, and loaded in Syringe A. The ATP and $MgCl_2$ concentrations in Syringe B resulted in a final free Mg^{2+} of 0.89 mM and the following [Mg·ATP]: 504 μM Mg·ATP: 1.1 mM ATP, 1.9 mM $MgCl_2$. 256 μM Mg·ATP: 0.55 mM ATP, 1.4 mM $MgCl_2$. 107 μM Mg·ATP: 0.23 mM ATP, 1.1 mM $MgCl_2$. 23 μM Mg·ATP: 0.050 mM ATP, 0.93 mM $MgCl_2$. 5.6 μM Mg·ATP: 0.012 mM ATP, 0.90 mM $MgCl_2$. 0 ATP: 0.890 mM $MgCl_2$. Each trace is the average of 2 stopped-flow mixing experiments.

concentration 2.6 sites were filled within the 1 ms dead time of the instrument. Binding of Mg·ATP to the first site is known to occur with high affinity (Senior and Al-Shawi, 1992; Senior *et al.*, 1992). A value for K_{d1}=5 nM was used to fit the Mg·ATP binding titration to a model with three sites of differing affinities, which gives values for K_{d2}=2.4 μM and K_{d3}=44.8 μM. This agrees with the K_{d2}=0.9 μM and K_{d3}=33 μM previously determined (Löbau *et al.*, 1997; Weber *et al.*, 1993). These data greatly strengthen our hypothesis that the initial burst of ATP hydrolysis is driven by binding of nucleotide to the third, low affinity catalytic site with a K_d for Mg·ATP which is very similar to the K_M for steady state Mg·ATP hydrolysis ((Weber and Senior, 2001) and Fig. 2.4.5A) and rotation of the γ subunit (Yasuda *et al.*, 2001).

A titration with ADP using the βY331W mutant F_1, under the same low free Mg^{2+} conditions as the quench-flow experiments, was also performed (Fig. 2.4.6B). Binding of ADP to the enzyme is rapid, and second order fits of the data show the rate is slightly slower than diffusion limited (on the order of $1x10^7$-$1x10^8$ $M^{-1}s^{-1}$). Using the extent of sites filled at 5 ms, the $K_{1/2}$ for rapid binding of ADP to all three sites was approximately 127 μM under these conditions. These data could be fit to a model assuming a single class of binding site, with a K_d for ADP of 80 μM. This value is used for the initial starting value for k_{+4}/k_{-4} in the modeling (Table 2.4.1), and is in very good agreement with the previously reported values of 83 μM and 100 μM (Lunardi *et al.*, 1988; Weber and Senior, 1997). In addition, it is similar to the K_I value of 120 μM determined for the inhibition of steady state hydrolysis due to increasing ADP concentrations (Fig. 2.4.5B). These results indicate that under the conditions used for our experiments, where ADP and

free Mg^{2+} concentrations are low, there is not enough Mg·ADP present to drive the enzyme into a Mg·ADP inhibited form.

2.4.6 Modeling data fits and simulations of pre-steady state reactions.

Our kinetic model as shown in Reaction Scheme 2 shows that a single nucleotide binds, undergoes reversible hydrolysis/synthesis, and releases from the enzyme in each cycle. Even though these steps occur in different catalytic sites and to different nucleotides, which is an essential aspect of the rotational catalytic mechanism as will be described in the *Discussion*, only single nucleotide binding and release steps in each cycle are necessary for the purposes of simulating the kinetic model. As will be described in detail in the following section, we emphasize that both the pre-steady state and steady state data are critical in constraining the possible kinetic steps and their values. Initial estimates of the rate constants for the model were determined as much as possible from the experimental results shown above. Importantly, both pre-steady state and steady state phases were fit by a single kinetic model and set of rate constants.

(*i*) The described model is a minimal model with the least number of steps required to achieve a confident fit. The basic steps of ATP binding, hydrolysis, and Pi and ADP release were taken from a scheme used to describe the reaction at a single catalytic site, also known as the unisite condition (Duncan and Senior, 1985; Grubmeyer *et al.*, 1982), although we emphasize that the multisite, steady state kinetics are different from the unisite reaction. All of the rate constants used to fit the data in Fig. 2.4.3 are faster than those determined in unisite conditions (Al-Shawi and Nakamoto, 1997; Grubmeyer *et al.*, 1982; Senior and Al-Shawi, 1992). In addition, a model with only the

TABLE 2.4.1A

Rate constants derived from kinetic fits. Rate constants from k_{+1} to k_{γ} are listed. Rate constants from k_{+3} to k_{-4}, and goodness-of-fit parameters are listed below in Table 2.4.1B

[Mg·ATP] μM	k_{+1} $M^{-1}s^{-1}$ $X10^{7}$	k_{-1} s^{-1} $x10^{3}$	K_1 M^{-1} $x10^{3}$	K_d^{ATP} μM	k_{+2} s^{-1}	k_{-2} s^{-1}	K_2	k_{γ} s^{-1}
4.8	4.0	2.0	2.0	50	94	95	1.0	24
17.8	3.0	1.6	1.9	53	100	98	1.0	29
29.2	4.5	1.8	2.5	40	140	140	1.0	30
62.0	4.2	2.1	2.0	50	140	140	1.0	30
105.6	4.2	2.1	2.0	50	170	110	1.5	29
259.9	4.0	2.1	1.9	53	170	110	1.5	30
Average	4.0±0.2	1.9±0.1	2.0±0.1	49±2	140±13	120±8	1.2±0.1	29±0.9

TABLE 2.4.1B

Rate constants derived from kinetic fits [a]

Listed are rate constants from k_{+3} to k_{-4}, and goodness-of-fit parameters.

[Mg·ATP]	k_{+3}	k_{-3}	K_3	K_d^{Pi}	k_{+4}	k_{-4}	K_4	K_d^{ADP}	R^2	*MSC* [b]
μM	s^{-1}	$M^{-1}s^{-1}$	M^{-1}	M	s^{-1}	$M^{-1}s^{-1}$	M^{-1}	μM		
			$x10^{-2}$			$x10^{6}$	$x10^{4}$			
4.8	200	8.9	4.4	22	250	3.0	1.2	83	0.997	4.92
17.8	210	12	5.8	17	380	4.0	1.0	95	0.997	5.08
29.2	210	12	5.8	17	380	4.5	1.2	85	0.997	5.08
62.0	210	14	6.7	15	380	4.5	1.2	85	0.998	5.56
105.6	210	14	6.7	15	380	4.5	1.2	85	0.998	5.56
259.9	200	13	6.6	15	380	4.5	1.2	85	0.994	4.40
Average	210±2	12±.0.8	6.0±0.4	17±1.1	360±22	4.2±0.2	1.2±0.0	86±2		

[a] Rate constants refer to Reaction Scheme 2.

[b] See *Experimental Procedures* for definition of MSC, the model selection criterion.

four unisite steps was not adequate to simulate the data. An additional slow step (Reaction Scheme 2, Step 3) was required to achieve a good fit to the data, the position of which in the order of the reaction was critical and will be discussed later. This minimal model uniquely simulates both the pre-steady state and steady state phases of hydrolysis.

(*ii*) The binding of Mg·ATP was very rapid as determined in Fig. 2.4.6A. The k_{+1} in the model fits is an apparent binding constant and is not quite as fast as the diffusion limited rate determined from Fig. 2.4.6A. We hypothesize, and it is shown in our model (discussed below), that this is due to Mg·ATP binding at one site and hydrolysis occurring at another site requiring transmission of information between the two sites. This cooperativity occurs in a finite time and therefore slows the apparent binding rate of Mg·ATP in the model. The ratio of k_{-1}/k_{+1} was approximated both from the K_M values and the K_d value for Mg·ATP calculated from Fig. 2.4.3, 2.4.5A, and 2.4.6A. The close similarity of the K_M value for Mg·ATP hydrolysis and the K_{d3} value indicates that catalysis is triggered by Mg·ATP binding to the third site.

(*iii*) The forward and reverse constants for the step of ATP hydrolysis (k_{+2} and k_{-2}) were not constrained in the model fitting. The best fits were achieved when the forward and reverse constants were approximately equal. Even when initial seed values were chosen where the two parameters differed, after performing the simplex and least-squares minimization with high stringency, the k_{+2}/k_{-2} ratio tended towards unity. This is in agreement with the model of Boyer and others ((Boyer *et al.*, 1973); see Ref. (Nakamoto *et al.*, 1999) for a review), indicating that ATP is undergoing reversible hydrolysis/synthesis with ADP and Pi at the site of chemistry. The sensitivity analysis

(Table 2.4.2, and described below) validates this notion in that the ratio of the forward and reverse reactions is a highly sensitive parameter, and small changes in the ratio greatly decreased the quality of the fit.

(*iv*) As described above, the rate limiting step (Step 3) was required to account for the observed initial burst of hydrolysis. The seed value for this step was approximated by the V_{max} (25.6 s^{-1}) for Mg·ATP under the same conditions (Fig. 2.4.5A). This step was not constrained in the model fitting – although it tended not to vary greatly. The order of this step in the reaction scheme was also directly tested (see *viii* below for description). This step could only follow hydrolysis (Step 2) and precede Pi release (Step 4). Previously it has been argued that a partial rotation of the γ subunit in ATP hydrolysis is associated with the decrease in affinity for Pi, allowing Pi release, a major energy yielding step in hydrolysis ((Al-Shawi *et al.*, 1997b); reviewed in Ref. (Nakamoto *et al.*, 1999)). The requirement for a slow step in the model, prior to Pi release further supports this hypothesis. This rate limiting step is therefore termed k_γ.

(*v*) One Pi is released per cycle of the enzyme in the steady state mode of the model. Pi release, k_{+3}, is not the rate limiting step so a relatively fast seed value (compared to k_γ) was used. If it were too slow, there would be significant product inhibition as the steady state progresses, and this is not seen in the data. Also the Pi release is constrained by the steady state hydrolysis rate. It has been shown that Pi does not bind productively to the enzyme in the absence of the transport sector F_O and a proton motive force (Al-Shawi *et al.*, 1990b; Al-Shawi and Senior, 1988; Al-Shawi and Senior, 1992; Grubmeyer *et al.*, 1982; Weber *et al.*, 1993), therefore an arbitrary slow value of 10

$M^{-1}s^{-1}$ was used for the k_{-3} seed value and does not affect progress of the reaction, and in fact very much smaller values for k_{-3} did not negatively affect fitting of the model to the data (described further in the *Sensitivity Analysis* below).

(*vi*) The rate of ADP binding, k_{-4}, was shown to be rapid from the βY331W titration in Fig. 2.4.6B, yet was slower than Mg·ATP binding, so the seed value for k_{-4} was slower than k_{+1}. The ratio of k_{+4}/k_{-4} was approximated from experimentally determined affinities. The K_I^{ADP} was determined under the same conditions (Fig. 2.4.5B) and the K_d for ADP was calculated from the βY331W titration (Fig. 2.4.6B, and also (Löbau *et al.*, 1997; Weber and Senior, 2001)). Using these data along with the determined k_{-4}, a seed value was calculated for the dissociation rate constant k_{+4}. These values were consistent with the requirement for a relatively fast rate of ADP release (k_{+4}). Similar to Pi, if the release of either product were too slow or rate limiting the steady state would slow due to product inhibition. Clearly, ADP release is not rate limiting in the steady state conditions shown in Fig. 2.4.3.

(*vii*) It is important to note that the pre-steady state and the steady state phases of hydrolysis are fit using the same rate constants. In addition, excellent fits to the data for a wide range of substrate concentrations were achieved with remarkably little variation in the rate constants (Table 2.4.1). These two facts emphasize the simplicity of the model and generate a high level of confidence in its validity.

(viii) Various alternate models were tested, and the results of the best attainable fits are shown in Fig. 2.4.8. One stipulation placed on these tests was that the experimentally determined parameters were not allowed to vary to unrealistic values.

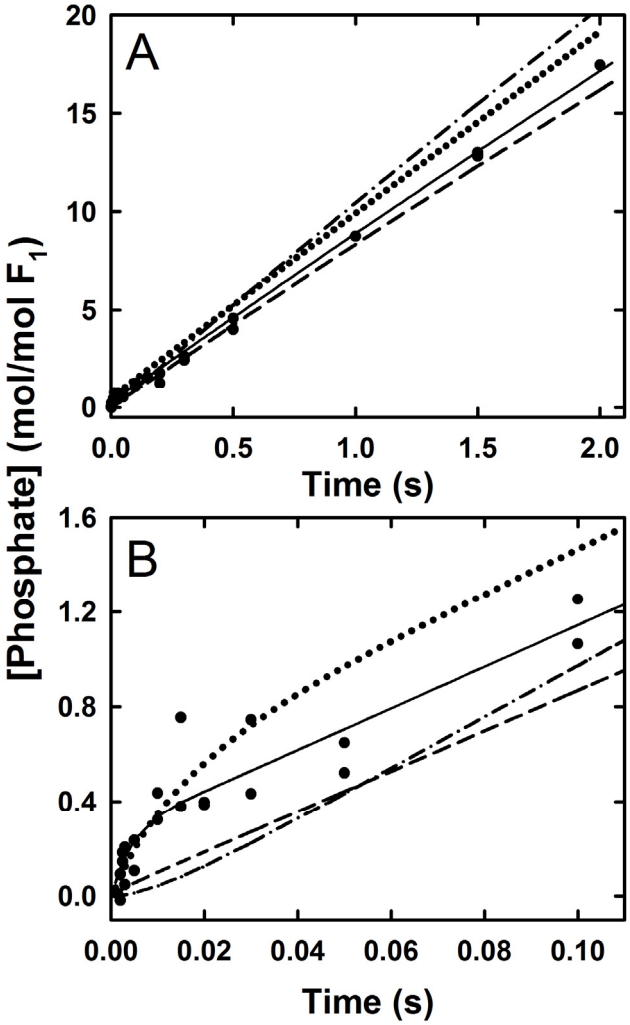

Figure 2.4.8. Comparison of alternate kinetic models.

The data points (●, same as those shown in Fig. 1) of the pre-steady state hydrolysis of F_1 at 62 μM Mg·ATP final concentration are used to attempt fits using alternate kinetic models. A. The complete time course up to 2.0 s, and B. the early time points up to 0.1s. The *solid line* is the best fit for our model using the parameters listed in Table 2.4.1 for the 62 μM Mg·ATP data set (MSC (see *Experimental Procedures* for definition): 5.56, R^2: 0.998). The other lines represent the best fits to alternate models as described in detail in the *Results*. The *dashed line* (----) is the best fit for a model lacking the rate limiting step, k_γ, which is essentially the uni-site model described elsewhere (Duncan and Senior, 1985; Grubmeyer et al., 1982) (MSC: 4.40, R^2: 0.994). The *dot and dashed line* (-·-·-) is the best fit for a model where k_γ occurs before Step 2, the hydrolysis/synthesis of ATP (MSC: 2.54, R^2: 0.964). The *dotted line* (····) is the best fit for a model where Pi release, k_{+3}, occurs before k_γ (MSC: 3.03, R^2: 0.978).

The 62 μM Mg·ATP data set was used to fit the alternate models, although other data sets at different Mg·ATP concentrations were also used to validate the results and ensure the results were not particular to one condition (results not shown). For comparison, the best fit for these data using our model (Reaction Scheme 2) is indicated by the solid line in Fig. 2.4.8.

The first model tested was essentially the unisite model of catalysis (Al-Shawi and Senior, 1992; Grubmeyer *et al.*, 1982), without the rate limiting step, k_{γ}. As can be seen from Fig. 2.4.8B (*dashed line*, ----), the model cannot simulate the burst of ATP hydrolysis in the pre-steady state. This emphasizes the need for a rate limiting step after hydrolysis in the reaction scheme in order to fit the burst. On the other hand, if k_{γ} and k_{+3}, the release of Pi, are combined in a single rate limiting step, the burst can be fit but the steady state is not (result not shown).

The order of k_{γ} within the reaction scheme was also verified using the following two test models: (1) placement of k_{γ} before Step 2, the hydrolysis/synthesis of ATP (*dot and dashed line*, -·-·), or (2) placement of k_{γ} after Pi release (*dotted line*, ····). The first model with k_{γ} before Step 2 also cannot account for the burst of hydrolysis and there is actually a slight lag evident in the early time course of Pi generated (Fig. 2.4.8B). The second model with k_{γ} after Pi release can simulate a burst but the burst is too slow and overshoots the data (Fig. 2.4.8B). Furthermore, this model fails to fit the steady state rate (Fig. 2.4.8A).

We also tested a model where the hydrolysis of ATP is irreversible (no k_{-2}), and the Pi release, k_{+3}, is fast. This possible reaction scheme would imply that the rate

limiting k_γ step occurs with hydrolysis of ATP. In this case, the steady state rate could be approximated, but the burst could not be fit (result not shown). This result was similar to the model where k_γ occurs before the step of chemistry. Our data are thus inconsistent with the model of Weber *et al*. (Weber *et al.*, 2000), a key element of which is the simultaneous release of phosphate with a k_{+2}-driven rotational conformational change.

The fits to a model where the rate limiting step, k_γ, is several fold faster than $k_{-\gamma}$ were of good quality, however the model where k_γ is essentially irreversible achieved the best fit (Fig. 2.4.8A and B, *solid line*; R^2=0.998; MSC=5.56). In comparison, the quality of the fit where k_γ and $k_{-\gamma}$ were constrained to equal values was much worse (MSC=3.03; data not shown), and when $k_{-\gamma}$ was large compared with k_γ (*e.g.* 4-fold greater) the model fit to the data was very poor (MSC=1.56), and resulted in pre-steady state and steady state rates which were far too slow. Although k_γ may not be irreversible, these analyses show that the reverse rate is much smaller than the forward reaction. This conclusion is consistent with the observations of single molecule behavior where the rotor very rarely takes a backwards step (Noji *et al.*, 1999; Yasuda *et al.*, 1998).

In summary, a minimal number of partial reactions provide an excellent fit to the pre-steady state and steady state data. We emphasize that the order of the partial reaction steps shown in Reaction Scheme 2 is a unique solution to all of the data and is consistent with observations in the literature.

2.4.7 Sensitivity Analysis

The sensitivity of each of the rate constants was determined (as described in *Experimental Procedures*) as a means to analyze which constants are important for fitting the model to the data and determining the rate of the reaction. Each of the constants was perturbed, one at a time (except where noted), and the new set of parameters was refined using the simplex technique to locate a region of minima. Following the parameter refinement, the non-linear least squares minimization algorithm was performed to finalize the model fit. The fit was analyzed statistically to determine the MSC value, which is the most sensitive way to evaluate the goodness-of-fit of the model using the new parameter set. Although an infrequent occurrence, model fits to the data that changed experimentally verified parameters to unrealistic values were considered bad fits.

Table 2.4.2 shows the results of the analysis. A 10-fold increase or decrease of each parameter individually, up to and including the rate limiting step (k_γ), was a perturbation not tolerated by the model. A change of 10-fold of those rate constants occurring after the rate limiting step in the reaction was not as detrimental to achieving a fit, although the quality of the fits were decreased substantially. The exception was k_{-3}, Pi binding, which was almost unaffected. This is consistent with previous studies that show Pi does not bind in a productive manner in the absence of a proton motive force and the F_O sector, *i.e.* that Pi release is essentially an irreversible reaction in the hydrolysis mode. A 10-fold increase or decrease of k_{+2} and k_{-2} together, thus retaining the ratio between ATP hydrolysis and synthesis, failed to fit. While the change in the k_{+2} and k_{-2} rates was

TABLE 2.4.2

Sensitivity analysis of kinetic constants: model selection criterion (MSC) values for fits using alternative kinetic constants.

Best fit MSC: 5.56	k_{+1}	k_{-1}	k_{+2}	k_{-2}	k_{+2}; k_{-2}[a]	k_{γ}	k_{+3}	k_{-3}	k_{+4}	k_{-4}
10 fold ↑	N.F.	N.F.	N.F.	N.F.	2.96[b]	N.F.	4.45	5.30	4.56	3.87
10 fold ↓	N.F.	N.F.	N.F.	N.F.	1.30	N.F.	3.12	5.30	2.38	5.09
2 fold ↑	2.35	2.31	N.F.	1.46	3.93	N.F.	4.85	5.30	5.39	5.39
2 fold ↓	2.29	2.37	1.13	1.18	3.76	1.08	5.44	5.44	5.38	5.20

The 62 μM [Mg·ATP] data set was used for the sensitivity analysis of the rate constants. Details of the procedure are described further in the *Experimental Procedures.*

[a] Both parameters are increased/decreased simultaneously, thus retaining the ratio of the parameter, K_2.

[b] The MSC (MicroMath_Research, 1995), which is defined in the *Experimental Procedures*, is a highly sensitive parameter for distinguishing between models and selects the best model that fits with simplicity and parsimony. The MSC is a relative value and should be compared to the best fit MSC of 5.56 for this data set (the higher the MSC value, the more appropriate the model).

NF: No fit, due to undefined parameters, negative MSC values or rate constants that were unrealistic.

more sensitive than any of the constants occurring after k_γ, it was not as sensitive as forcing the ATP hydrolysis/synthesis ratio, K_2, away from unity.

In order to establish a more rigorous criterion for sensitivity, the analysis was performed once more, but with a 2-fold increase or decrease of the parameter values. Similar to the 10-fold perturbations the parameters leading up to and including k_γ were very sensitive to perturbation. The parameters after the rate limiting step were almost insensitive to the 2-fold perturbation, with the exception of k_{+3}, Pi release. This shows that the rate of Pi release does affect the rate of the reaction.

The fact that the rate constants up to k_γ were more sensitive than those after this step gives credence to the fact that k_γ is the rate limiting step, and emphasizes that its order in the reaction is critical. Significantly it has the smallest window within which its value can accurately describe the data. Overall, even the relatively non-sensitive parameters do not tolerate a 10-fold change, which in enzymatic terms is relatively small. The more sensitive parameters (those occurring before and including k_γ) do not tolerate even a 2-fold change in the rates, thus giving us a high level of confidence in our model.

2.5 Discussion

The pre-steady state kinetics of ATP binding and hydrolysis of the F_1-ATPase in the rotational catalytic mode have been determined for the first time. A high concentration of Mg·ATP was used to start the reaction in order to fill all three catalytic sites, which was required to achieve full promotion of ATP hydrolytic activity and to

efficiently couple γ subunit rotation to hydrolysis for the reasons already outlined in the *Introduction*. Experimental results from several laboratories were taken together to conclude that Mg·ATP was required at high enough concentration ($>10^{-5}$ M) to occupy the low affinity site in order for the enzyme to enter a cooperative rotational catalytic mode. The data clearly showed that upon rapid mixing of the enzyme with high concentrations of Mg·ATP, it *immediately* entered into a rotational catalysis mode.

In multisite catalysis all of the rate constants are much faster than those determined for unisite conditions and an additional rate limiting step must be added, which comes prior to Pi and ADP release (see *Results* and Ref. (Al-Shawi *et al.*, 1997b; Al-Shawi *et al.*, 1989; Duncan and Senior, 1985; Grubmeyer *et al.*, 1982)). The faster rate constants necessitated the use of millisecond mixing, which was apparent from the time course of hydrolysis shown in Fig. 2.4.3B and 2.4.3C. Resolution of the burst of ATP hydrolysis provided constraints which were critical in defining the kinetic model and rate constants of the partial reactions. Importantly, the same kinetic model and rate constants could be used to fit and simulate both pre-steady state and steady state phases accurately. *Thus, we found that it was valid to use the pre-steady state rate constants to describe partial reaction rates in the steady state.* A variety of models were tested systematically and a unique solution was found that was able to fit all the data from a wide range of substrate concentrations. Furthermore, the kinetic model presented in this paper is consistent with important properties of the enzyme characterized in previous publications (reviewed in (Nakamoto *et al.*, 1999)).

Several lines of evidence indicate that Mg·ADP inhibition is not observed in the pre-steady state hydrolysis data presented here. First, the active site titration of the pre-steady state burst shows that the enzyme is essentially 100% active with one site per F_1 molecule carrying out reversible hydrolysis/synthesis of ATP immediately after rapid mixing with substrate. Second, the kinetics of the longer steady state hand-mixing measurements were the same as the steady state kinetics of the rapid mixing experiments. The data could not be fit if the rate constant for ADP release was slower, as shown by the sensitivity analysis. Finally, a single set of rate constants would not be adequate to describe both the pre-steady state and steady state data if there was a conversion between Mg·ADP inhibited and uninhibited forms of the enzyme.

The experimentally demonstrated reaction sequence and kinetic rate constants were incorporated into a rotational catalytic model shown in graphical form in Fig. 2.4.9. Although the same rate constants were used to describe both the pre-steady state and the steady state, the first cycle is presented separately from the subsequent steady state cycles because two ATP and one ADP are bound rather than the one ATP and two ADP + Pi bound in the steady state mode (see below). Rapid addition of Mg·ATP to the enzyme shows that substrate associates with all three sites in a diffusion limited manner (Fig. 2.4.6). Binding of the higher Mg·ATP concentrations to the catalytic sites of the βY331W enzyme in the fluorescence stopped-flow traces shows that the initial binding is completed within the 1 ms dead time of the instrument. This is faster than the calculated rate constant for binding, k_{+1}, determined from the model fits (see Table 2.4.1).

Figure 2.4.9. Graphical representation of the rotational catalytic pathway from pre-steady state into steady state hydrolysis.

The three site rotational reaction scheme is depicted for the F_1 enzyme in the hydrolysis mode of catalysis. The model is discussed in detail in the text. The relative arrangement of the β subunit conformations are as viewed from the "top" of the complex towards the membrane. The three site conformations, β_{DP} (green), β_{TP} (yellow) and β_E (red) are as presented by Abrahams *et al*. (8) and β_{HC} (purple) refers to the "half closed" intermediate conformation structural described by Menz *et al*. (65) and incorporated into a mechanistic model of F_1 rotational catalysis by others (e.g. Senior *et al*.; Ref. (*4*)). In the starting conformation (upper left) the exact conformation of the initial state of the enzyme is rather ambiguous, therefore dashed lines are used to indicate the likely conformations. The non-catalytic α subunits are omitted for clarity. The central asymmetric shape represents the position of the γ subunit during the course of catalysis. The intermediate rotation of 80° and the completion of rotation to the next 120° position correspond to the observed dwell positions (Shimabukuro et al., 2003; Yasuda et al., 2001). The brackets on the left indicate the mode of kinetics corresponding to the data presented in this paper. The steps of the first cycle responsible for the pre-steady state kinetics are represented by the top two rows. The burst of hydrolysis occurs through the relatively rapid binding step (k_{+1}) to the step of chemistry (k_{+2}). The binding of two ATP to β_{TP} and β_E only occurs in the first turnover and the asterisk for the first k_{+3} indicates that there is no Pi to release in the pre-steady state. In the steady state (surrounding the circular blue arrows in the third and fourth rows), only one ATP binds per cycle to the β_E site. We also note that the β_{TP} site does not hydrolyze bound ATP unless ATP is also bound to the β_E site thus converting it to the β_{HC} conformation (between k_1 and k_2). The position of the γ subunit is offset 120° for each cycle in the steady state mode of the enzyme. The rate limiting transition state for pre- and steady state catalysis as described in Al-Shawi *et al.* (58) and Nakamoto *et al.* (2) occurs during the k_γ rotation step.

Fig. 2.4.9

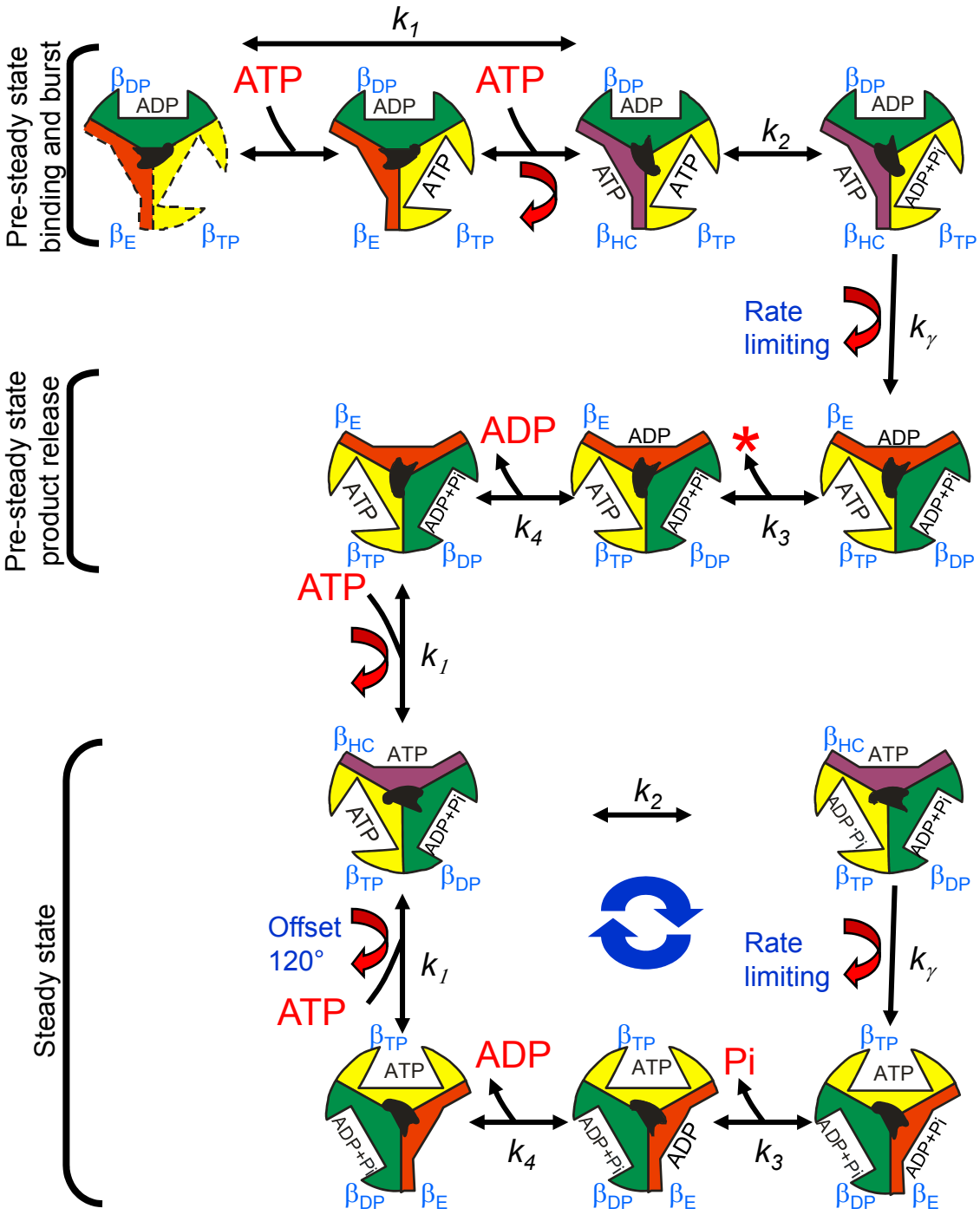
Pre-steady state binding and burst
Pre-steady state product release
Steady state
k_1
ATP
ADP
k_2
Rate limiting
k_γ
k_4
k_3
Offset 120°
Pi
β_{DP}
β_{TP}
β_{HC}
β_E
ADP+Pi
ADP·Pi

The slightly slower than expected k_{+1} probably reflects the partial rotation that takes place to put β_{TP} in a state that undergoes reversible hydrolysis/synthesis. Previous kinetic analysis of sub-millisecond rotational behavior of single molecules resolved a brief pause in γ subunit rotation that defined two partial rotation steps (Shimabukuro *et al.*, 2003; Yasuda *et al.*, 2001). The first substep, corresponding to the 80° rotation (Shimabukuro *et al.*, 2003), occurred in an ATP dependent manner and was assigned to ATP binding. In the pre-steady state cycle (shown in the top two rows of Fig. 2.4.9), we hypothesize a sequential cooperative binding of ATP. In our model, ATP binding to the third site, β_E. drives the partial 80° γ subunit rotation and forces the change of the β_E conformer (red) into the half-closed (β_{HC}, purple) conformer, which was structurally observed by Menz *et al*. (Menz *et al.*, 2001), and incorporated into a catalytic model by Senior *et al*. (4). In the hydrolysis direction this partial rotation is not a rate limiting step, but it activates the β_{TP} site by putting it in a conformation that can carry out reversible hydrolysis/synthesis, k_{+2}/k_{-2}. The similar value for the K_d of Mg·ATP binding to the low affinity site and the K_M for the extent of the burst of Mg·ATP hydrolysis (Fig. 2.4.3 and 2.4.2) support this notion, as does the fact that ATP hydrolysis is clearly not rate limiting to the reaction (Fig. 2.4.3B, 2.4.3C and Table 2.4.1). In addition, the ratio of ATP hydrolysis/synthesis rates (K_2) at the active site was found to be close to unity in the rotational catalytic mode, similar to the unisite mode of the enzyme, and consistent with the binding change mechanism of Boyer (Boyer, 1975; Boyer, 1993). In the synthesis direction, we hypothesize that the partial rotation is the energy requiring step that changes

the conformational state from β_{TP} to β_E thus decreasing the affinity for ATP and allowing its release from the enzyme (Al-Shawi *et al.*, 1997b).

We needed to add a kinetic step, k_γ, to account for the burst of ATP hydrolysis. Moreover, to simulate both the pre-steady state and steady state phases of the data, k_γ must follow hydrolysis and precede the release of Pi, k_{+3}. Models in which k_γ and k_{+3} were combined into the same step, or k_{+3} preceded k_γ, or k_{+3} was much faster, failed to give satisfactory fits to either the pre-steady state or steady state phases. Consistent with this conclusion, Masaike *et al.* (Masaike *et al.*, 2002) detected an ATP-dependent fluorescence intensity change of a tryptophan near the catalytic site which indicated a conformational shift. The fluorescence changed with a rate slower than nucleotide binding, but occurred with the same kinetics as Pi release. Previously we presented an extensive Arrhenius analysis of steady state data of the γMet23 to Lys mutant enzyme which perturbed the interactions between the stator β and rotor γ subunits (Al-Shawi *et al.*, 1997b). Our results suggested that the rate limiting transition state occurred during γ subunit rotation between hydrolysis and release of Pi and we now present pre-steady state kinetic data that show the conformational change must occur after hydrolysis. Taken together, it is clear that the rate limiting transition state occurs during the 40° partial rotation observed by Shimbakuro *et al.* (Shimabukuro *et al.*, 2003), which we now call k_γ. It is likely that k_γ involves several partial reactions, but the chemical approach used in this paper cannot distinguish these steps and modeling the step as a single rate constant is sufficient for the purposes of fitting the kinetic data.

Furthermore, the data presented show that k_γ and Pi release are essentially irreversible because it is likely that they are the major energy producing steps of the hydrolysis pathway. This is in agreement with experimental evidence in the synthesis direction where an input of energy from the proton motive force is required for Pi binding (Al-Shawi *et al.*, 1997b). This is also in agreement with the rotational behavior of F_1 which is observed not to reverse the direction of rotation in the presence of high Mg·ATP concentrations (Noji *et al.*, 1997; Yasuda *et al.*, 1998). The model indicates that γ subunit rotation, in the direction of hydrolysis, drives the conformational change, which leads to a decrease in affinity for Pi and converts the β_{DP} conformation to β_E, allowing release of products. Depicted in the first cycle of the model (Fig. 2.4.9, asterisk at the first k_{+3}) there is no Pi released due to γ rotation because there is no Pi in the β_{DP} site from a previous cycle of hydrolysis. Mg·ATP binds to the newly vacated β_E to trigger the next round of hydrolysis. We also note that product release, either Pi or ADP, cannot be rate limiting, otherwise a product bound form of the enzyme would accumulate during the steady state, slowing the steady state rate.

One catalytically competent site is expected based on the many unisite studies which have unequivocally established that a catalytically active, high affinity site is available for ATP binding and hydrolysis. In the pre-steady state and steady state, our data (Fig. 2.4.3) show that only one site is hydrolyzing ATP per cycle. However, earlier reports have hinted that a second site is catalytically competent. A second site was implied by the x-ray crystallographic structure of the bovine F_1 obtained in the presence of ADP and AlF_4^- by Menz *et al*. (Menz *et al.*, 2001). In this structure, the two catalytic

sites in the β_{TP} and β_{DP} subunits had very similar conformations and both had ADP·AlF_4^- bound. Similarly, Nadanaciva *et al*. (Nadanaciva *et al.*, 2000) found that two of the *E. coli* F_1 catalytic sites could attain transition state conformations using Mg·ADP plus fluoroscandium. In addition, Weber *et al*. (Weber *et al.*, 1996), using the βF148W mutant whose fluorescence differentiates between bound ADP and ATP, found one mol of ATP and two mol of ADP were bound in conditions of maximal ATPase rates. The only model consistent with all of these results is that one site is in the process of hydrolyzing ATP and the other is holding ADP + Pi that was produced in the previous cycle. In this case, β_{TP} must be the site of catalysis. This conclusion is in contrast to other models including Menz *et al*. (Menz *et al.*, 2001) and Senior *et al*. (Senior *et al.*, 2002) that suggest that β_{DP} is the site of chemistry. Such models do not account for the cooperativity of the three sites, or the average occupancy of the sites, almost three, in steady state conditions (Weber *et al.*, 1993). The sequence order of β subunit conformations through a rotation cycle in the direction of hydrolysis is β_E-β_{HC}-β_{TP}-β_{DP}, therefore, the site of catalysis cannot be β_{DP} otherwise there would be two sites containing ATP and one site with ADP. It was previously hypothesized that site β_{DP} also has bound Pi based on the apparent positive cooperativity of phosphate in the activation of ATP synthesis (Al-Shawi *et al.*, 1997b). ATP synthesis has a sigmoidal dependence upon Pi concentration with a Hill coefficient close to 2 suggesting that there are two molecules of Pi bound during steady state ATP synthesis. We earlier hypothesized that the conserved and essential amino acid αArg376 (Le *et al.*, 2000) plays the critical role of retaining product Pi in the catalytic site until it is released as the β_{DP} is converting to the

β_E site. These results suggest that Pi is released from β_{DP}, therefore it follows that Pi is not released until the cycle after which it was produced. In this manner, we suggest that the enzyme is able to utilize the binding energy of Pi to maintain efficient coupling between catalysis and rotation.

The order of the partial reactions presented above provides us with a framework to understand how the F_1-ATPase maintains coupling between catalysis and rotation. The enzyme requires that the rate limiting step, k_γ, occurs after the reversible hydrolysis/synthesis reaction and prior to Pi release. Clearly, if Pi is released without coupling to rotation, coupling efficiency decreases. This is the case with the replacement of the conserved γ subunit Met23 with Lys. The mutant enzyme allows a pathway where Pi can be released without rotation (Al-Shawi *et al.*, 1997b). This same mutant enzyme also had a higher K_M for Pi in ATP synthesis, which implied that the perturbation of the interaction between γ and β subunits blocked the ability of the catalytic site to achieve the proper conformation for binding Pi. Furthermore, Arrhenius analysis of the mutant enzyme showed that the amino acid replacement directly affected the rate limiting transition state of steady state ATP hydrolysis (Al-Shawi *et al.*, 1997a). Taken together, our analyses show that the F_1 enzyme maintains efficient coupling by requiring that Pi can only be released after the rate limiting 40° rotation step, k_γ.

3. Role of γ subunit rotation in the kinetic pathway: kinetics of γ–β cross-linked, rotation-inhibited F_1-ATPase.

A rotor-stator cross-link in the F_1 ATPase blocks the rate limiting step of rotational catalysis.
Joanne A. Baylis Scanlon, Marwan K. Al-Shawi, Robert K. Nakamoto, 2008 *J.B.C.* July 15. Manuscript M804858200.

3.1 Abstract

The F_OF_1 ATP synthase couples the functions of H^+ transport and ATP synthesis/hydrolysis through the efficient transmission of energy mediated by rotation of the centrally located γ, ε and *c* subunits. In order to understand the γ subunit role in the catalytic mechanism we previously determined the partial rate constants and devised a minimal kinetic model for the rotational hydrolytic mode of the F_1-ATPase enzyme that uniquely fits the pre-steady state and steady state data (Baylis Scanlon, J. A., Al-Shawi, M. K., Le, N. P., Nakamoto, R. K. (2007) *Biochemistry* 46, 8785-8797). Here we directly test the model using two single cysteine mutants, βD380C and βE381C, which can be used to reversibly inhibit rotation upon formation of a cross-link with the conserved γCys87. In the pre-steady state, the γ-β cross-linked enzyme at high Mg·ATP conditions retained the burst of hydrolysis but was not able to release Pi. These data

show that the rate-limiting rotation step, k_γ, occurs after hydrolysis and before Pi release. This analysis provides additional insights into how the enzyme achieves efficient coupling and implicates the βGlu381 residue for proper formation of the rate-limiting transition state involving γ subunit rotation.

3.2 Introduction

The F_OF_1-ATP synthase, located in energy-transducing membranes, utilizes the electrochemical gradient of H^+ or Na^+ to synthesize ATP from ADP and Pi. Under anaerobic conditions the bacterial enzyme can function as an ATPase, coupled to pump protons across the membrane to generate a $\Delta\mu_{H+}$. Proton transport is mediated by the membrane-embedded F_O sector (ab_2c_{10}), and is separated by a distance greater than 120 Å from the three catalytic sites where ATP hydrolysis/synthesis occurs on the membrane extrinsic F_1 segment ($\alpha_3\beta_3\gamma\delta\varepsilon$) (for reviews see (Boyer, 1997; Boyer, 2002; Junge *et al.*, 2001; Nakamoto *et al.*, 2000; Weber, 2003)). This distance indicates a complicated mechanism for effectual, efficient transmission between the two disparate functions. It is now well established that the enzyme functions as a molecular motor (Nishio *et al.*, 2002; Noji *et al.*, 1997; Tanabe *et al.*, 2001), transmitting energy between F_1 and F_O through rotation of the central stalk subunits, γ, ε and the ring of *c* subunits (for reviews see (Nakamoto *et al.*, 2008; Yoshida *et al.*, 2001))

The F_1 complex can be reversibly stripped from the membrane and functions as a soluble ATPase. In describing the first high resolution x-ray structure, Abrahams *et al.*

(Abrahams *et al.*, 1996) named each catalytic β subunit for the nucleotide bound at that site: β_{TP} for the ATP analog adenosine 5′-(β,γ-imido)triphosphate (AMPPNP[1]), β_{DP} for ADP-bound, and the structurally open β_E empty site (Fig. 3.2.1). The three sites have vastly differing affinities for Mg·ATP (Weber *et al.*, 1993), $K_{d1}=10^{-10}$, $K_{d2}=10^{-6}$, $K_{d3}=10^{-4}$ M^{-1}, exhibiting negative cooperativity in nucleotide binding. At low sub-stochiometric Mg·ATP concentrations, characteristics of the basic catalytic reaction have been elucidated in unisite catalytic conditions (Al-Shawi and Senior, 1992; Grubmeyer *et al.*, 1982). At higher substrate concentrations, the enzyme enters the multisite hydrolysis mode which is 10^5-10^6 times faster than unisite catalysis due to the high positive cooperativity among the sites with respect to promotion of catalysis (Cross *et al.*, 1982; Grubmeyer and Penefsky, 1981; Wise *et al.*, 1984). The K_d for the binding of Mg·ATP to the low affinity catalytic site (Weber *et al.*, 1993) matches the K_M for Mg·ATP hydrolysis (Baylis Scanlon *et al.*, 2007; Weber *et al.*, 1996) and K_M for rotation in the direct observation of single F_1 molecules (Yasuda *et al.*, 2001). Rotational catalysis requires the concerted, sequential participation of all three catalytic sites as they pass through the three different conformations (Ariga *et al.*, 2007; Baylis Scanlon *et al.*, 2007; Ren *et al.*, 2006). For these reasons, we have argued (Al-Shawi *et al.*, 1997b) that reversible hydrolysis/synthesis of ATP occurs in the β_{TP} site, and product Pi and ADP are released after the site converts from β_{DP} to β_E (Baylis Scanlon *et al.*, 2007). Further evidence using fluorescence resonance energy transfer confirmed that the β_{TP} site is the high affinity site (Mao and Weber, 2007).

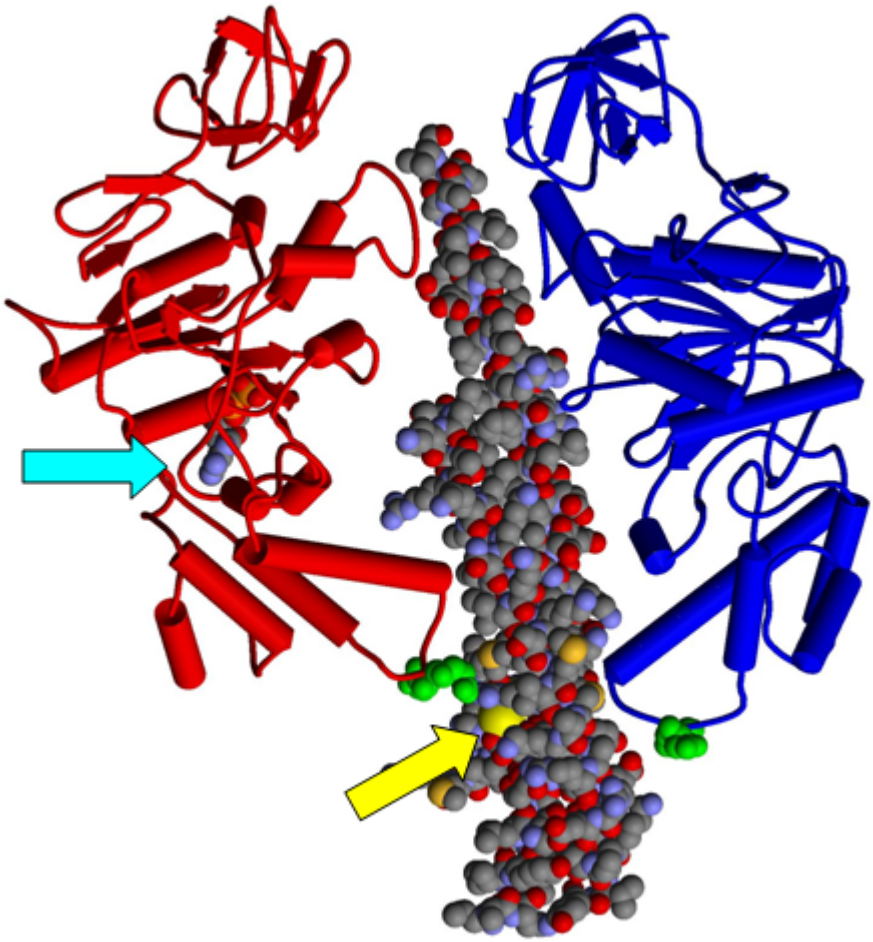

Figure 3.2.1. The βD^{380}ELSEED^{386} motifs relative to the catalytic sites.
Two of the β subunit conformers, β_{DP} (red) and β_E (blue) and the coiled-coil region of the γ subunit (space filling representation) from the x-ray structure of Abrahams *et al.* (Abrahams *et al.*, 1994). ADP bound to β_{DP} is shown in the space filling model (cyan arrow). βAsp380 and βGlu381 (*E. coli* numbering) are shown in green space filling representation near the "bottom" of the β subunits in the βDELSEED loop. γCys87 is indicated by the yellow arrow.

Single molecule experiments have observed that each major 120° step in γ subunit rotation occurs in two substeps: the 80° substep that is dependent on Mg·ATP concentration, followed by a 40° substep that is not affected by Mg·ATP concentration (Shimabukuro *et al.*, 2003). Attempts to elucidate the role of rotation in the enzymatic mechanism using the single molecule approach include analysis of γ subunit substeps (Shimabukuro *et al.*, 2003; Yasuda *et al.*, 2001), and concurrent visualization of the binding and release of fluorescent nucleotide (Nishizaka *et al.*, 2004). However, the structural and mechanistic coordination of γ subunit rotation and the kinetics of the elemental chemical hydrolysis reaction steps cannot be delineated by these studies and the chemomechanical coupling of the enzyme remains not fully understood.

Using pre-steady state analysis we recently determined the partial reactions of the multisite ATPase hydrolytic pathway, and that the rate limiting step occurs after the reversible hydrolysis/synthesis step and just prior to release of Pi (Baylis Scanlon *et al.*, 2007). The following reaction scheme was adequate to describe the multisite kinetic pathway (Baylis Scanlon *et al.*, 2007):

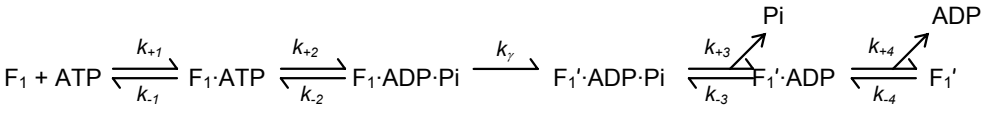

[Reaction Scheme 3]

We conjectured that the rate limiting step involves the 40° rotation and therefore called it k_γ. The pre-steady state kinetics of this step were critical in allowing us to determine its order in the reaction scheme which provided tremendous insight into the rotational

catalytic mechanism. Even though we could directly determine several of the partial reaction rate constants, assignment of k_γ to the rotation step in the pre-steady was not confirmed.

In this work we test our model that the rate limiting step k_γ involves rotation of the γ subunit. In order to assay the rotation steps we decided to use a rotor-stator, γ subunit to β subunit, disulfide bond, with the premise that a cross-link would block rotation and therefore stop the partial reactions involving rotation. Such disulfides have been previously observed between the native Cys at position 87 in the *Escherichia coli* γ and Cys substitutions in the conserved β D380-ELSEE-D386 motif, either at βAsp380 (Duncan *et al.*, 1995b) or βGlu381 (Aggeler *et al.*, 1995a) (Fig. 3.2.1). For example, Garcia and Capaldi reported that the γ-β cross-linked F_1 had nearly normal unisite kinetic behavior demonstrating that unisite catalysis is independent of the γ subunit rotation (García and Capaldi, 1998). We reasoned that cross-linking the rotor to the stator would lock the position, or at least greatly restrict, the rotation of the γ subunit and therefore prevent the kinetic steps that require rotation. We report here that our data do indeed show this to be the case. Preventing the rotation results in a slower pre-steady state burst of ATP hydrolysis and blocks the release of Pi. These data are consistent with the functional assignments of the catalytic sites where β_{TP} is the high affinity site carrying out reversible hydrolysis/synthesis, and β_{DP} is the site from which product Pi and ADP are released after it converts to β_E (Baylis Scanlon *et al.*, 2007). We also found that mild perturbations of the β^{380}DELSEED^{386} function by βE381C causes uncoupling of catalysis and rotation by affecting the establishment of the optimal catalytic conformation resulting

in a bypass in the reaction pathway. In the alternate pathway, γ subunit rotation becomes disengaged from hydrolysis thus perturbing its ability to pump protons.

Evidence presented in this paper suggests the 40° rotation is associated with k_{γ}, and the enzyme needs to acquire the conformation after the 80° rotation substep to achieve positive cooperativity for the promotion of catalysis.

3.3 Experimental Procedures

3.3.1 F_OF_1 strains and plasmids.

The single cysteine mutations (βD380C and βE381C) were introduced into plasmid pUβSE derived from a modified pUC18 vector containing a portion of *uncD* (γ-subunit gene) between *Sac*I and *Eco47*III restriction sites (Ketchum *et al.*, 1998). Site-directed mutagenesis was performed with the QuickChange kit from Stratagene (La Jolla, CA), using the following primers: βE381C; 5'-CTGAAAGACATCATCGCCACCCTGGGTATGGATTGCCTTTCTGAAGAAGACA AACTGGTGG-3' and βD380C; 5'-CGCCATCCTGGGTATGTGTGAACTTTCTGAAGAAGACAAACTGG -3' (where the underlined letters show the converted β-subunit codons GAA→TGC and GAT→TGT, respectively). Both mutations were isolated on the *Sac*I to *Eco47*III fragment and ligated individually into the high copy number plasmid pBWU13 (Moriyama *et al.*, 1991). Colonies were screened for the insert with a PCR approach using Taq Master Mix (Qiagen, Valencia, CA). Introduction of each mutation in the expression plasmid was

verified by DNA sequencing. Mutant F_OF_1 complexes were expressed in the *atp* operon-deleted strain, DK8 (Klionsky *et al.*, 1984).

The amino-terminal polyhistidine-tagged ε subunit (His-ε was expressed in *E. coli* strain BL21(DE3)*pLysS* (Andrews *et al.*, 2001) and purified as described in (Baylis Scanlon *et al.*, 2007).

All molecular biology manipulations were done according to manufacturers' instructions or according to procedures described in Sambrook *et al.* (Sambrook *et al.*, 1989).

3.3.2 Preparation and characterization of mutant F_OF_1 enzymes.

Oxidative phosphorylation-dependent growth of mutant strains was determined on minimal defined media containing 0.2% sodium succinate as a sole carbon source (Moriyama *et al.*, 1991; Senior *et al.*, 1984).

Membrane vesicles containing F_OF_1 were prepared as previously described (Futai *et al.*, 1974) from cells grown to mid-log phase in a minimal salt medium supplemented with 1.1% glucose, amino acids, thiamine and 50 μg/ml ampicillin at 37 °C (Moriyama *et al.*, 1991). F_1 expression levels in the membrane preparations were analyzed using a quantitative immunoblot assay using polyclonal antibodies against *E. coli* F_1 α subunits (kindly provided by Dr. Alan Senior, University of Rochester). Purified F_1 was used as a standard as described previously (Al-Shawi *et al.*, 1997a).

The formation of ATP- or NADH-dependent electrochemical gradients of protons across inside-out inner membrane vesicles was assessed by monitoring acridine orange

fluorescence quenching at 530 nm as previously described (Moriyama *et al.*, 1991; Shin *et al.*, 1992)

3.3.3 Preparation of F_1 enzymes.

Cells for F_1 purification were grown at 37 °C in minimal media supplemented with 1.1% glucose, amino acids, thiamine and 50 μg/ml ampicillin. F_1 was isolated and purified as described (Al-Shawi and Senior, 1992). The purity and subunit composition of F_1 preparations were checked by SDS-PAGE analysis (Laemmli, 1970) and by comparison of steady state ATP hydrolysis rates with those previously reported (Aggeler *et al.*, 1995a; Andrews *et al.*, 2001; Duncan *et al.*, 1995a).

3.3.4 Cross-linking of F_1 mutants.

The βD380C mutant F_1 was cross-linked by reacting with 5,5'-dithiobis-(2-nitrobenzoate) (DTNB) based on conditions described previously (Duncan *et al.*, 1995a). The enzyme was thawed and stored at room temperature, diluted to ~2.5 mg/ml, treated with 1 mM tris(2-carboxyethyl) phosphine hydrochloride (TCEP) for 20 minutes, then passed over a Sephadex G50 centrifuge column (Penefsky, 1979) to remove TCEP, nucleotides and to exchange the buffer into Buffer 1 (25 mM TES·KOH pH 8.0, 1 mM $MgSO_4$, 10% glycerol). Mutant F_1 was incubated with 2.5 μM DTNB for 1 hour to induce cross-linking. After incubation, the enzyme was again passed over a centrifuge column to remove oxidizing reagent and exchange the buffer into Buffer 2 (25 mM TES-KOH, 0.244 mM $MgCl_2$, 0.2 mM EDTA, pH 7.5 at 25 °C) in preparation for pre-steady state measurements. The βE381C mutant was treated in the same manner as the βD380C

mutant but to induce the γ–β cross-link 50 μM $CuCl_2$ was used for 1 hour (García and Capaldi, 1998). Incubation with DTNB or $CuCl_2$ overnight did not significantly increase cross-linking efficiency, nor affect ATPase activity of wild-type F_1. Interestingly, neither mutant F_1 achieved a maximal cross-linking yield when treated with the oxidizing reagent optimized for the other.

3.3.5 Pre-steady state multisite hydrolysis of ATP.

[γ-^{32}P]ATP hydrolysis was measured in the millisecond time range using a Kintek RQF-3 rapid quench-flow apparatus (Austin, TX) with circulating water temperature control. The uncross-linked F_1 was prepared for pre-steady state experiments by removing bound nucleotides and exchanging the enzyme into Buffer 2 as described previously (Baylis Scanlon *et al.*, 2007).

In the rapid mixing device (1:1 mixing volume ratio) syringe A contained purified F_1 (with an additional equimolar concentration of ε subunit) (Baylis Scanlon *et al.*, 2007) in Buffer 2, and syringe B contained 25 mM TES-KOH, 0.2 mM EDTA, 0.5 mM [γ-^{32}P]ATP and 0.46 mM $MgSO_4$, pH 7.5 at 25 °C, resulting in final concentrations of 104 μM and 50 μM for Mg·ATP and free Mg^{2+}, respectively. The samples were processed according to the two step procedure described previously (Baylis Scanlon *et al.*, 2007) in order to minimize the background due to the high concentration of [γ-^{32}P]ATP in the experiments. The amount of [^{32}P]Pi generated was determined by Cerenkov counting in 0.2 M Tris base.

3.3.6 Unisite binding and hydrolysis of ATP.

F_1 was prepared as described above for the multisite experiments except that the final centrifuge column was equilibrated with unisite buffer (50 mM Tris base, 50 mM MOPS, 4.5 mM K_2SO_4 and 0.5 mM $MgSO_4$ adjusted to pH 7.5 with H_2SO_4). Reactions were performed at 23 °C, and were initiated by adding 15 µl of [γ-^{32}P]ATP to F_1 while rapidly mixing. The final molar mix ratio of ATP to F_1 was approximately 0.1. The reactions were quenched at varying times with 550 µl of 50 mM Tris-SO_4, pH 8.0, 1 mM KH_2PO_4, 4.5 mM ATP, 2.8 mM $MgSO_4$, 8.2% v/v $HClO_4$. The total ^{32}Pi generated was determined by the acid molybdate precipitation method of Sugino and Miyoshi (Sugino and Miyoshi, 1964), and Cerenkov counting in 15 ml of 0.2 M Tris base. The rate of [γ-^{32}P]ATP binding was measured by the hexokinase trap method modified slightly from that described previously (García and Capaldi, 1998; Senior *et al.*, 1992). Briefly, the unisite reactions were started as described above, but at times shown 200 µl of hexokinase solution (unisite buffer with 2 mg/ml hexokinase (purified from Baker's yeast at ~170 units/mg), 4.4 mg/ml glucose and an extra 2.5 mM $MgSO_4$) was added, and the reaction allowed to proceed for 10 seconds before quenching with 2 N HCl containing 1 mM Pi. Samples were boiled for 7 minutes to hydrolyze the unreacted [γ-^{32}P]ATP, and the ^{32}Pi was removed by acid molybdate precipitation. The amount of [^{32}P]-glucose-6-phosphate formed was determined by measuring the radioactivity of the supernatant by Cerenkov counting in Tris base.

3.3.7 Pre-steady state Pi release.

Pi release was followed by the fluorescence intensity change of (7-diethylamino-3-((((2-maleimidyl)ethyl)amino)carbonyl) coumarin)-labeled phosphate binding protein (MDCC-PBP, Ref. (Brune *et al.*, 1998; White *et al.*, 1997)). Phosphate binding protein was expressed from *E. coli* strain ANCC75 (*leu purE trp his argG strA phoS64 met thi)* harboring plasmid pSN5182/7 (kindly provided by Dr. Martin Webb, MRC, Mill Hill, London) and prepared as previously described (Brune *et al.*, 1998). Un-reacted label was separated from MDCC-PBP by passage over a PD-10 desalting column (all chromatography materials were from Amersham Biosciences). Unlabeled phosphate binding protein and Pi-insensitive MDCC-PBP were removed by passage over a Q-Sepharose column and a Mono-Q column, respectively (Brune *et al.*, 1998). The final preparation had a 12-15-fold increase in fluorescence at 465 nm on binding Pi, indicating that the protein was largely Pi free.

Removal of contaminating inorganic phosphate from buffers, the final enzyme preparation and the stopped-flow spectrometer, required a "Pi-mop," assembled as described by Nixon *et al*. (Nixon *et al.*, 1998). The "Pi-mop" sequesters Pi into the stable ribose-5-phosphate molecule through a coupled enzyme system. Bacterial purine nucleoside phosphorylase (PNPase) and 7-methylguanosine (MEG) converts phosphate and ribose to ribose-1-phosphate, which is then modified by phosphodeoxiribomutase (PDRM) in the presence of $MnCl_2$ and α-D-glucose 1,6-bis-phosphate to form the stable ribose-5-phosphate.

PNPase, MEG, and α-D-glucose 1,6-bis-phosphate were purchased from Sigma Chemicals. Purified PDRM was made by amplifying the *E. coli* PDRM gene from strain XL1 Blue genomic DNA by PCR using primers: 5'-ACTCCATGGAACGTGCATTTATTATGGTTCTGGACTCATTCGG-3' and 5'-ATGCTCGAGTCAGAACATTTGCTTTGCCATATTCCATATCAG-3'. The primers included an *NcoI* site over the ATG start codon and an *XhoI* site downstream of the native stop codon (the restriction sites are depicted by the underscored sequences). The open reading frame was verified by sequencing the entire insert, which was then ligated into the pHIS-Parallel1 vector (Sheffield *et al.*, 1999), and used for expression in BL21(DE3) cells (Invitrogen, Carlsbad, CA). The PDRM protein was purified from cell lysates *via* an amino terminal $(His)_6$ affinity tag.

The kinetics of Pi release were followed in an Applied Photophysics SX.18MV-R stopped-flow spectrometer (Surrey, UK). The fluorescence change of MDCC-PBP was monitored at the excitation wavelength of 425 nm with a 455 nm emission cutoff filter. The syringe contents, listed in the figure legends, were essentially the same as for the rapid quench flow experiments except for the lack of radioactivity and addition of 20 μM MDCC-PBP. The Pi binding response of MDCC-PBP fluorescence was calibrated using known Pi concentrations in the stopped-flow at fixed photomultiplier voltage.

4.3.8 Kinetic analysis.

The experimental data fitting program, Scientist Version 2.0 (Micromath Research, Inc., St Louis, Missouri), was used to fit the experimental data by numerical integration of differential equations previously described in detail (Baylis Scanlon *et al.*,

2007). The calculated rate constants were evaluated based on the least squares regression value, R^2, and Model Selection Criteria (M.S.C.) (see Ref. (MicroMath_Research, 1995) used in Baylis Scanlon *et al.* (Baylis Scanlon *et al.*, 2007)) values from statistical analyses performed to determine the goodness-of-fit.

3.3.9 General methods and materials.

Except where [γ-^{32}P]ATP was used, steady state ATPase activities were determined as previously described (Al-Shawi *et al.*, 1997a) using the Taussky and Shorr colorimetric method (Taussky and Shorr, 1953). The nucleotide content of cross-linked and uncross-linked F_1 was determined by an ion exchange HPLC assay using a Titansphere TiO_2 column (Alltech Assoc., Deerfield, IL) as described in (Baylis Scanlon *et al.*, 2007). Protein concentrations were determined using the method of Lowry *et al.* (1951) and in most instances cross-checked by the Amido Black protein assay (Kaplan and Pedersen, 1985). The algorithm of Fabiato and Fabiato was used to determine the concentrations of Mg·ATP and free Mg^{2+} (Fabiato and Fabiato, 1979). Gel electrophoresis was performed according to Laemmeli (Laemmli, 1970) using the NuPAGE gel system (Invitrogen, Carlsbad, CA) and Tris/Glycine 4-12% gradient gels. [γ-^{32}P]ATP was purchased from GE Biosciences (Piscataway, NJ). All other chemicals were the highest grade commercially available.

3.4 Results

3.4.1 Characterization of Cys mutants and cross-linked enzymes.

It was previously shown that a disulfide bond can be induced between the native γ subunit Cys87 and a Cys substitution in place of either β subunit Asp380 (Duncan *et al.*, 1995a; Duncan *et al.*, 1995b) or Glu381 (Aggeler *et al.*, 1995a) (Fig. 3.2.1). The β subunit residues are part of the conserved βD380-ELSEE-D386 motif, the loop near the carboxyl terminus that interacts directly with the γ subunit which, in part, establishes the conformational asymmetry of the catalytic sites during the course of rotational catalysis (Kaibara *et al.*, 1996). Perturbations of the γ-β interaction affect steady state catalysis as well as coupling efficiency between ATP hydrolysis/synthesis and rotation (Al-Shawi *et al.*, 1997a; Nakamoto *et al.*, 1995)

Growth yields of βE381C and βD380C mutant strains on minimal-defined solid medium, with sodium succinate as the sole carbon source, were similar to wild-type, indicating functional F_OF_1 enzymes competent enough to achieve net synthesis of ATP by oxidative phosphorylation. The expression levels of βE381C and βD380C F_OF_1 complexes in the inner membranes were measured quantitatively by immunoblot and were similar to wild-type F_OF_1 expression (Table 3.4.1). The steady state ATPase activities of F_OF_1-containing membranes of both mutants were also comparable to wild-type (Table 3.4.1). Proton pumping of mutant F_OF_1 into inside-out inner membranes was measured by acridine orange fluorescence quenching, and is shown in Fig. 3.4.1. The NADH-driven ΔpH for βE381C and βD380C membranes were similar to wild-type (Fig.

3.4.1A) indicating the membranes from the mutant strains were not intrinsically more permeable to protons than wild-type membranes. This assay verifies that mutant F_1 binds to F_O, and is stable but is also used to determine the quality of the membrane preparations as a control for ATP-driven ΔpH. ATP-driven fluorescence quenching was only 25% for the βE381C membranes compared with 85% and 82% for wild-type and βD380C, respectively. The βE381C mutant is able to sustain growth on succinate because its proton pumping ability, while impaired, is not completely abolished. The reduced ability of the βE381C mutant to form an ATP-driven pH gradient, despite similar expression level and ATPase activity to wild-type, indicates that catalysis and transport are not efficiently coupled in this mutant. In contrast, the βD380C mutant enzyme is functionally similar to wild-type in H^+ pumping ability, and appears to have well coupled catalysis and transport.

Table 3.4.1

ATP hydrolysis activities of membranes containing F_OF_1 and purified F_1 before and after induction of the γ–β cross link by oxidizing reagent.
Conditions of assays are described under *Experimental Procedures.*

		ATP Hydrolysis [a]					
			Isolated F_1				
Mutation	F_OF_1 Expression [a]	Membranes [b]	Untreated [c]	After induction of γ–β cross-link [c, d]	After treatment with 20 mM DTT [c]	Untreated	Untreated
						K_M [e]	k_{cat}/K_M [e]
	%	*μmol Pi/min/mg*	s^{-1}	s^{-1}	s^{-1}	*μM*	$s^{-1}M^{-1}$
Wild-type	12 ± 3	8.0 ± 0.9	95 ± 3	n/d [f]	n/d [f]	45	$5.9x10^5$
βE381C	20 ± 4	8.0 ± 1.9	120 ± 4	4.0 ± 0.9 [g]	130 ± 2	42	$1.0x10^6$
βD380C	15 ± 2	5.0 ± 0.9	84 ± 2	1.2 ± 0.02 [g]	77 ± 3	37	$1.1x10^6$

[a] Expression of F_OF_1 on membranes was determined by quantitative immunoblot as outlined in *Experimental Procedures*, and values expressed as % of total membrane protein, n = 4.
[b] Membrane assays contained 1 μM CCCP.
[c] ATPase activites, under saturating ATP conditions, were measured in 50 mM Hepes-KOH, 10 mM ATP, 5 mM $MgSO_4$, pH 7.5 at 30 °C, with an ATP regenerating system of 5 mM phospho(enol)pyruvate (PEP) and 50 μg/ml pyruvate kinase.
[d] The γ–β cross link was induced by treatment with 50 μM $CuCl_2$ for βE381C-F_1, and by treatment with 25 μM DTNB for βD380C-F_1.
[e] Values for K_M and k_{cat} were determined by measuring ATPase activity as a function of Mg·ATP concentration under conditions maintaining a low free Mg^{2+} concentration of 50 μM. The buffer consisted of 25 mM TES-KOH, 0.2 mM EDTA, and varying amounts of Na_2-ATP (25 μM - 10 mM) and $MgCl_2$ (0.269 mM - 4.57 mM), pH 7.5 at 25 °C, with an ATP regenerating system of 2 mM PEP, 50 μg/ml pyruvate kinase.
[f] n/d: Experiment was not repeated here. Duncan *et al.* have already shown there is no effect of either DTNB or DTT on wild-type activity (Duncan *et al.*, 1995).
[g] Activity was fully inhibitable by 1 mM sodium azide, indicating the extent of uncross-linked enzyme.

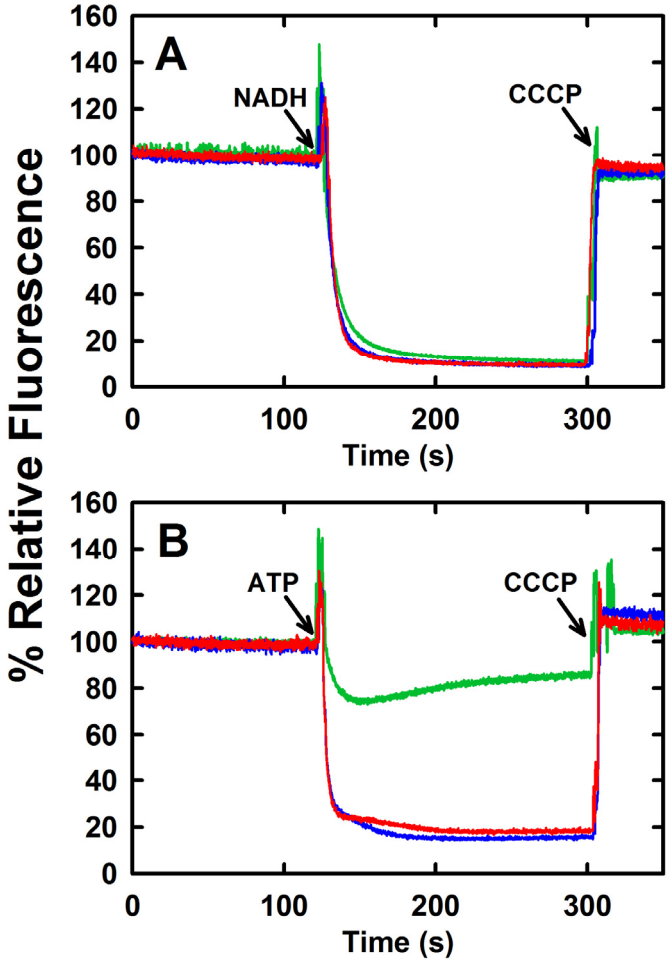

Figure 3.4.1. NADH- or ATP-dependent proton electrochemical gradient formation by mutant F_OF_1 in membranes.

200 μg of membrane vesicle protein from strain DK8, harboring plasmid pBWU13 wild-type of carrying the mutations for βE381C or βD380C, were suspended in 2 ml of buffer containing 10 mM HEPES-KOH, 300 mM KCl, 5 mM $MgCl_2$, 1 μM valinomycin, and 1 μM acridine orange at pH 7.5, with vigorous mixing. Fluorescence intensity at 530 nm (excitation at 460 nm) was monitored at 25 °C. *A*, NADH-driven quenching. Proton pumping was initiated at the indicated time (*arrow*) by addition of 1 mM NADH. *B*, ATP-driven quenching. Proton pumping was initiated at the indicated time (*arrow*) by addition of 1 mM ATP. 1 μM carbonylcyanide-*m*-chlorophenylhydrazone (*CCCP*) was added, as indicated (*arrows*) to abolish the proton gradient and establish the maximum fluorescence value. The fluorescence traces are depicted as follows: wild-type (blue),

βD380C (red), βE381C (green). The traces are representative of those from several trials.

Steady state ATP hydrolysis rates of βE381C-F_1 and βD380C- F_1 were measured as a function of Mg·ATP concentration (10 μM to 4.3 mM) under conditions of a low free Mg^{2+} concentration of 50 μM, in the presence of an ATP regenerating system, at 25 °C and pH 7.5. βE381C-F_1 had a k_{cat} value of 41 s^{-1} and K_M of 42 μM. βD380C-F_1 had a k_{cat} of 41 s^{-1} and K_M of 37 μM (Table 3.4.1). These were similar to wild-type values measured under the same conditions (k_{cat} of 26.6 s^{-1} and K_M of 45 μM). The specificity constants (k_{cat}/K_M: βE381C-F_1, $1.0x10^6$ $s^{-1}M^{-1}$ βD380C-F_1, $1.1x10^6$ $s^{-1}M^{-1}$) were also similar to wild-type ($5.9x10^5$ $s^{-1}M^{-1}$), hence verifying that the mechanism of ATP hydrolysis in F_1 is not drastically altered by the cysteine substitutions.

3.4.2 Formation of the cross-link between γCys87 and βE381C or βD380C.

The disulfide bond forms to a slight degree without the presence of oxidizing agents in the βE381C mutant, but not in the βD380C mutant (Fig. 3.4.2A and 3.4.2B, Lane 1). To maximize cross-linking, 50 μM copper chloride or 25 μM DTNB was used to induce cross-linking of γCys87 to βE381C-F_1 or βD380C-F_1, respectively. A small percentage (~0.5%) of the β subunits cross-link to form a homodimer (Fig. 3.4.2), however this level is insignificant compared to the γ-β dimer, and is not enough to affect the kinetic analyses described below. Consistent with previous reports (Aggeler and Capaldi, 1992; García and Capaldi, 1998), the formation of the γ-β disulfide bond is effective in inhibiting the steady state turnover of both mutant enzymes (Table 3.4.1). There still remained ~1% of the maximal activity for the cross-linked βD380C-F_1 and

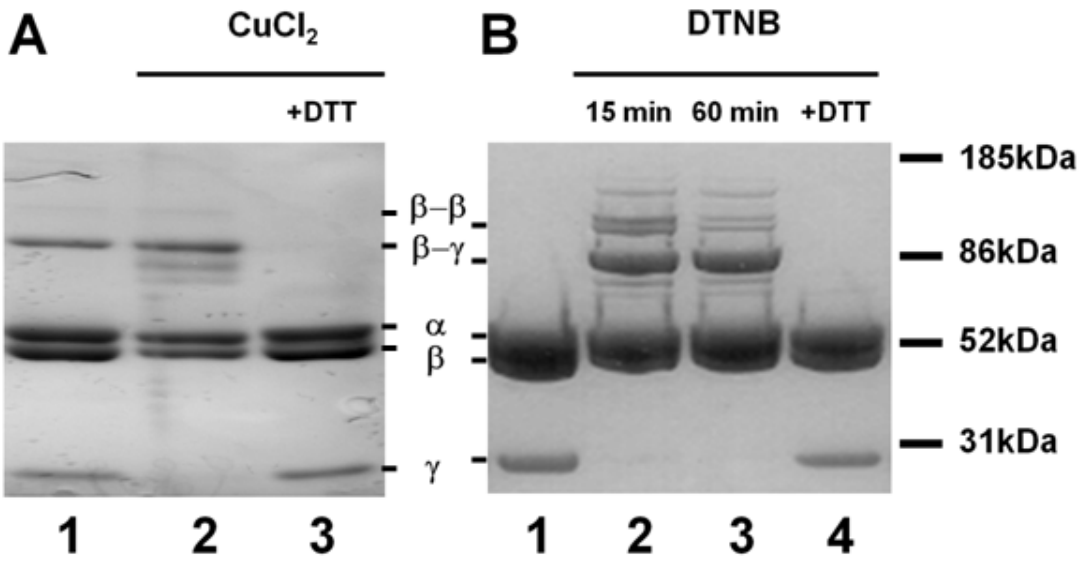

Figure 3.4.2. Reversible γ–β disulfide bond formation between native γCys87 and βE381C or βD380C.

A, βE381C-F_1 was treated with 50 μM $CuCl_2$ and aliquots were taken for SDS/PAGE and ATPase assays (activities listed in Table I). Lane 1. Initial sample, no treatment. Lane 2. βE381C-F_1 after 1 hour incubation with $CuCl_2$. Lane 3. βE381C-F_1 incubated for 30 min with 10 mM DTT following the reaction with $CuCl_2$. B, βD380C-F_1 was treated with 25 μM DTNB and aliquots were taken for SDS/PAGE and ATPase assays (activities listed in Table I). Lane 1. Initial sample, pretreatment. Lane 2. βD380C-F_1 after 15 min incubation with DTNB. Lane 3. βD380C-F_1 after 60 min incubation with DTNB. Lane 4. βD380C-F_1 incubated for 30 min with 10 mM DTT after the reaction with DTNB. Note that the gels are slightly overloaded to emphasize the complete disappearance of the γ subunit into the γ-β cross-linked product.

~5% of activity for βE381C-F_1. We questioned whether this slow rate of hydrolysis was due to the slow unisite mode of catalysis (García and Capaldi, 1998) or due to the small amount of uncross-linked enzyme. The residual activity for each enzyme was examined by treatment with 1 mM sodium azide (NaN_3), as this compound apparently affects catalytic site cooperativity, and thus only inhibits F_1-ATPase multisite activity with no effect on unisite activity (Noumi *et al.*, 1987). The NaN_3 treatment verified that the activity measured after cross-linking was due almost entirely to uncross-linked enzyme. This corroborates observations that the level of inhibition of activity for γCys87-βE381C-F_1 correlated with the yield of cross-linking (García and Capaldi, 1998). Addition of 10 mM dithiothreitol (DTT) removed the disulfide bond and restored steady state activity for both mutants (Table 3.4.1). In the case of βE381C the activity level for the DTT treated enzyme was higher than the initial rate due to complete reduction of the small fraction of cross-linked enzyme present prior to addition of $CuCl_2$. There was no effect on wild-type steady state membrane ATPase activity by $CuCl_2$, DTNB or DTT, as shown by (Duncan *et al.*, 1995b).

3.4.3 Unisite binding and hydrolysis of [γ-^{32}P]ATP.

The unisite kinetic activity was examined in order to determine the elementary rate constants, and thus whether either β^{380}DELSEED^{386} mutation or γ–β cross-link perturbed the mechanism of the enzymatic reaction at the high affinity catalytic site, which is believed to be the β_{TP} conformer (Baylis Scanlon *et al.*, 2007; Mao and Weber, 2007). Unisite parameters for βE381C-F_1, both cross-linked, and uncross-linked, were

TABLE 3.4.2A

Rate constants and kinetically calculated binding constants of cross-linked and non-cross-linked enzymes. Rate constants for constants from k_{+1} to k_{γ} are listed here. Rate constants for k_{-3} to k_{-4} are listed in the Table continued below.

	k_{+1}	k_{-1}	K_1	k_{+2}	k_{-2}	K_2	k_{γ}	R^2	*MSC*
	$M^{-1}s^{-1}$	s^{-1}	M^{-1}	s^{-1}	s^{-1}		s^{-1}		
unisite									
Wild-type [a]	1.1×10^{5}	2.5×10^{-5}	4.4×10^{9}	0.12	0.043	2.8			
βE381C [b]	5.3×10^{5}	6.0×10^{-4}	8.8×10^{8}	1.2 [c]	1.2 [c]	1.0		0.998 [c]	3.23 [c]
βE381C(γ–β)[b]	6.1×10^{5}	3.1×10^{-2}	2.0×10^{7}	1.3 [c]	0.5 [c]	2.6 [c]		0.998 [c]	3.96 [c]
βD380C	6.5×10^{5}	7.3×10^{-2}	8.9×10^{6}	1.8	1.2	1.5		0.997	3.31
βD380C(γ–β)	1.8×10^{5}	2.4×10^{-2}	7.5×10^{6}	0.54	0.15	3.6		0.998	4.27
multisite									
Wild-type [e]	4.0×10^{7}	1.9×10^{3}	2.1×10^{4}	140	120	1.2	29	0.997	5.10
βE381C	5.5×10^{7}	3.7×10^{3}	1.5×10^{4}	150	110	1.4	426	0.998	5.47
βE381C(γ–β)	2.2×10^{5}	6.1×10^{-3}	3.6×10^{7}	120	80	1.5	0	0.958	1.77
βD380C	4.4×10^{7}	2.1×10^{3}	2.1×10^{4}	270	150	1.8	38	0.999	6.30
βD380C(γ–β)	2.3×10^{5}	5.2×10^{-3}	4.4×10^{7}	63	17	3.8	0	0.972	2.60

TABLE 3.4.2B

Rate constants and kinetically calculated binding constants of cross-linked and non-cross-linked enzymes. Rate constants from k_{-3} to k_{-4} are listed here.

	k_{+3}	k_{-3}	K_{-3}	k_{+4}	k_{-4}	K_{-4}	*Turnover* (V_{max})	R^2	*MSC*
	s^{-1}	$M^{-1}s^{-1}$	M^{-1}	s^{-1}	$M^{-1}s^{-1}$	M^{-1}	s^{-1}		
unisite									
Wild-type [a]	1.2×10^{-3}	4.8×10^{-4}	0.4	1.6×10^{-3}	1.8×10^{2}	1.1×10^{5}			
βE381C [b]	2.2×10^{-2}	N.D [d]	N.D.	2.2×10^{-3}	N.D.	N.D.		0.998 [c]	3.23 [c]
βE381C(γ–β)[b]	2.8×10^{-2}	N.D.	N.D.	7.7×10^{-3}	N.D.	N.D.		0.998 [c]	3.96 [c]
βD380C	2.5×10^{-3}	N.D.	N.D.	N.D.	N.D.	N.D.		0.997	3.31
βD380C(γ–β)	6.4×10^{-4}	N.D.	N.D.	N.D.	N.D.	N.D.		0.998	4.27
multisite									
Wild-type [e]	210	13	0.062	360	4.2×10^{6}	1.2×10^{4}	27	0.997	5.10
βE381C	220	17	0.077	540	8.2×10^{6}	1.5×10^{4}	41	0.998	5.47
βE381C(γ–β)	0 (1.5) [f]	0	0	0	0	0	(0.44) [f]	0.958	1.77
βD380C	267	26	0.1	826	4.0×10^{5}	4.8×10^{2}	41	0.999	6.30
βD380C(γ–β)	0 (0.8) [f]	0	0	0	0	0	(0.16) [f]	0.972	2.60

[a] Values taken from Ref. (14).

[b] Values taken from Ref. (28).

[c] Values calculated from primary data (28).

[d] N.D. Not determined.

[e] Values taken from Ref. (18).

[f] In parentheses is the value of azide-inhibitable Pi release due to a small fraction of non-cross-linked enzyme. See text for details.

determined by Garcia and Capaldi (García and Capaldi, 1998), and their rate constants are listed in Table 3.4.2. Their omission of values for k_{+2} and k_{-2} necessitated a refitting of their primary data, which was achieved without much change in the other rate constants. They noted an increased rate of ATP binding (k_{+1}) compared with their measurements for wild-type F_1, although the value was comparable with other previously published results for the wild-type enzyme (Al-Shawi and Senior, 1992), also listed in Table 3.4.2 for reference. The βE381C-F_1 enzyme had an ATP off rate, k_{-1} 24-fold faster than wild-type, and a lower affinity for ATP. It also showed slightly increased rates of unisite activity compared to wild-type, due mostly to higher rates of ATP hydrolysis (k_{+2}) and Pi release (k_{+3}), although importantly, the hydrolysis/synthesis ratio, K_2, was essentially unchanged either by the mutation or by cross-link formation.

Fig. 3.4.3 shows the hydrolysis of substochiometric amounts of [γ-^{32}P]ATP by βD380C-F_1 and γ-β cross-linked βD380C-F_1. The total [^{32}P]Pi (enzyme-bound [^{32}P]Pi plus [^{32}P]Pi released to the medium) was determined by directly quenching samples with acid. The glucose/hexokinase trap additionally measured [γ-^{32}P]ATP bound to F_1. These two experiments allow derivation of ATP binding (k_{+1}), ATP release (k_{-1}), the ATP hydrolysis/synthesis rates (k_{+2}, k_{-2}), and Pi release (k_{+3}) from fits of the data using a minimal unisite reaction scheme (ATP binding through Pi release, see also *Introduction 1.5.1,* Reaction Scheme 1) (Al-Shawi and Senior, 1992). The elemental rate constants are listed in Table 3.4.2. The parameters for both the βD380C-F_1 and γ-β cross-linked βD380C-F_1 enzymes were very similar to those measured for the wild-type enzyme, with the exception of faster rates for ATP release (k_{-1}), resulting in a lower affinity for ATP,

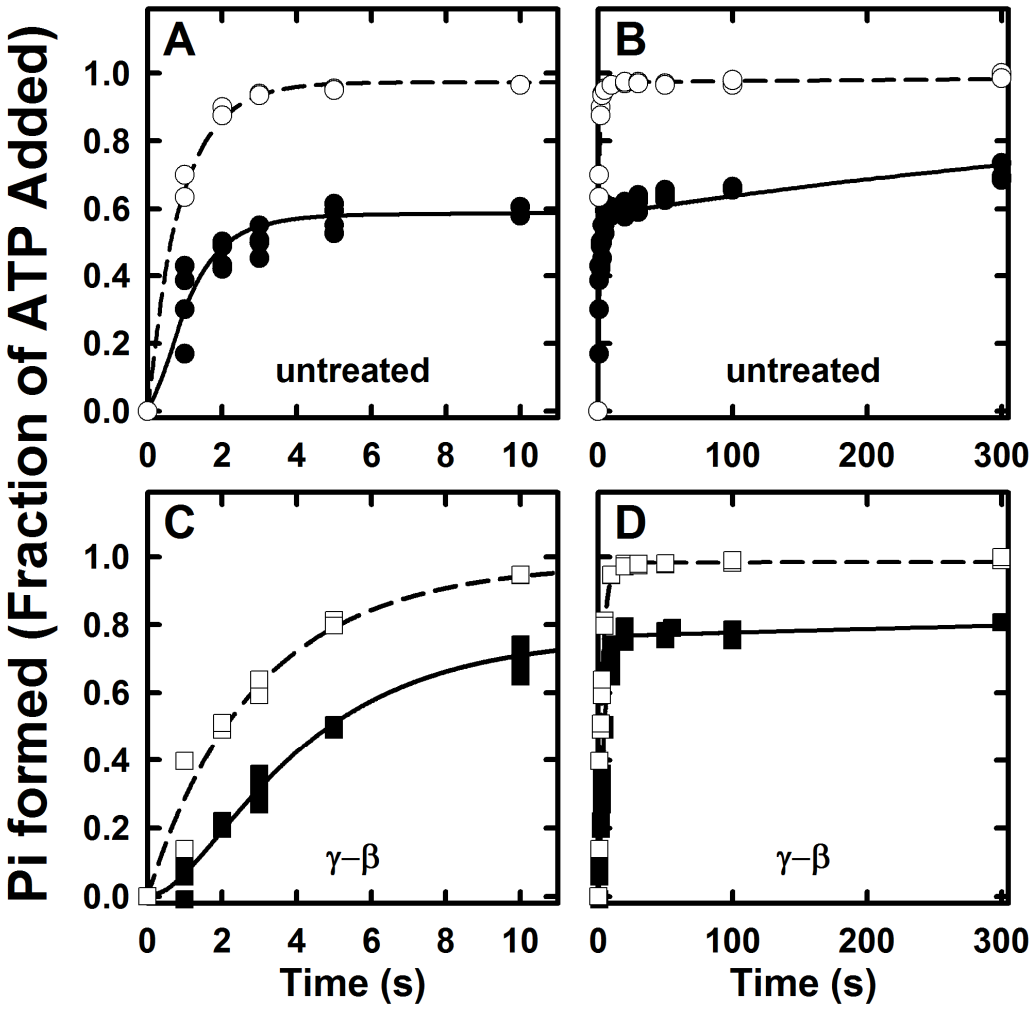

Figure 3.4.3. Unisite hydrolysis of βD380C-F_1 and γ–β cross-linked βD380C-F_1.

F_1 was prepared either by exchanging into unisite buffer, or by treatment with DTNB and then exchanging into unisite buffer, as described in *Experimental Procedures*. Hydrolysis was initiated by adding 0.1 μM [γ-^{32}P]ATP to 1 μM F_1 (with equimolar ε added) in unisite buffer (50 mM Tris-OH, 50 mM MOPS, 4,5 mM K_2SO_4 and 0.5 mM $MgSO_4$ adjusted to pH 7.5 with H_2SO_4 at 25 °C). A, the early time points, and B, the complete time course for the βD380C-F_1 acid-quenched hydrolysis (●), and bound [γ-^{32}P]ATP (○) measured in parallel by the hexokinase trap method. C, the early time points, and D, the complete time course for the γ–β cross-linked βD380C-F_1 reactions. At the times indicated samples were quenched directly with acid (■), and bound [γ-^{32}P]ATP (□) was measured in parallel by the hexokinase trap method. The lines indicated are the best fits to the data, and the parameters are listed in Table 3.4.2.

even greater than the effect described above for the βE381C mutant. Results from cold chase experiments corroborated this finding where addition of excess unlabeled ATP failed to promote ATP hydrolysis in βD380C-F_1 previously incubated with [γ-^{32}P]ATP, and actually decreased bound [γ-^{32}P]ATP (data not shown). This is consistent with a fast ATP off-rate, k_{-1}, which allows the excess cold chase of ATP to displace the enzyme-bound [γ-^{32}P]ATP. Importantly, the ATP hydrolysis/synthesis equilibrium constant, K_2, was not changed by the βD380C mutation nor by the γ-β cross-linked enzyme, with values close to unity in accordance with Boyer's binding change mechanism (Boyer, 1975; Boyer, 1993). In summary, unisite analysis shows that neither Cys mutation disrupts the mechanism of ATP hydrolysis at the high affinity catalytic site, although there is a decreased affinity for ATP. In addition, the βD380C unisite rate constants are essentially unaltered upon formation of the γ-β cross-link, in agreement with measurements of the βE381C enzyme (García and Capaldi, 1998), and verifying that the mechanism of unisite hydrolysis of ATP at the high affinity catalytic site does not involve γ subunit rotation.

3.4.4 Pre-steady state multisite hydrolysis of [γ^{32}P]ATP.

We previously determined the partial reaction rate constants of the catalytic pathway involving γ subunit rotation by analyzing the pre-steady state kinetics of multisite ATP hydrolysis (Baylis Scanlon *et al.*, 2007). Our data showed that rapid mixing with high Mg·ATP concentrations put the enzyme immediately into a rotational catalytic mode. Similar conditions were used in this study, for the same rationale.

Briefly, nucleotide occupancy of all three catalytic sites is needed to ensure the enzyme enters the rotational catalytic mode (Weber *et al.*, 1993; Yasuda *et al.*, 2001), and low free Mg^{2+} conditions are used to avoid the inhibitory effects of high concentrations of this ion (Al-Shawi *et al.*, 1988; Kanazawa *et al.*, 1980). Reaction conditions used for the time course of ATP hydrolysis are a compromise to satisfy these requirements, but also necessitate use of radioactive [γ-^{32}P]ATP because of the small amounts of substrate hydrolyzed in the first few turnovers. We also wished to limit the total radioactivity to keep the background at a reasonable level. The final concentrations after mixing are 0.5 μM F_1, 0.352 mM $MgCl_2$ and 0.25 mM [γ-^{32}P]ATP to give [Mg^{2+}_{free}]=49 μM and [Mg·ATP]=105 μM at pH 7.5 and 25 °C. This Mg·ATP concentration is approximately 2.5-fold higher than the K_M for steady state ATP hydrolysis (42 μM and 37 μM for βE381C and βD380C, respectively, and 45 μM for wild-type F_1, Table 3.4.1). Based on the affinity constants from Senior and coworkers (Löbau *et al.*, 1997; Weber and Senior, 2001), and our previous work monitoring pre-steady state nucleotide binding (Baylis Scanlon *et al.*, 2007), this is an adequate concentration of Mg·ATP to fill two sites completely and the third site partially.

We previously showed that the rate limiting step, k_γ, can be distinguished by pre-steady state analysis of Mg·ATP hydrolysis in the millisecond time regime (Baylis Scanlon *et al.*, 2007). The pre-steady state hydrolysis of βE381C-F_1 and βD380C-F_1 before and after treatment with the oxidizing reagent, and the curve fits to the data are shown in Fig. 3.4.4 and 3.4.5, respectively. After preparation of the F_1 for the reaction, the nucleotide contents of each sample were determined to be close to 4.0 mol of

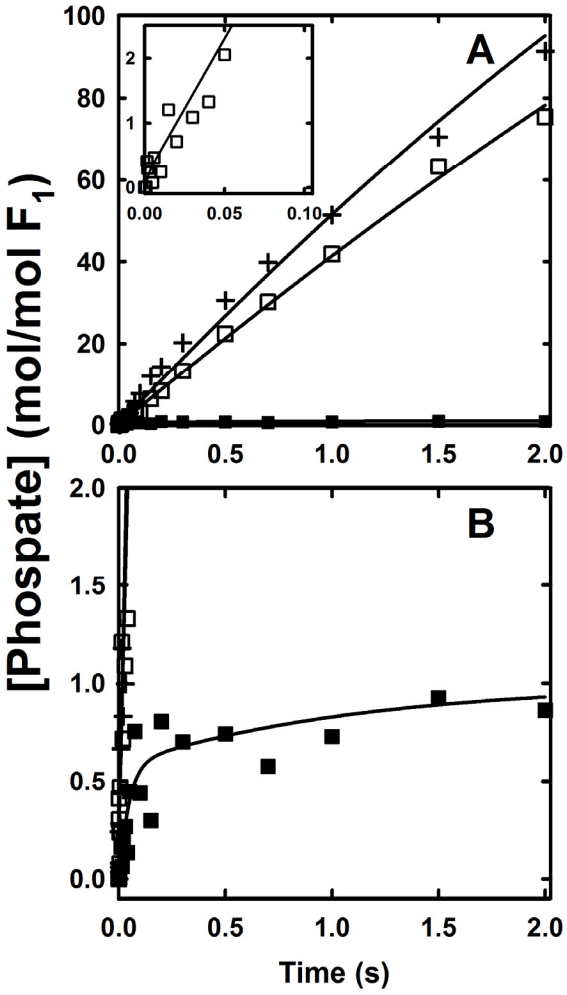

Figure 3.4.4. Pre-steady state hydrolysis of βE381C-F_1 before and after induction of γ–β cross-link.

A. the complete time course up to 2.0 s. *Inse*t, the early time points up to 0.1 s of uncross-linked sample. *B*. the complete time course with expanded y-axis to show the γ–β cross-linked sample. Purified F_1 was prepared as described in *Experimental Procedures* giving 4.0 ± 0.1 mol nucleotide bound per mol F_1, equimolar ε was added, and the sample diluted to 1 μM in 25 mM TES-KOH, 0.244 mM $MgCl_2$, 0.2 mM EDTA, pH 7.5 at 25 °C and loaded into Syringe A of the chemical quench instrument. Syringe B contained 25 mM TES-KOH, 0.46 mM $MgCl_2$, 0.20 mM EDTA, 0.50 mM [γ-^{32}P]ATP, pH 7.5 at 25 °C (final concentrations: 0.5 μM F_1, 0.352 mM $MgCl_2$, 0.25 mM [γ-^{32}P]ATP; [Mg^{2+}_{free}]= 49 μM, [Mg·ATP]=105 μM). [^{32}P]Pi produced is reported in mol of Pi per mol of F_1 for untreated F_1 (□), F_1 incubated with 50 μM $CuCl_2$ to form the γ–β cross-linked sample (■) and F_1 incubated with 10 mM DTT after $CuCl_2$ treatment (+). The *solid lines* are the best fits of each data set to our model, using the parameters listed in Table 3.4.2.

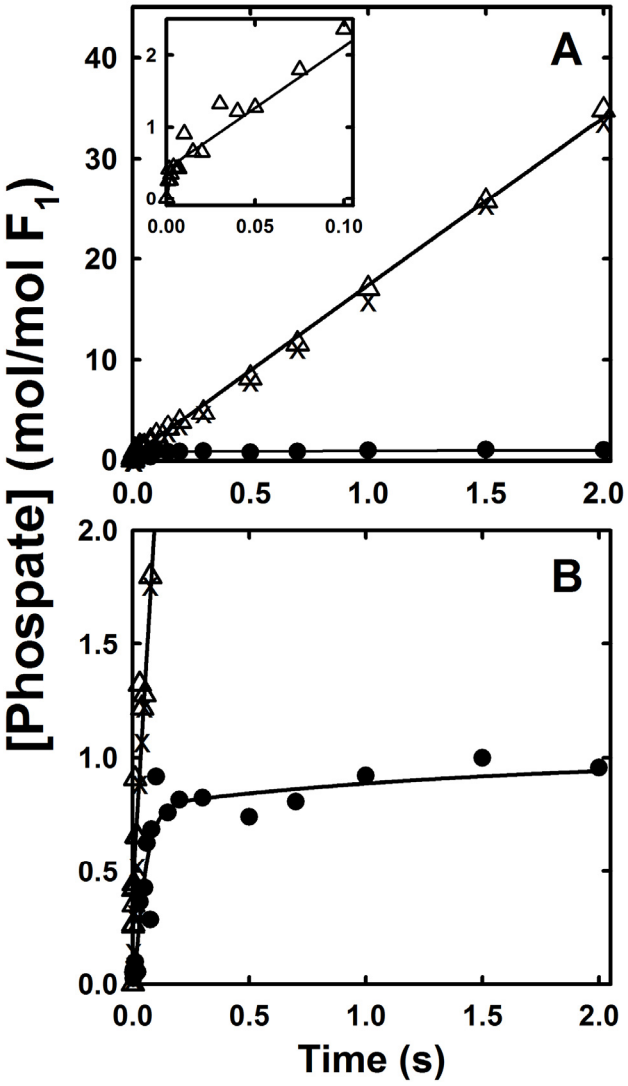

Figure 3.4.5. Pre-steady state hydrolysis of βD380C-F_1 before and after induction of γ–β cross-link.

A. the complete time course up to 2.0 s. *Inset*, the early time points up to 0.1 s of uncross-linked sample. *Note the y-axis scales compared to Fig. 5*. B, the complete time course with expanded y-axis to show the γ–β cross-linked sample. Preparation of F_1 and reaction conditions are essentially the same as the experiments in Fig. 5, except that βD380CF_1 is treated with 25 μM DTNB to induce the γ–β cross-link formation. Untreated F_1 (○) initially containing 4.0 ± 0.1 nucleotides, F_1 after DTNB incubation to induce γ–β cross-link (●), containing 3.9 ± 0.1 nucleotides, and DTT treated F_1 to reduce the γ–β cross-link (x). The *solid lines* are the best fits of each data set to our model, using the parameters listed in Table 3.4.2.

nucleotides bound per mol F_1, and are listed in the appropriate figure legends. We assume that 3 moles of nucleotide are bound to the non-catalytic α subunits and 1 mole of ADP is bound to the β_{DP} site (Baylis Scanlon *et al.*, 2007).

As described in the *Experimental Procedures* and explained in our previous analysis (Baylis Scanlon *et al.*, 2007), the pre-steady state kinetics of ATP hydrolysis provide adequate constraints to define a unique model for the partial reaction pathway. The same model (Reaction Scheme 1 and Table 3.4.2) was used to fit the kinetics of the cross-linked enzymes. Rate constants for the fits are listed in Table 3.4.2. Our rate constants for ATP binding for wild-type and both untreated mutants are consistent with the ATP k_{on} value of 2.6×10^7 $M^{-1}s^{-1}$ determined from single molecule experiments (Yasuda *et al.*, 2001). The total time courses of the reactions (Fig. 3.4.4A and 3.4.5A) show the cross-link was effective in inhibiting the steady state turnover in both mutants (closed symbols). The very slow hydrolysis and Pi production by the cross-linked enzymes, observed in the longer time course, are completely azide-inhibitable and due to the small amount of uncross-linked complex. The steady state hydrolysis was restored upon addition of 10 mM DTT for both enzymes ("+" and "x" symbols). The βE381C enzyme hydrolytic activity, after addition of DTT, was increased to a rate ~10% faster than the untreated sample (Fig. 3.4.4A), due to the presence of ~10% of cross-linked enzyme in the untreated sample (Fig. 3.4.2A, Lane 1). The steady state hydrolysis rates under the quench flow conditions are consistent with those under maximal ATP hydrolysis conditions, listed in Table 3.4.1, such that the activity of the DTT treated sample is ~10% faster than untreated sample.

Further examination of the untreated βE381C enzyme (before addition of $CuCl_2$) yields important insights into the coupling function of the enzyme. As seen in the inset of Fig. 3.4.4A, depicting the early time course of the reaction, the untreated βE381C has no initial burst of hydrolysis, and therefore no substantially slower step after hydrolysis which would cause product accumulation. The rate constants for the data fits are listed in Table 3.4.2, and comparison of the βE381C enzyme to wild-type shows similar rates for ATP binding and unbinding (k_{+1} and k_{-1}), which reflects the affinity for ATP of the low affinity catalytic site, β_E (see *Introduction*). The hydrolysis and synthesis rates (k_{+2} and k_{-2}) are also similar, yielding a K_2 value close to unity, and showing the hydrolysis reaction at the active site is essentially unperturbed. The major functional difference of the βE381C mutant becomes evident when comparing rates of k_γ, previously defined as the rate-limiting step and attributed, at least in part, to γ subunit rotation (Baylis Scanlon *et al.*, 2007). The βE381C enzyme has an extremely fast k_γ, which is not rate-limiting to the reaction. This is very different from the wild-type enzyme which displays an initial burst of hydrolysis (Baylis Scanlon *et al.*, 2007), and can only be fit by a reaction scheme that includes a relatively slow step after hydrolysis and before product release (Baylis Scanlon *et al.*, 2007). The βE381C enzyme proceeds through a different catalytic pathway where k_γ is not the rate-limiting step which we hypothesize is not associated with γ subunit rotation (see *Discussion*). Our results confirm the importance of the γ-β^{380}DELSEED^{386} interaction in coupling efficiency.

In contrast to the βE381C mutant, the pre-steady state activity of the uncross-linked βD380C-F_1 is very similar to wild-type with an initial burst of hydrolysis in the

first few milliseconds, after which the enzyme enters the steady state Fig. 3.4.5A (inset). The parameters for the fits are also very similar to the wild-type rate constants, notably in (1) the affinity for ATP, giving a K_d^{ATP} for the third site similar to the K_M for ATP hydrolysis, (2) the hydrolysis/synthesis ratio, K_2, close to one, and (3) the value of k_γ, the rate-limiting step of the reaction.

Fig. 3.4.4B and 3.4.5B each have an expanded y-axis to allow clear illustration of the time course of Mg·ATP hydrolysis by the cross-linked enzymes. Both enzymes exhibit a burst of hydrolysis despite the γ-β rotation-inhibiting cross-link. Thereafter the hydrolysis is severely abrogated. The initial burst is slower, but of a similar amplitude as wild-type, showing that inhibition of rotation does not prevent the first turnover of Mg·ATP hydrolysis. Moreover, the burst amplitude shows that simultaneous hydrolysis at multiple sites does not occur, and thus hydrolysis follows a sequential mechanism involving only a single site at any instant during catalysis.

It is also important to note that the rate constants for the fits of both cross-linked enzymes are similar suggesting that the functional uncoupling between catalysis and proton pumping observed in the steady state for the βE381C enzyme (Fig. 3.4.1B) is due to perturbation of γ subunit rotation, which presumably does not occur in the cross-linked enzyme (see *Discussion*). This is consistent with our previous thermodynamic analyses which suggested that the transition state for the steady state reaction occurs during γ subunit rotation between hydrolysis and release of Pi (Al-Shawi *et al.*, 1997b; Ketchum *et al.*, 1998).

The cross-linked enzymes had an ATP on rate (k_{+1}) which was 2 orders of magnitude slower, and an ATP off rate (k_{-1}) 5 orders of magnitude slower compared to the untreated enzyme. The hydrolysis/synthesis ratio, K_2, remained close to that for wild-type, still showing no great perturbation of the catalytic mechanism. Importantly the rates of ATP hydrolysis (k_{+2}) and resynthesis (k_{-2}) are similar to the untreated mutant enzymes and wild-type under multisite conditions, indicating that the positive cooperativity for ATP hydrolysis (Cross *et al.*, 1982) remains essentially intact despite inhibition of γ rotation.

3.4.5 Pi release for βD380C-F_1.

We will now focus on the βD380C enzyme because it is better coupled and therefore is more representative of the coupled pathway. We showed previously that the order of k_γ in the reaction was critical and occurs after hydrolysis but before Pi release (Baylis Scanlon *et al.*, 2007). The prediction from our model was that all steps after rotation should be inhibited in the γ-β cross-linked enzyme. In order to test this directly we followed the release of Pi from the βD380C enzyme by measuring the fluorescence intensity change of the MDCC-labeled phosphate binding protein (MDCC-PBP, see *Experimental Procedures* and (Brune *et al.*, 1998)). This protein binds Pi very fast (k_{on} = 1.36×10^8 $M^{-1}s^{-1}$) with high affinity (K_d is approximately 0.1 μM), and is an accurate probe for Pi in solution at low concentrations (Brune *et al.*, 1994). The release of Pi from βD380C-F_1 was monitored by 20 μM MDCC-PBP in the fluorescence stopped-flow spectrometer (see *Experimental Procedures*) using essentially the same reaction

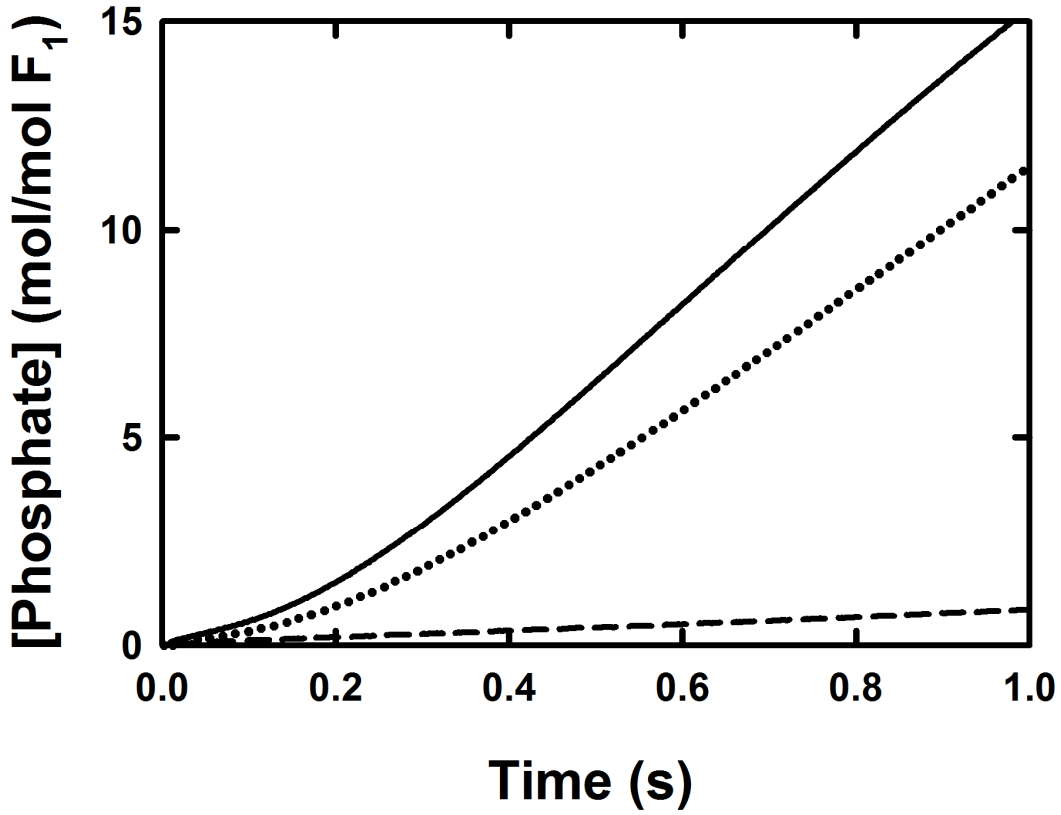

Figure 3.4.6. Pre-steady release of Pi by βD380C-F_1.

Details are given in the *Experimental Procedures* for the stopped-flow set up. F_1 was prepared as described in the *Experimental Procedures*, giving 4.0 ± 0.1 mol nucleotide bound per mol F_1, equilibrated with 25 mM TES/KOH, 0.244 mM $MgCl_2$, 0.2 mM EDTA pH 7.5 at 25 °C, diluted to 1 μM with the same buffer, and loaded in Syringe A. The ATP and $MgCl_2$ concentrations in Syringe B resulted in a final free Mg^{2+} of ~50 μM and 105 μM Mg·ATP. The stopped-flow syringe also contained 20 μM MDCC-PBP. The traces of MDCC-PBP fluorescence show Pi released from the enzyme, and was calibrated by measuring the fluorescence response to known concentrations of Pi. The response loses linearity above ~16 μM due to saturation of Pi binding. Each trace is the average of at least 3 stopped-flow mixing experiments. The noise in the averaged data is within the thickness of the lines shown. The *solid line* shows the Pi release from the untreated F_1, the *dashed line* depicts that from the γ–β cross-linked F_1 and the *dotted line* is the Pi release from the partially reduced cross-linked sample after incubation with 5 mM DTT.

conditions as the quench flow experiment. Calibration experiments demonstrate that the fluorescence response of MDCC-PBP to rapid addition of 1 - 20 μM Pi is within the 1 - 2 ms deadtime of the stopped-flow instrument (data not shown). Ideally the rate of Pi release from F_1 would be directly determined from this experiment, however upon further examination it was evident that the PBP interacts both directly and indirectly with F_1, resulting in a slight inhibition of ATP hydrolysis (data not shown). Although this negates quantitative analysis of the data, qualitative analysis can still yield valuable information. The Pi release data are valid up to ~16 μM of released Pi due to the limiting amount of MDCC-PBP. Around this point, the fluorescence signal begins to saturate and no longer follows the hydrolysis kinetics. It is clear that upon formation of the rotation-inhibiting γ-β cross-link, the enzyme is prevented from releasing product Pi (Fig. 3.4.6). There is a very slow residual rate of Pi release but this is due to a small amount of uncross-linked enzyme in the sample. Upon addition of DTT, the rate of Pi release increases, and approaches the initial rate before treatment with DTNB. In this particular case the DTT treated enzyme had a slightly slower steady state rate due to incomplete reduction of the γ-β cross-link. This demonstrates the reversible nature of the blockage of Pi release and that it is dependent on disulfide bond formation.

In the cases of the non-cross-linked enzymes, we note that there is no burst of Pi release as shown for βD380C-F_1 (Fig. 3.4.6), but rather a lag before Pi is released which indicates a delay between hydrolysis of Mg·ATP (Fig. 3.4.5A) and the release of Pi, and emphasizes the hydrolytic step is kinetically distinct from k_γ and Pi release. Above all, these results show that γ subunit rotation, while not essential for the first cycle of ATP

hydrolysis, is absolutely integral for decreasing the enzyme affinity for Pi, thus enabling F_1 to release Pi and enter into the steady state mode of hydrolysis.

3.5 Discussion

3.5.1 γ-β cross-link blocks the rotation step, k_γ.

γ-β cross-link blocks the rotation step, k_γ. The γ87Cys-β cross-link is effective in inhibiting steady state activity for both the βD380C and βE381C enzymes (Table 3.4.1, Fig. 3.4.4 and 3.4.5) under high Mg·ATP conditions, consistent with the notion that inhibition of rotation prevents the enzyme from entering the steady state mode. It is obvious from the multisite fit parameters in Table 3.4.2 that the steps most affected by cross-linking are k_γ, and steps subsequent to k_γ in the reaction scheme. k_γ is arrested and aside from a low rate of Pi release, which was shown to be due to a very small fraction of uncross-linked enzyme, the data could be well fit to a minimal model with no steps subsequent to the hydrolytic step (k_{+2}). Pi release is the major energy producing process in the hydrolysis mode based on evidence from the synthesis direction that productive Pi binding requires an input of energy (Al-Shawi *et al.*, 1997b), and does not occur without the F_O transport moiety and a proton motive force (Al-Shawi *et al.*, 1990b; Al-Shawi and Senior, 1988; Al-Shawi and Senior, 1992; Grubmeyer *et al.*, 1982; Weber *et al.*, 1993). Concurring with this is the unidirectional rotation of F_1 which does not rotate in reverse under high Mg·ATP conditions (Noji *et al.*, 1997; Yasuda *et al.*, 1998). Product Pi is not released from the γ-β cross-linked enzyme, as demonstrated by use of the PBP-MDCC Pi

detection system (Fig. 3.4.6), indicating that the γ subunit cannot rotate to carry out the power stroke which is required to release Pi. Clearly the enzyme is stuck at the hydrolysis step. Additional evidence that k_γ involves γ subunit rotation step is provided by unisite analysis, which does not require a rate-limiting step to fit the data, and shows no change in the rate constants upon γ-β cross-link formation (Table 3.4.2 and (García and Capaldi, 1998)).

3.5.2 γ-β cross-linked enzymes assume the 80° conformation, and allow assignment of catalytic sites.

The γ-β cross-linked enzymes retain the burst of ATP hydrolysis (Fig. 3.4.4B and 3.4.5B), showing that the enzyme can hydrolyze substrate during the first cycle despite the rotation-inhibiting cross-link. However, direct effects on the rotational behavior of single molecules of F_1 incubated with the slowly hydrolysable substrate, ATPγS (Nishizaka *et al.*, 2004; Shimabukuro *et al.*, 2003), and of F_1 complexes containing the hydrolysis-impeding βE190D mutation (Ariga *et al.*, 2007), show that hydrolysis occurs during the dwell after the 80° γ subunit rotation, and before the 40° γ subunit rotation. We can reconcile these results by considering the conformational state of the cross-linked enzyme. The data are consistent with the γ-β cross-link rigidly locking the enzyme in a conformation similar to that achieved after the 80° rotation, depicted by the *red symbols* (§) in Fig 8. This is in agreement with the conclusion from the fluorescence study by Yasuda *et al.* (Yasuda *et al.*, 2003) that the crystal structures solved by the Walker group

(Abrahams *et al.*, 1994; Braig *et al.*, 2000; Gibbons *et al.*, 2000; Stock *et al.*, 1999) are more similar to the 80° conformation of the enzyme.

In fact, the conformation of the cross-linked enzyme allows us to distinguish between unisite and multisite rotational catalysis. Under multisite conditions, when rotation is inhibited by the γ-β cross-link, the rate of the hydrolytic burst is slower (Fig. 3.4.4B and 3.4.5B), due to 2 orders of magnitude slower ATP binding (k_{+1}), and 5 orders of magnitude slower ATP unbinding (k_{-1}), compared to the uncross-linked and wild-type enzymes (Table 3.4.2). We note that these rates for k_{+1} and k_{-1} are similar to all enzymes in unisite conditions, therefore unisite experiments and cross-linked multisite behavior reflect binding of Mg·ATP to the same site, β_{TP}. This is in contrast to the rates of ATP binding and unbinding in the multisite uncross-linked and wild-type enzymes which we have previously shown are due to binding to the low affinity β_E site (Baylis Scanlon *et al.*, 2007).

3.5.3 Effect of β^{380}DELSEED^{386} mutations on the high affinity catalytic site, β_{TP}.

The parameter fits to the unisite data of the βE381C and βD380C enzymes elucidate slight but significant differences between the two mutants. Based on the unisite experiments (Table 3.4.2), the βE381C mutant has an affinity for ATP that is similar to wild-type, while the effect of the βD380C mutation is to decrease the affinity of the β_{TP} catalytic site for ATP, by about 500-fold. Upon formation of the γ-β cross-link, differences between the mutants are no longer apparent. Both cross-linked enzymes exhibit a decreased affinity for Mg·ATP at the β_{TP} site, compared with wild-type, because

both have 2 orders of magnitude lower affinity (k_{+1}/k_{-1}) in unisite conditions (Table 3.4.1).

The two β^{380}DELSEED^{386} Cys mutations examined here have increased unisite rates of ATP hydrolysis, k_{+2}, and resynthesis, k_{-2}, (Table 3.4.2)however they do not have a drastic effect on altering the catalytic mechanism, because the catalytic equilibrium constant, K_2, and the specificity constant, k_{cat}/K_M, remain unaltered from wild-type values. The βE381C and βD380C mutations appear to affect the conformation of the high affinity catalytic site, β_{TP}, as indicated by the lower affinity in unisite conditions and in the cross-linked enzyme under multisite conditions. In contrast analysis of multisite catalysis shows these mutations do not seem to have much influence on β_E (Table 3.4.2) because k_{+1} and k_{-1} of uncross-linked and wild-type enzymes are not affected. These results demonstrate the role of specific βDELSEED residues, and their interaction with the γ subunit, in establishing the proper conformation of the catalytic site at the proper time during rotational catalysis. This conclusion was previously made by analysis of γ subunit mutations (Al-Shawi *et al.*, 1997a), and is particularly interesting considering that the βDELSEED motif is physically distant from the nucleotide binding sites (Fig. 3.2.1).

3.5.4 Role of the βGlu381 of the β^{380}DELSEED^{386} motif in chemomechanical coupling.

The marked functional differences between the two β^{380}DELSEED^{386} single Cys mutants become more apparent in the multisite mode of rotational catalysis, and are particularly interesting because of their adjacent positions in the sequence. The βD380C mutant has very similar characteristics to wild-type, and the transmission of coupling

energy between the two distinct functions of proton translocation and ATP hydrolysis/synthesis is intact, *i.e.* it is a well coupled enzyme. This mutant can be used as a close representation of the activity and behavior of the wild-type enzyme. In contrast to the βD380C mutant, the βE381C mutant behaves in a manner dissimilar to the wild-type enzyme with characteristics indicating that catalysis and rotation are not efficiently coupled in this enzyme. Interestingly, Garcia and Capaldi used the βE381C enzyme (García and Capaldi, 1998) and must have been measuring an uncoupled enzyme. This would not affect their conclusions as most of their measurements were of unisite kinetics and transmission of coupling information requires γ subunit rotation and consequently participation of all three catalytic sites (Weber *et al.*, 1993). Indeed, functional differences in coupling between the βE381C and βD380C mutants are alleviated when the γ-β cross-link is induced, validating the conclusion that the high energy transition state involves the power stroke rotation of the γ subunit, and specific interactions at the γ-β interface are critical for proper transmission of coupling energy (Al-Shawi *et al.*, 1997a).

The multisite kinetic rate constants of the uncross-linked βE381C-F_1 were very similar to wild-type, with the exception of k_γ (Table 3.4.2). This enzyme hydrolyzes ATP faster than wild-type due to a much faster k_γ (Table 3.4.2), which is no longer the rate-limiting step of the reaction. The power stroke is no longer fully engaged in this mutant as it likely slips frequently, and goes through a different pathway, allowing the enzyme to release Pi without complete rotation of γ. An analogy for this fast, yet unproductive hydrolysis is the revving of a car engine with a partially disengaged or slipping clutch.

The β^{380}DELSEED^{386} loop in a sense is the clutch motif which engages the γ subunit to cause rotation.

The uncoupling between the catalytic reaction and the rate-limiting rotation step, k_γ, is likely the cause of inefficient transmission of information to the F_O transport sector (Fig. 3.4.1B). We propose that the alternate, uncoupled pathway does not involve full rotation of the γ subunit. The γ and ε subunits are not mutated, neither is the F_O complex, therefore for each ATP hydrolyzed, a complete 120° rotation of γ should drive H^+ transport. The 80° degree ATP-dependent rotation step is unaffected in the βE381C mutant, based on the similar rates of ATP binding and unbinding (k_{+1} and k_{-1}), and ATP hydrolysis and resynthesis (k_{+2}, k_{-2}). Whereas, in contrast, k_γ, the rate-limiting step correlated with the 40° substep, is severely perturbed such that it is two orders of magnitude faster, and appears to be the step that slips. Complete inhibition of rotation by the γCys87-βE381C cross-link prevents Pi release and abrogates enzyme activity after the first cycle. The alternate pathway is also inhibited by the cross-link showing that partial rotation is necessary for activity. In the alternate pathway, it is likely that the slip of the rotation allows the γ subunit to fall back to the position prior to the 80° substep for a new cycle of hydrolysis (Al-Shawi *et al.*, 1997b). We speculate the mechanism for this involves Pi release from the β_{TP} site instead of the β_{DP} site (Fig. 3.4.7), without the 40° rotation of γ, thereby altering the timing and coupling between rotation and Pi release.

The much higher rate constant for k_γ implies a lower transition state for the alternate, uncoupled pathway so the βE381C mutation has made this bypass pathway in the reaction more likely. This is reminiscent of the γM23K mutation which established

that an alternative pathway of hydrolysis can exist (Nakamoto *et al.*, 1999). Thermodynamic analysis of the γM23K mutation revealed that inefficient communication of coupling energy, from the catalytic sites to the F_O transport sector, was due to increased energy of interaction between γ and β possibly caused by an extra ionized hydrogen bond between the mutant and βGlu381 (Al-Shawi *et al.*, 1997a). The γM23K mutant impeded k_γ, the rate-limiting transition state, and resulted in a slip or branch in the pathway allowing unproductive dissipation of energy (Al-Shawi *et al.*, 1997a; Al-Shawi and Nakamoto, 1997; Ketchum *et al.*, 1998). Importantly this resulted in a 50-fold increase in the rate of Pi release (Al-Shawi and Nakamoto, 1997), emphasizing that the very tight association between k_γ and Pi release is required for efficient coupling.

βE381C-F_1 may rotate under a load as seen by Hara *et al*. (Hara *et al.*, 2000) who observed similar torque generation by the Bacillus PS3 thermophilic enzyme with an Ala mutation at the β381 position. They suggested that the side chain charges of the β^{380}DELSEED^{386} motif do not play a role in torque generation, and proposed a stearic role for the loop in driving the γ subunit rotation. However, it is expected that a slipping mutation would either generate full torque or not at all during a slip. In the single molecule studies, slip events cannot be distinguished. In other words, the limitation of these measurements is that the catalytic reaction, especially release of products cannot be observed concurrent with observations of rotation.

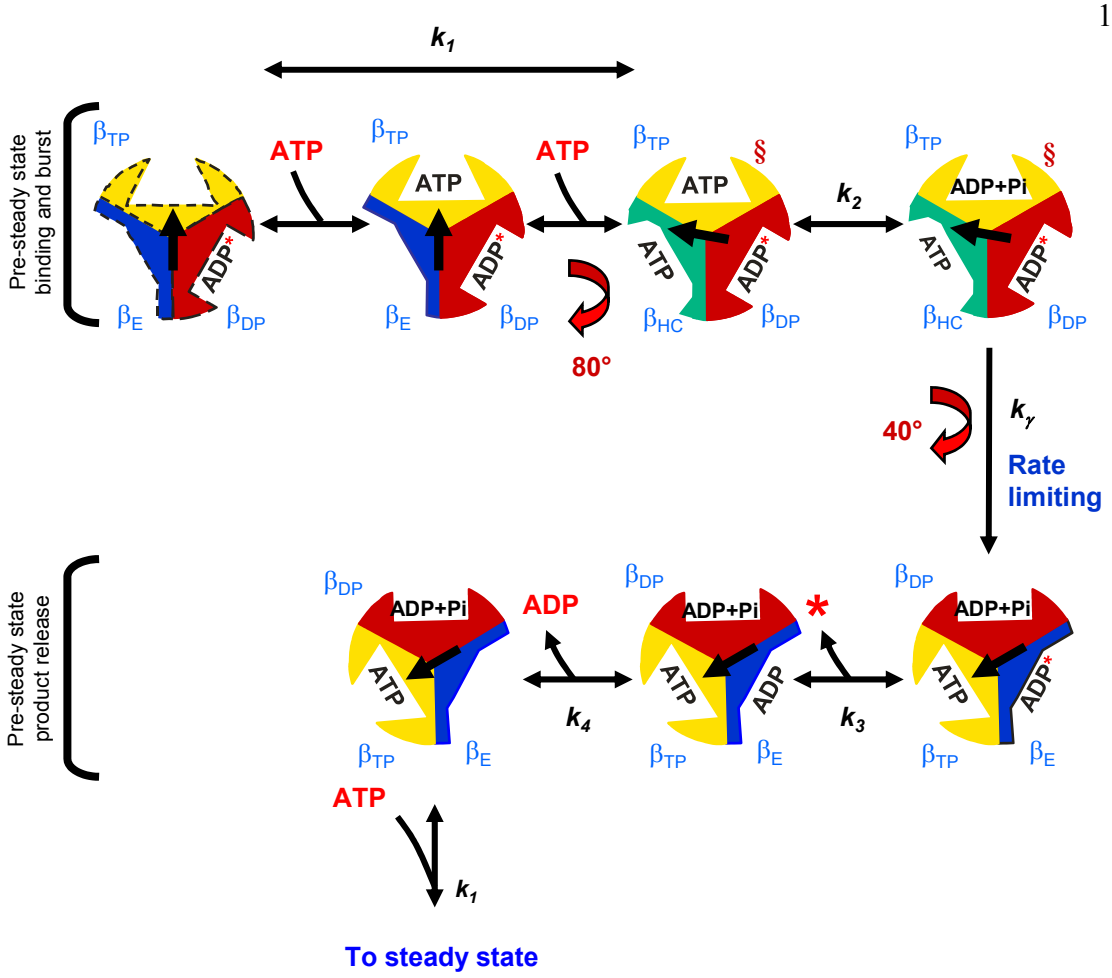

Figure 3.4.7. Graphical representation of the pre-steady state to steady state pathway.

See text for discussion of the model. The relative arrangement of the γ subunit conformations are as viewed from the "bottom" of the complex from the membrane. The conformations of the catalytic sites are labeled as β_{DP}, β_{TP}, β_{E}, and β_{HC} (the half closed conformation described in Menz *et al*. (Menz *et al.*, 2001)). The a subunits were omitted for clarity. The central arrow represents the relative position of the γ subunit during the course of multi-site catalysis. The intermediate rotation of 80° and the completion of rotation to the next 120° position corresponds to the dwell positions observed by Yasuda *et al*. (Yasuda *et al.*, 2001). The red symbols (§) depict the steps in the pathway we propose are closest to the conformation of the cross-linked enzyme. We propose that unisite hydrolysis of ATP by the wild-type enzyme occurs in a conformation similar to that depicted prior to the 80° rotation step where ATP is bound only to the β_{TP} site, and no nucleotide is bound to the β_{E} site. In the steady state, the position of the γ subunit is offset 120° for each cycle in the steady state. The asterisk indicates that there is no Pi release in the first pre-steady state cycle (see (Baylis Scanlon *et al.*, 2007) for discussion).

Further evidence for the role of the β^{380}DELSEED^{386} region comes from rotational behavior of F_1 containing γ subunits with truncated axels (Furuike *et al.*, 2008). The region of the β subunits which interact with the γ subunit at the point where γ extends from the central cavity of the $\alpha_3\beta_3$ ring, were seen to be important in directing γ rotation by blocking backward diffusion, thus ensuring efficient torque generation (Furuike *et al.*, 2008). The authors also implicated the N- and C-termini of the γ helices and their interactions with the β subunit as being important for the "rapid progress of catalysis" (Furuike *et al.*, 2008). This is consistent with our observations of positive catalytic cooperativity being unaffected by the γ–β cross-link formation (Table 3.4.2), implicating a region of γ–β interaction, other than the region around the β^{380}DELSEED^{386} motif, as mediating positive catalytic cooperative effects.

3.5.5 Implications for our model of rotational catalysis.

Our model remains essentially the same as that previously published (Baylis Scanlon *et al.*, 2007). We have modified the graphical representation to show only the pre-steady state steps of the reaction, and to illustrate enzyme rotation as viewed from the "bottom" or direction of the membrane for consistency with model illustrations presented by investigators measuring single particle rotation behavior (Fig. 3.4.7). Our analysis in this paper clarifies the roles of each site where binding of ATP to β_E promotes the hydrolysis/synthesis rates occurring in β_{TP}, which occurs even in the cross-linked

enzymes. β_{DP} retains products of hydrolysis from the previous cycle and releases them after it changes conformation to β_E. Our results indicate that perturbation of the 40° rotation step leading to product release is responsible for the alternate, uncoupled pathway of the βE381C enzyme. This is consistent with observations of others (Adachi *et al.*, 2007; Ariga *et al.*, 2007; Nishizaka *et al.*, 2004), that ATP bound to the β_E site in the first cycle, when γ is at 0°, is hydrolyzed during the second 120° cycle, specifically after γ has rotated through 200° (120° + 80°) (Fig. 3.4.7). However, our model differs from theirs in that we propose that ADP is released after β_{DP} converts to β_E (after completion of the third cycle when γ has rotated through 360°). This is in keeping with the results of Weber *et al*. (Weber *et al.*, 1993) that the three catalytic sites are almost always occupied with nucleotide during steady state. A temperature-sensitive, ADP-dependent reaction intermediate for the Bacillus PS3 thermophilic enzyme was recently detected at low temperatures. This intermediate occurred before the 80° substep during the ATP binding dwell, and was assigned to ADP release (Watanabe *et al.*, 2008). These results are in agreement with our model where ADP is released after the γ subunit has completed a 360° rotation cycle, before binding of another ATP molecule to that site.

A recent study of the timing of Pi release and γ subunit rotation (Adachi *et al.*, 2007), in contrast to our data, suggests that Pi is released before the 40° rotational

substep, based on the effects on the substeps upon incubation with Pi. While we agree with their conclusion that the Pi release reaction is directly coupled to the 40° rotation, our data suggest that Pi is not released before the rate-limiting rotation step k_γ. Ariga *et al.* (Ariga *et al.*, 2007) defined a "third catalytic event," an extended dwell occurring between the 80° and 40° substeps in the third cycle, and attributed this to Pi release from the single βE190D mutated catalytic site of a hybrid F_1 complex (in the β_{DP} conformation at this point in the cycle) (Fig. 1.5.4). Our data are consistent with Pi release after the 40° rotation step, therefore we suggest this dwell is due to slowed ATP catalysis at the adjacent (wild-type) β_{TP} catalytic site. It is certainly possible that perturbations at one site are readily communicated to the other catalytic sites due to the highly cooperative nature of the enzyme. We could only fit the pre-steady state data with k_γ preceding k_{+3} (Baylis Scanlon *et al.*, 2007). In addition, if Pi were released before the k_γ step, we would expect that K_2 would be dramatically altered. Blocking k_γ by the cross-link did not perturb the K_2 ratio, therefore there must be an intervening, energy producing step between hydrolysis, k_{+2}, and Pi release, k_{+3}.

This analysis further elucidates the role for each partial rotation in the multisite reaction. The 40° rotational substep is associated with k_γ, the rate-limiting step, and the 80° substep with the conformation required for the promotion of catalysis. Several lines of evidence lead to these conclusions. k_γ was previously determined to occur after hydrolysis and before Pi release (Baylis Scanlon *et al.*, 2007), and single molecule studies place the 40° substep after hydrolysis (Shimabukuro *et al.*, 2003). Here we showed k_γ, and steps subsequent to k_γ, were severely perturbed when rotation was blocked by the γ-β

cross-link under multisite conditions. In the unisite mode, which does not involve γ subunit rotation, there was no change in the rate constants upon formation of the γ-β cross-link. Analysis of the βE381C uncoupling mutant revealed that k_γ was affected by the mutation, consistent with previous studies which implicated the specific interaction between this residue and the γ subunit at Met23 and Arg242 for proper formation of the rate-limiting transition state hypothesized to involve γ subunit rotation (Al-Shawi *et al.*, 1997a; Ketchum *et al.*, 1998). Essentially in each case where k_γ is perturbed, K_2 is unaffected showing k_γ is independent of hydrolysis. The 80° rotational substep allows the enzyme to achieve the conformation required for the promotion of catalysis. This was shown by the cross-linked enzymes, which in multisite conditions show unperturbed positive catalytic cooperativity with promoted rates of hydrolysis and resynthesis of ATP (k_{+2} and k_{-2}) similar to uncross-linked enzymes and wild-type. Further evidence comes from the uncross-linked F_1 with the βE381C mutation in which the ATP binding/unbinding (k_{+1}, k_{-1}) and ATP hydrolysis/resynthesis (k_{+2}, k_{-2}) parameters are unaltered, even though k_γ was strongly perturbed. Together, these results link the 80° ATP-dependent substep to the promoted catalytic rates.

4. Perspectives

A reasonable argument could be made that the F_OF_1 ATP synthase is the most important protein for multicellular life, so central is its role in metabolism and bioenergetics. It couples the electrical and chemical energy of the ion gradient across the membrane to the chemical reaction of ATP synthesis or hydrolysis through an incredibly efficient rotary mechanism. The mechanism by which it transduces these various types of energy remains enigmatic. High resolution structures of the complete F_O complex would provide information on the molecular details of subunit interactions and help to elucidate the ion transport mechanism. Further structures of the F_1 domain representing different states along the catalytic pathway, and assignment of these to specific steps of the chemical reaction are needed to understand the rotational catalytic cycle at the molecular level. Finally higher resolution structures of the F_OF_1 ATP synthase would reveal specifics of the multiple subunit interactions required for function of the holoenzyme. In addition, structures of the *E. coli* and Bacillus PS3 complexes are required for interpretation of the extensive amount of biochemical, mutagenic and rotational data obtained from these enzymes, in relation to the molecular structure. However while greater structural information is needed, the F_OF_1 enzyme is dynamic and thermodynamically and kinetically complex so static structures are only part of the process towards understanding enzyme function.

A kinetic and thermodynamic approach yields important mechanistic information, critical for understanding the complex, multi-component process of rotational catalysis.

Mutagenic analyses combined with unisite reaction kinetics of ATP hydrolysis, thermodynamic analyses, and nucleotide binding measurements, identified critical residues and their roles in the catalytic mechanism (reviewed in (Senior *et al.*, 2002; Weber and Senior, 2000; Weber and Senior, 2004). However, determination of which partial reaction step was affected under physiological, multisite conditions was not previously possible. This work provides the chemical framework to address such issues, because for the first time, under conditions involving all three catalytic sties, the kinetic rate constants for Mg·ATP hydrolysis by the wild-type F_1-ATPase in the rotational catalytic mode have been assessed. In addition, thermodynamic calculations may now be performed on the kinetic rate constants of the partial reactions of rotational catalysis in a similar manner as was performed on unisite parameters (Al-Shawi *et al.*, 1989; Al-Shawi *et al.*, 1990b). The intermediate thermodynamic states of multisite catalysis can then be compared to the unisite relative transition and ground energy levels, which will provide information on the cooperative promotion of catalysis by the enzyme. It is reasonable to anticipate that complementing mutagenesis with pre-steady state kinetic and thermodynamic analyses will prove to be a powerful combination to address many of the yet unresolved questions in the field.

One area, not yet fully understood, is the chemomechanical coupling of F_1-ATPase. The analysis of the cross-linked enzymes clarified the order of the rate-limiting step, k_γ, in the reaction mechanism, solidified the conclusion that it is indeed a rotation step and revealed aspects of the roles of the rotational substeps. However, further insights into the role of rotation in the catalytic mechanism may be gained by taking

advantage of mutant enzymes that cause abnormal rotation or coordination of rotation of the γ subunit and perturb the kinetics of the steady state ATP hydrolytic reaction. An example of such a mutation is the βSer174 to Phe (βS174F) substitution which was shown to be mechanically defective by reducing torque generated by the enzyme (Iko *et al.*, 2001). Another substitution at this position (βS174L) is thought to be defective at the step of hydrolysis and several other residues that appear to be important for torque generation in the local domain that interact with βSer174 have been identified. ((Nakanishi-Matsui *et al.*, 2007)). Further study of such mutant enzymes may be revealing of the torque generating mechansm Another candidate for furthering the understanding of the chemomechanical coupling mechanism is F_1 with the γT106C mutation labeled with N-[4-[7-(diethylamino)-4-methyl]coumarin-3-yl)]maleimide (CM). This labeled enzyme exhibits a fluorescence response of CM upon ATP binding correlated with a conformational change of γ (Turina and Capaldi, 1994) and may be useful for monitoring more directly the pre-steady state kinetics of γ subunit movement upon addition of Mg·ATP.

Another essential aspect of enzyme function, involving coordinated, complicated, inter- and intra-subunit interactions throughout the entire complex, is the coupling between the catalytic and transport mechanisms. The details of how such a large enzyme achieves efficient communication between disparate functions, by preventing dissipation of energy through alternate pathways, is difficult to dissect. Determination of the pre-steady state kinetics of the βE381C mutant provided insights into the role of the $\beta D^{380}ELSEED^{386}$ motif in the coupling function of the enzyme. Further examination of

several mutants which have been shown to alter the transition state energy of the enzyme, and disrupt coupling efficiency may help unravel the complex interplay between catalytic substeps and transport. Similar analysis may be performed on the γM23K mutant F_1, which interacts with βGlu381 and γArg242, and also perturbs coupling efficiency of the enzyme (Al-Shawi *et al.*, 1997a; Al-Shawi and Nakamoto, 1997). At higher temperatures the greater prevalence of an alternate uncoupled pathway in the γM23K mutant, and its effect on the rotational step, can be tested and would further our understanding of the role of this region (near γMet23, γArg242 and βGlu381, see Fig. 1.6.1), and specifically the role of the γMet23 residue, in rotational catalysis. Other residues important for efficient coupling were identified by mutagenesis and second site suppressor mutations of γM23K, and are located in the region of the γ terminal α-helix around γGln269-Ala280 (Nakamoto *et al.*, 1995; Nakamoto *et al.*, 1993). Further analysis of these would help understand the role of the domain (γ18-35, γ236-246 and γ269-280), which is critical for efficient coupling and catalytic function. Analyses of these will be useful for testing and refining our model of the rotational catalytic mechanism.

A significant area for further research is the role of the ε subunit in the regulation of enzyme activity. This is an extension of our work on the βE381C mutant, as the regulation is mediated in part through the ε C-terminal interaction with the $\beta D^{380}ELSEED^{386}$ motif (Hara *et al.*, 2001). The C-terminus of the ε subunit is proposed to function as a ratchet, which interacts with the $\alpha_3\beta_3$ hexamer allowing ATP synthesis, but inhibiting ATP hydrolysis during enzyme turnover (Tsunoda *et al.*, 2001b). If this

hypothesis is correct, mutagenesis combined with kinetic and thermodynamic analyses under steady state conditions could reveal the role of the interaction between the C-terminus of the ε subunit and the $\alpha_3\beta_3$ hexamer during enzyme turnover. ε also plays a role in coupling (Capaldi and Schulenberg, 2000; Cipriano and Dunn, 2006; Peskova and Nakamoto, 2000). We have observed empirically that Cys mutations in the $\beta D^{380}ELSEED^{386}$ cause ε to dissociate more readily, particularly in the partially uncoupled βE381C mutant (unpublished data, Baylis Scanlon, J. A. and Lin, S.-K.). The uncoupling effect on the enzyme may be due to parital dissociation of ε (Cipriano and Dunn, 2006). However, the C-terminal helix of ε interacts with the $\beta D^{380}ELSEED^{386}$ motif, therefore disruption of this interaction may alter the energetics of transition state formation and therefore the rate-limiting rotational step. ε has a low affinity for ATP, and upon binding ATP assumes the "down" or folded conformation (Iino *et al.*, 2005). Perhaps this conformation, with the C-terminal folded near the interface of interaction with the *c*-ring (see Fig. 1.5.3C) is required to maintain efficient coupling. Further analysis could provide insight into the role of the ε subunit, and its isomerization state in regulation and coupling which is critical to efficient enzyme function, and is not fully understood. It is also important to note that single molecule rotational studies deplete the enzyme of ε, which potentially uncouples rotation from catalysis and may explain certain discrepancies, particularly in the timing of product Pi and ADP release.

Although kinetic analyses in F_1 have provided invaluable mechanistic insights these have not been applied extensively to F_O and F_OF_1. Given the enzyme's physiological role is ATP synthesis and/or proton pumping, the obvious avenue to pursue

is to apply the pre-steady state kinetics approach to ATP hydrolysis and synthesis in the F_OF_1 enzyme. This would provide information useful for understanding the H^+ transport mechanism and ultimately the electro-chemomehanical coupling. An interesting aspect of the transport mechanism is that there are two components of $\Delta\mu_{H+}$ (the membrane potential and pH gradient) that are not kinetically equivalent, and that a membrane potential threshold is critical for ATP synthesis (Dimroth *et al.*, 2000). Interestingly, the requirement for the membrane potential in ATP synthesis has been attributed to the interaction of F_1 with F_O because isolated F_O transports H^+ across the membrane with a pH gradient alone (Feniouk *et al.*, 2004). One can speculate that the obligatory role of the membrane potential is mediated through the ε subunit. This aspect of transport is an intriguing area for further study. In addition, analysis of mutants with disrupted coupling efficiency, and their effects on the kinetics of hydrolysis and synthesis of ATP in F_OF_1, will be crucial to understanding the mechanism of coupling between catalysis and transport in the enzyme.

5. References

Abrahams, J.P., S.K. Buchanan, M.J. van Raaij, I.M. Fearnley, A.G.W. Leslie, and J.E. Walker. 1996. The structure of bovine F_1-ATPase complexed with the peptide antibiotic efrapeptin. *Proc. Natl. Acad. Sci. U. S. A.* 93:9420-9424.

Abrahams, J.P., A.G.W. Leslie, R. Lutter, and J.E. Walker. 1994. Structure at 2.8 Å resolution of F_1-ATPase from bovine heart mitochondria. *Nature*. 370:621-628.

Adachi, K., K. Oiwa, T. Nishizaka, S. Furuike, H. Noji, H. Itoh, M. Yoshida, and K. Kinosita, Jr. 2007. Coupling of rotation and catalysis in F_1-ATPase revealed by single-molecule imaging and manipulation. *Cell*. 130:309-21.

Aggeler, R., S.X. Cai, J.F.W. Keana, T. Koike, and R.A. Capaldi. 1993. The γ subunit of the *Escherichia coli* F_1-ATPase can be cross-linked near the glycine-rich loop region of a β subunit when ADP+Mg^{2+} occupies catalytic sites but not when ATP+Mg^{2+} is bound. *J. Biol. Chem.* 268:20831-20837.

Aggeler, R., and R.A. Capaldi. 1992. Cross-linking of the γ subunit of the *Escherichia coli* ATPase (ECF_1) via cysteines introduced by site-directed mutagenesis. *J. Biol. Chem.* 267:21355-21359.

Aggeler, R., and R.A. Capaldi. 1996. Nucleotide-dependent movement of the ε subunit between α and β subunits in the *Escherichia coli* F_1F_O-type ATPase. *J. Biol. Chem.* 271:13888-13891.

Aggeler, R., G. Grüber, and R.A. Capaldi. 1998. Trapping of conformations of the *Escherichia coli* F_1 ATPase by disulfide bond formation. *FEBS Lett.* 426:37-40.

Aggeler, R., M.A. Haughton, and R.A. Capaldi. 1995a. Disulfide bond formation between the COOH-terminal domain of the β subunits and the γ and ε subunits of the *Escherichia coli* F_1-ATPase. *J. Biol. Chem.* 270:9185-9191.

Aggeler, R., I. Ogilvie, and R.A. Capaldi. 1997. Rotation of a γ-ε subunit domain in the *Escherichia coli* F_1F_O-ATP synthase complex. *J. Biol. Chem.* 272:19621-19624.

Aggeler, R., F. Weinreich, and R.A. Capaldi. 1995b. Arrangement of the ε subunit in the *Escherichia coli* ATP synthase from the reactivity of cysteine residues introduced at different positions in this subunit. *Biochim. Biophys. Acta*. 1230:62-68.

Ahmad, Z., and A.E. Senior. 2005a. Identification of phosphate binding residues of Escherichia coli ATP synthase. *J Bioenerg Biomembr*. 37:437-40.

Ahmad, Z., and A.E. Senior. 2005b. Involvement of ATP synthase residues alphaArg-376, betaArg-182, and betaLys-155 in Pi binding. *FEBS Lett*. 579:523-8.

Akaike, H. 1974. A new look at the statistical model identification. *IEEE Trans. Automat. Contrl.* 19:716-723.

Akaike, H. 1976. What is Akaike Information Criterion? *Math. Sciences*. 14:5-11.

Aksimentiev, A., I.A. Balabin, R.H. Fillingame, and K. Schulten. 2004. Insights into the molecular mechanism of rotation in the Fo sector of ATP synthase. *Biophys J.* 86:1332-44.

Al-Shawi, M.K., C.J. Ketchum, and R.K. Nakamoto. 1997a. Energy coupling, turnover, and stability of the F_OF_1 ATP synthase are dependent on the energy of interaction between g and b subunits. *J. Biol. Chem.* 272:2300-2306.

Al-Shawi, M.K., C.J. Ketchum, and R.K. Nakamoto. 1997b. The *Escherichia coli* F_OF_1 γM23K uncoupling mutant has a higher $K_{0.5}$ for Pi. Transition state analysis of this mutant and others reveals that synthesis and hydrolysis utilize the same kinetic pathway. *Biochemistry*. 36:12961-12969.

Al-Shawi, M.K., and R.K. Nakamoto. 1997. The mechanism of energy coupling in the F_OF_1-ATP synthase: the uncoupling mutation, γM23K, disrupts the use of binding energy to drive catalysis. *Biochemistry*. 36:12954-12960.

Al-Shawi, M.K., D. Parsonage, and A.E. Senior. 1988. Directed mutagenesis of the strongly conserved aspartate 242 in the β-Subunit of *Escherichia coli* proton-ATPase. *J. Biol. Chem.* 263:19633-19639.

Al-Shawi, M.K., D. Parsonage, and A.E. Senior. 1989. Kinetic characterization of the unisite catalytic pathway of seven β-subunit mutant F_1-ATPases from *Escherichia coli*. *J. Biol. Chem.* 264:15376-15383.

Al-Shawi, M.K., D. Parsonage, and A.E. Senior. 1990a. Adenosine triphosphatase and nucleotide binding activity of isolated β-subunit preparations from *Escherichia coli* F_1F_o-ATP synthase. *J. Biol. Chem.* 265:5595-5601.

Al-Shawi, M.K., D. Parsonage, and A.E. Senior. 1990b. Thermodynamic analyses of the catalytic pathway of F_1-ATPase from *Escherichia coli*. *J. Biol. Chem.* 265:4402-4410.

Al-Shawi, M.K., and A.E. Senior. 1988. Complete kinetic and thermodynamic characterization of the unisite catalytic pathway of *Escherichia coli* F_1-ATPase. *J. Biol. Chem.* 263:19640-19648.

Al-Shawi, M.K., and A.E. Senior. 1992. Catalytic sites of *Escherichia coli* F_1-ATPase. Characterization of unisite catalysis at varied pH. *Biochemistry*. 31:878-885.

Allen, R.D., C.C. Schroeder, and A.K. Fok. 1989. An investigation of mitochondrial inner membranes by rapid-freeze deep-etch techniques. *J Cell Biol*. 108:2233-40.

Andrews, S.H., Y.B. Peskova, M.K. Polar, V.B. Herlihy, and R.K. Nakamoto. 2001. Conformation of the γ subunit at the γ-ε-c interface in a complete *Escherichia coli* F_1-ATPase complex by site-directed spin labeling. *Biochemistry*. 40:10664-10670.

Angevine, C.M., and R.H. Fillingame. 2003. Aqueous access channels in subunit a of rotary ATP synthase. *J. Biol. Chem.* 278:6066-74.

Angevine, C.M., K.A. Herold, and R.H. Fillingame. 2003. Aqueous access pathways in subunit a of rotary ATP synthase extend to both sides of the membrane. *Proc. Natl. Acad. Sci. U. S. A.* 100:13179-83.

Angevine, C.M., K.A. Herold, O.D. Vincent, and R.H. Fillingame. 2007. Aqueous access pathways in ATP synthase subunit a. Reactivity of cysteine substituted into transmembrane helices 1, 3, and 5. *J. Biol. Chem.* 282:9001-7.

Ariga, T., E. Muneyuki, and M. Yoshida. 2007. F1-ATPase rotates by an asymmetric, sequential mechanism using all three catalytic subunits. *Nat. Struct. Mol. Biol.* 14:841-6.

Arnold, I., K. Pfeiffer, W. Neupert, R.A. Stuart, and H. Schagger. 1998. Yeast mitochondrial F1F0-ATP synthase exists as a dimer: identification of three dimer-specific subunits. *Embo J*. 17:7170-8.

Arselin, G., M.F. Giraud, A. Dautant, J. Vaillier, D. Brethes, B. Coulary-Salin, J. Schaeffer, and J. Velours. 2003. The GxxxG motif of the transmembrane domain of subunit e is involved in the dimerization/oligomerization of the yeast ATP synthase complex in the mitochondrial membrane. *Eur J Biochem*. 270:1875-84.

Assadi-Porter, R.M., and R.H. Fillingame. 1995. Proton-translocating carboxyl of subunit *c* of F_1F_O H^+-ATP synthase: the unique environment suggested by the pKa determined by ^1H NMR. *Biochemistry*. 34:16186-16193.

Baylis Scanlon, J.A., M.K. Al-Shawi, N.P. Le, and R.K. Nakamoto. 2007. Determination of the partial reactions of rotational catalysis in the F_1-ATPase. *Biochemistry*. 46:8785-97.

Birkenhäger, R., M. Hoppert, G. Deckers-Hebestreit, F. Mayer, and K. Altendorf. 1995. The F_O complex of the *Escherichia coli* ATP synthase: investigation by electron spectroscopic imaging and immunoelectron microscopy. *J. Eur. Biochem.* 230:58-67.

Bottcher, B., L. Schwarz, and P. Graber. 1998. Direct indication for the existence of a double stalk in CF0F1. *J Mol Biol*. 281:757-62.

Boyer, P., R.L. Cross, and W. Momsen. 1973. A new concept for energy coupling in oxidative phosphorylation based on a molecular explanation of the oxygen exchange reactions. *Proc. Natl. Acad. Sci. U. S. A.* 70:2837-2839.

Boyer, P.D. 1975. A model for conformational coupling of membrane potential and proton translocation to ATP synthesis and to active transport. *FEBS Lett.* 58:1-6.

Boyer, P.D. 1979. The binding-change mechanism of ATP synthesis. *In* Membrane Bioenergetics. C.P. Lee, G. Schatz, and L. Ernster, editors. Addison-Wesley, Reading, MA. 461-479.

Boyer, P.D. 1989. A perspective of the binding change mechanism for ATP synthesis. *FASEB J.* 3:2164-2178.

Boyer, P.D. 1993. The binding change mechanism for ATP synthase-some probabilities and possibilities. *Biochim. Biophys. Acta*. 1140:215-250.

Boyer, P.D. 1997. The ATP synthase-a splendid molecular machine. *Annu. Rev. Biochem.* 66:717-749.

Boyer, P.D. 2002. Catalytic site occupancy during ATP synthase catalysis. *FEBS Lett.* 512:29-32.

Braig, K., R.I. Menz, M.G. Montgomery, A.G.W. Leslie, and J.E. Walker. 2000. Structure of bovine mitochondrial F_1-ATPase inhibited by Mg^{2+}-ADP and aluminium fluoride. *Structure*. 8:567-573.

Brune, M., J.L. Hunter, J.E. Corrie, and M.R. Webb. 1994. Direct, real-time measurement of rapid inorganic phosphate release using a novel fluorescent probe and its application to actomyosin subfragment 1 ATPase. *Biochemistry*. 33:8262-71.

Brune, M., J.L. Hunter, S.A. Howell, S.R. Martin, T.L. Hazlett, J.E.T. Corrie, and M.R. Webb. 1998. Mechanism of inorganic phosphate interaction with phosphate binding protein from *Escherichia coli*. *Biochemistry*. 37:10370-10380.

Bulygin, V.V., T.M. Duncan, and R.L. Cross. 1998. Rotation of the ε subunit during catalysis by *Escherichia coli* F_OF_1-ATP synthase. *J. Biol. Chem.* 273:31765-31769.

Burwick, N.R., M.L. Wahl, J. Fang, Z. Zhong, T.L. Moser, B. Li, R.A. Capaldi, D.J. Kenan, and S.V. Pizzo. 2005. An Inhibitor of the F1 subunit of ATP synthase (IF1) modulates the activity of angiostatin on the endothelial cell surface. *J Biol Chem*. 280:1740-5.

Bustos, D.M., and J. Velours. 2005. The modification of the conserved GXXXG motif of the membrane-spanning segment of subunit g destabilizes the supramolecular species of yeast ATP synthase. *J Biol Chem*. 280:29004-10.

Buzhynskyy, N., P. Sens, V. Prima, J.N. Sturgis, and S. Scheuring. 2007. Rows of ATP synthase dimers in native mitochondrial inner membranes. *Biophys J*. 93:2870-6.

Cain, B.D., and R.D. Simoni. 1989. Proton translocation by the F_1F_o ATPase of *Escherichia coli*: mutagenic analysis of the *a* subunit. *J. Biol. Chem.* 264:3292-3300.

Capaldi, R.A., R. Aggeler, E.P. Gogol, and S. Wilkens. 1992. Structure of the *Escherichia coli* ATP synthase and role of the γ and ε subunits in coupling catalytic site and proton channeling functions. *J. Bioenerg. Biomemb.* 24:435-439.

Capaldi, R.A., and B. Schulenberg. 2000. The epsilon subunit of bacterial and chloroplast F(1)F(0) ATPases. Structure, arrangement, and role of the epsilon subunit in energy coupling within the complex. *Biochim Biophys Acta*. 1458:263-9.

Carbajo, R.J., F.A. Kellas, M.J. Runswick, M.G. Montgomery, J.E. Walker, and D. Neuhaus. 2005. Structure of the F1-binding domain of the stator of bovine F1Fo-ATPase and how it binds an alpha-subunit. *J Mol Biol*. 351:824-38.

Carelli, V., A. Baracca, S. Barogi, F. Pallotti, M.L. Valentino, P. Montagna, M. Zeviani, A. Pini, G. Lenaz, A. Baruzzi, and G. Solaini. 2002. Biochemical-clinical correlation in patients with different loads of the mitochondrial DNA T8993G mutation. *Arch Neurol*. 59:264-70.

Cipriano, D.J., and S.D. Dunn. 2006. The role of the epsilon subunit in the Escherichia coli ATP synthase. The C-terminal domain is required for efficient energy coupling. *J Biol Chem*. 281:501-7.

Collinson, I.R., M.J. Runswick, S.K. Buchanan, I.M. Fearnley, J.M. Skehel, M.J. van Raaij, D.E. Griffiths, and J.E. Walker. 1994. F_O membrane domain of ATP synthase from bovine heart mitochondria: purification, subunit composition, and reconstitution with F_1-ATPase. *Biochemistry*. 33:7971-7978.

Cross, R.L., C. Grubmeyer, and H.S. Penefsky. 1982. Mechanism of ATP hydrolysis by beef heart mitochondrial ATPase: rate enhancements resulting from cooperative interactions between multiple catalytic sites. *J. Biol. Chem.* 257:12101-12105.

Cross, R.L., and C.M. Nalin. 1982. Adenine nucleotide binding sites on beef heart F_1-ATPase: evidence for three exchangeable sites that are distinct from three noncatalytic sites. *J. Biol. Chem.* 257:2874-2881.

Cruz, J.A., C.A. Radkowski, and R.E. McCarty. 1997. Functional Consequences of Deletions of the N Terminus of the [epsilon] Subunit of the Chloroplast ATP Synthase. *Plant Physiol*. 113:1185-1192.

Das, A.M. 2003. Regulation of the mitochondrial ATP-synthase in health and disease. *Mol Genet Metab*. 79:71-82.

Del Rizzo, P.A., Y. Bi, and S.D. Dunn. 2006. ATP synthase b subunit dimerization domain: a right-handed coiled coil with offset helices. *J Mol Biol*. 364:735-46.

Del Rizzo, P.A., Y. Bi, S.D. Dunn, and B.H. Shilton. 2002. The "second stalk" of *Escherichia coli* ATP synthase: structure of the isolated dimerization domain. *Biochemistry*. 41:6875-6884.

Deming, S.N., and S.L. Morgan. 1979. The use of linear models and matrix least squares in clinical chemistry. *Clin. Chem.* 25:840-855.

Dickson, V.K., J.A. Silvester, I.M. Fearnley, A.G. Leslie, and J.E. Walker. 2006. On the structure of the stator of the mitochondrial ATP synthase. *Embo J*. 25:2911-8.

Dimroth, P., G. Kaim, and U. Matthey. 2000. Crucial role of the membrane potential for ATP synthesis by F(1)F(o) ATP synthases. *J Exp Biol*. 203:51-9.

Dimroth, P., C. von Ballmoos, and T. Meier. 2006. Catalytic and mechanical cycles in F-ATP synthases. Fourth in the Cycles Review Series. *EMBO Rep*. 7:276-82.

Dimroth, P., C. von Ballmoos, T. Meier, and G. Kaim. 2003. Electrical power fuels rotary ATP synthase. *Structure*. 11:1469-73.

Dittrich, M., S. Hayashi, and K. Schulten. 2003. On the mechanism of ATP hydrolysis in F1-ATPase. *Biophys J*. 85:2253-66.

Dittrich, M., S. Hayashi, and K. Schulten. 2004. ATP hydrolysis in the betaTP and betaDP catalytic sites of F1-ATPase. *Biophys J*. 87:2954-67.

Dittrich, M., and K. Schulten. 2005. Zooming in on ATP hydrolysis in F_1. *J. Bioenerg. Biomembr.* 37:441-444.

Dmitriev, O., P.C. Jones, W. Jiang, and R.H. Fillingame. 1999a. Structure of the membrane domain of subunit *b* of the *Escherichia coli* F_OF_1 ATP synthase. *J. Biol. Chem.* 274:15598-15604.

Dmitriev, O.Y., F. Abildgaard, J.L. Markley, and R.H. Fillingame. 2002. Structure of Ala24/Asp61 --> Asp24/Asn61 substituted subunit c of Escherichia coli ATP synthase: implications for the mechanism of proton transport and rotary movement in the F0 complex. *Biochemistry*. 41:5537-47.

Dmitriev, O.Y., P.C. Jones, and R.H. Fillingame. 1999b. Structure of the subunit *c* oligomer in the F_1F_O ATP synthase: model derived from solution structure of the monomer and cross-linking in the native enzyme. *Proc. Natl. Acad. Sci. U. S. A.* 96:7785-7790.

Dudkina, N.V., J. Heinemeyer, W. Keegstra, E.J. Boekema, and H.P. Braun. 2005. Structure of dimeric ATP synthase from mitochondria: an angular association of monomers induces the strong curvature of the inner membrane. *FEBS Lett*. 579:5769-72.

Dudkina, N.V., S. Sunderhaus, H.P. Braun, and E.J. Boekema. 2006. Characterization of dimeric ATP synthase and cristae membrane ultrastructure from Saccharomyces and Polytomella mitochondria. *FEBS Lett*. 580:3427-32.

Duncan, T.M., V.V. Bulygin, Y. Zhou, M.L. Hutcheon, and R.L. Cross. 1995a. Rotation of subunits during catalysis by *Escherichia coli* F_1-ATPase. *Proc. Natl. Acad. Sci. U. S. A.* 92:10964-10968.

Duncan, T.M., and A.E. Senior. 1985. The defective proton-ATPase of *uncD* mutations of *Escherichia coli*: two mutations which affect the catalytic mechanism. *J. Biol. Chem.* 260:4901-4907.

Duncan, T.M., Y. Zhou, V. Bulygin, M.L. Hutcheon, and R.L. Cross. 1995b. Probing interactions of the *Escherichia coli* F_OF_1 ATP synthase β and γ subunits with disulphide cross-links. *Biochem. Soc. Trans.* 23:736-741.

Dunn, S.D. 1982. The isolated γ subunit of *Escherichia coli* F_1 ATPase binds the ε subunit. *J. Biol. Chem.* 257:7354-7359.

Dunn, S.D., and J. Chandler. 1998. Characterization of a $b_2\delta$ complex from *Escherichia coli* ATP synthase. *J. Biol. Chem.* 273:8646-8651.

Dunn, S.D., and M. Futai. 1980. Reconstitution of a functional coupling factor from the isolated subunits of *Escherichia coli* F_1 ATPase. *J. Biol. Chem.* 255:113-118.

Dunn, S.D., L.A. Heppel, and C.S. Fullmer. 1980. The NH_2-terminal portion of the α subunit of *Escherichia coli* F_1 ATPase is required for binding the δ subunit. *J. Biol. Chem.* 255:6891-6896.

Dunn, S.D., D.T. McLachlin, and M. Revington. 2000. The second stalk of *Escherichia coli* ATP synthase. *Biochim. Biophys. Acta*. 1458:356-363.

Dunn, S.D., V.D. Zadorozny, R.G. Tozer, and L.E. Orr. 1987. ε subunit of *Escherichia coli* F_1-ATPase: effects on affinity for aurovertin and inhibition of product release in unisite ATP hydrolysis. *Biochemistry*. 26:4488-4493.

Elston, T., H. Wang, and G. Oster. 1998. Energy transduction in ATP synthase. *Nature*. 391:510-513.

Fabiato, A., and F. Fabiato. 1979. Calculator programs for computing the composition of the solutions containing multiple metals and ligands used for experiments in skinned muscle cells. *J. Physiol. (Paris)*. 75:463-505.

Feniouk, B.A., M.A. Kozlova, D.A. Knorre, D.A. Cherepanov, A.Y. Mulkidjanian, and W. Junge. 2004. The proton-driven rotor of ATP synthase: ohmic conductance (10 fS), and absence of voltage gating. *Biophys J*. 86:4094-109.

Feniouk, B.A., T. Suzuki, and M. Yoshida. 2006. The role of subunit epsilon in the catalysis and regulation of FOF1-ATP synthase. *Biochim Biophys Acta*. 1757:326-38.

Fillingame, R.H., C.M. Angevine, and O.Y. Dmitriev. 2002. Coupling proton movements to c-ring rotation in F(1)F(o) ATP synthase: aqueous access channels and helix rotations at the a-c interface. *Biochim Biophys Acta*. 1555:29-36.

Fillingame, R.H., C.M. Angevine, and O.Y. Dmitriev. 2003. Mechanics of coupling proton movements to c-ring rotation in ATP synthase. *FEBS Lett*. 555:29-34.

Fillingame, R.H., and O.Y. Dmitriev. 2002. Structural model of the transmembrane Fo rotary sector of H+-transporting ATP synthase derived by solution NMR and intersubunit cross-linking in situ. *Biochim Biophys Acta*. 1565:232-45.

Fillingame, R.H., W. Jiang, and O.Y. Dmitriev. 2000. Coupling H^+ transport to rotary catalysis in F-type ATP synthases: structure and organization of the transmembrane rotary motor. *J. Exp. Biol.* 203:9-17.

Fraga, D., and H. Fillingame. 1991. Essential residues in the polar loop region of subunit *c* of *Escherichia coli* F_1F_o ATP synthase defined by random oligonucleotide-primed mutagenesis. *J. Bacteriol.* 173:2639-2643.

Fraga, D., and R.H. Fillingame. 1989. Conserved polar loop region of *Escherichia coli* subunit *c* of the F_1F_o H^+-ATPase: glutamine 42 is not absolutely essential, but substitutions alter binding and coupling. *J. Biol. Chem.* 264:6796-6803.

Fraga, D., J. Hermolin, and R.H. Fillingame. 1994a. Transmembrane helix-helix interactions in F_O suggested by suppressor mutations to $Ala^{24}\rightarrow Asp/Asp^{61}\rightarrow Gly$ mutant of ATP synthase subunit *c*. *J. Biol. Chem.* 269:2562-2567.

Fraga, D., J. Hermolin, M. Oldenburg, M.J. Miller, and R.H. Fillingame. 1994b. Arginine 41 of subunit *c* of Escherichia coli H^+-ATP synthase is essential in binding and coupling of F_1 to F_O. *J. Biol. Chem.* 269:7532-7537.

Friedl, P., J. Hoppe, R.P. Gunsalus, O. Michelsen, K. von Meyenburg, and H.U. Schairer. 1983. Membrane integration and function of three F_o subunits of the ATP synthase of *Escherichia coli*. *EMBO J.* 2:99-103.

Froehlich, J.P., J.V. Sullivan, and R.L. Berger. 1976. A chemical quenching apparatus for studying rapid reactions. *Anal. Biochem.* 73:331-341.

Furuike, S., M.D. Hossain, Y. Maki, K. Adachi, T. Suzuki, A. Kohori, H. Itoh, M. Yoshida, and K. Kinosita. 2008. Axle-less F1-ATPase rotates in the correct direction. *Science*. 319:955-8.

Futai, M. 1977. Reconstitution of the coupling factor, F_1, of *Escherichia coli*. *Biochem. Biophys. Res. Commun.* 79:1231-1237.

Futai, M., P.C. Sternweis, and L.A. Heppel. 1974. Purification and properties of reconstitutively active and inactive adenosinetriphosphatase from *Escherichia coli*. *Proc. Natl. Acad. Sci. U. S. A.* 71:2725-2729.

García, J.J., and R.A. Capaldi. 1998. Unisite catalysis without rotation of the γ-ε domain in *Escherichia coli* F_1-ATPase. *J. Biol. Chem.* 273:15940-15945.

Garcia, J.J., I. Ogilvie, B.H. Robinson, and R.A. Capaldi. 2000. Structure, functioning, and assembly of the ATP synthase in cells from patients with the T8993G mitochondrial DNA mutation. Comparison with the enzyme in Rho(0) cells completely lacking mtdna. *J Biol Chem*. 275:11075-81.

Gibbons, C., M.G. Montgomery, A.G.W. Leslie, and J.E. Walker. 2000. The structure of the central stalk in bovine F_1-ATPase at 2.4 Å resolution. *Nature Struct. Biol.* 7:1055-1061.

Giraud, M.F., P. Paumard, V. Soubannier, J. Vaillier, G. Arselin, B. Salin, J. Schaeffer, D. Brethes, J.P. di Rago, and J. Velours. 2002. Is there a relationship between the supramolecular organization of the mitochondrial ATP synthase and the formation of cristae? *Biochim Biophys Acta*. 1555:174-80.

Girvin, M.E., V.K. Rastogi, F. Abildgaard, J.L. Markley, and R.H. Fillingame. 1998. Solution structure of the transmembrane H^+-transporting subunit *c* of the F_1F_O ATP synthase. *Biochemistry*. 37:8817-8824.

Gogol, E.P., R. Aggeler, M. Sagermann, and R.A. Capaldi. 1989a. Cryoelectron microscopy of *Escherichia coli* F_1 adenosinetriphosphatase decorated with monoclonal antibodies to individual subunits of the complex. *Biochemistry*. 28:4717-4724.

Gogol, E.P., U. Lücken, T. Bork, and R.A. Capaldi. 1989b. Molecular architecture of *Escherichia coli* F_1 adenosinetriphosphatase. *Biochemistry*. 28:4709-4716.

Grabar, T.B., and B.D. Cain. 2003. Integration of b subunits of unequal lengths into F1F0-ATP synthase. *J Biol Chem*. 278:34751-6.

Gresser, M.J., J.A. Myers, and P.D. Boyer. 1982. Catalytic site cooperativity of beef heart mitochondrial F_1 adenosine triphosphatase: correlations of initial velocity, bound intermediate, and oxygen exchange measurements with an alternating three-site model. *J. Biol. Chem.* 257:12030-12038.

Grubmeyer, C., R.L. Cross, and H.S. Penefsky. 1982. Mechanism of ATP hydrolysis by beef-heart mitochondrial ATPase: rate constants for elementary steps in catalysis at a single site. *J. Biol. Chem.* 257:12092-12100.

Grubmeyer, C., and H.S. Penefsky. 1981. Cooperativity between catalytic sites in the mechanism of action of beef heart mitochondrial adenosine triphosphatase. *J. Biol. Chem.* 256:3728-3734.

Hara, K.Y., Y. Kato-Yamada, Y. Kikuchi, T. Hisabori, and M. Yoshida. 2001. The role of the betaDELSEED motif of F1-ATPase: propagation of the inhibitory effect of the epsilon subunit. *J Biol Chem*. 276:23969-73.

Hara, K.Y., H. Noji, D. Bald, R. Yasuda, K. Kinosita, and M. Yoshida. 2000. The role of the DELSEED motif of the β subunit in rotation of F_1-ATPase. *J. Biol. Chem.* 275:14260-14263.

Hasler, K., O. Panke, and W. Junge. 1999. On the stator of rotary ATP synthase: the binding strength of subunit δ to $(\alpha\beta)_3$ as determined by fluorescence correlation spectroscopy. *Biochemistry*. 38:13759-65.

Hermolin, J., O.Y. Dmitriev, Y. Zhang, and R.H. Fillingame. 1999. Defining the domain of binding of F_1 subunit ε with the polar loop of F_O subunit *c* in the *Escherichia coli* ATP synthase. *J. Biol. Chem.* 274:17011-17016.

Hermolin, J., and R.H. Fillingame. 1989. H^+-ATPase activity of *Escherichia coli* F_1F_o is blocked after reaction of dicyclohexylcarbodiimide with a single proteolipid (subunit *c*) of the F_o complex. *J. Biol. Chem.* 264:3896-3903.

Hoppe, J., P. Friedl, H.U. Schairer, W. Sebald, K. von Meyenburg, and B.B. Jørgensen. 1983. The topology of the proton translocating F_o component of the ATP synthase from *Escherichia coli* K12: studies with proteases. *EMBO J.* 2:105-110.

Houstek, J., A. Pickova, A. Vojtiskova, T. Mracek, P. Pecina, and P. Jesina. 2006. Mitochondrial diseases and genetic defects of ATP synthase. *Biochim Biophys Acta*. 1757:1400-5.

Hundal, T., B. Norling, and L. Ernster. 1983. Lack of ability of trypsin-treated mitochondrial F1-ATPase to bind the oligomycin-sensitivity conferring protein (OSCP). *FEBS Lett*. 162:5-10.

Iino, R., T. Murakami, S. Iizuka, Y. Kato-Yamada, T. Suzuki, and M. Yoshida. 2005. Real-time monitoring of conformational dynamics of the epsilon subunit in F1-ATPase. *J Biol Chem*. 280:40130-4.

Iko, Y., Y. Sambongi, M. Tanabe, A. Iwamoto-Kihara, K. Saito, I. Ueda, Y. Wada, and M. Futai. 2001. ATP synthase F1 sector rotation: defective torque generation in the b subunit Ser-174 to Phe mutant and its suppression by second mutations. *J. Biol. Chem.* 276:47508-47511.

Issartel, J.-P., J. Lunardi, and P.V. Vignais. 1986. Characterization of exchangeable and nonexchangeable bound adenine nucleotides in F_1-ATPase from *Escherichia coli*. *J. Biol. Chem.* 261:895-901.

Itoh, H., A. Takahashi, K. Adachi, H. Noji, R. Yasuda, M. Yoshida, and K. Kinosita. 2004. Mechanically driven ATP synthesis by F1-ATPase. *Nature*. 427:465-8.

Iwamoto, A., J. Miki, M. Maeda, and M. Futai. 1990. H^+-ATPase γ subunit from *Escherichia coli*: role of the conserved carboxylic terminal region. *J. Biol. Chem.* 265:5043-5048.

Jiang, W., and R.H. Fillingame. 1998. Interaction helical faces of subunits *a* and *c* in the F_1F_O ATP synthase of *Escherichia coli* defined by disulfide cross-linking. *J. Biol. Chem.* 95:6607-6612.

Jiang, W., J. Hermolin, and R.H. Fillingame. 2001. The preferred stoichiometry of c subunits in the rotary motor sector of Escherichia coli ATP synthase is 10. *Proc Natl Acad Sci U S A*. 98:4966-71.

Jones, P.C., J. Hermolin, and R.H. Fillingame. 2000. Mutations in single hairpin units of genetically fused subunit *c* provide support for a rotary catalytic mechanism in F_OF_1 ATP synthase. *J. Biol. Chem.* 275:11355-11360.

Jones, P.C., W. Jiang, and R.H. Fillingame. 1998. Arrangement of the multicopy H^+-translocating subunit *c* in the membrane sector of the *Escherichia coli* F_1F_O ATP synthase. *J. Biol. Chem.* 273:17178-17185.

Junge, W., H. Lill, and S. Engelbrecht. 1997. ATP synthase: an electrochemical transducer with rotatory mechanics. *Trends Biochem. Sci.* 263:420-423.

Junge, W., O. Panke, D.A. Cherepanov, K. Gumbiowski, M. Muller, and S. Engelbrecht. 2001. Inter-subunit rotation and elastic power transmission in F0F1-ATPase. *FEBS Lett.* 504:152-60.

Kaibara, C., T. Matsui, T. Hisabori, and M. Yoshida. 1996. Structural asymmetry of F_1-ATPase caused by the g subunit generates a high affinity nucleotide binding site. *J. Biol. Chem.* 271:2433-2438.

Kaim, G., and P. Dimroth. 1999. ATP synthesis by F-type ATP synthase is obligatorily dependent on the transmembrane voltage. *Embo J*. 18:4118-27.

Kanazawa, H., Y. Horiuchi, M. Takagi, Y. Ishino, and M. Futai. 1980. Coupling factor F_1 ATPase with defective β subunit from a mutant of *Escherichia coli*. *J. Biochem. (Tokyo)*. 88:695-703.

Kaplan, R.S., and P.L. Pedersen. 1985. Determination of microgram quantities of protein in the presence of milligram levels of lipid with amido black 10B. *Anal. Biochem.* 150:97-104.

Kato-Yamada, Y. 2005. Isolated epsilon subunit of Bacillus subtilis F1-ATPase binds ATP. *FEBS Lett*. 579:6875-8.

Kato-Yamada, Y., D. Bald, M. Koike, K. Motohashi, T. Hisabori, and M. Yoshida. 1999. ε subunit, an endogenous inhibitor of bacterial F_1-ATPase, also inhibits F_OF_1-ATPase. *J. Biol. Chem.* 274:33991-33994.

Kato-Yamada, Y., H. Noji, R. Yasuda, K. Kinosita, and M. Yoshida. 1998. Direct observation of the rotation of ε subunit in F_1-ATPase. *J. Biol. Chem.* 273:19375-19377.

Kato, S., M. Yoshida, and Y. Kato-Yamada. 2007. Role of the epsilon subunit of thermophilic F1-ATPase as a sensor for ATP. *J Biol Chem*. 282:37618-23.

Ketchum, C.J., M.K. Al-Shawi, and R.K. Nakamoto. 1998. Intergenic suppression of the γM23K uncoupling mutation in F_OF_1 ATP synthase by βGlu-381 substitutions: the role of the β^{380}DELSEED^{386} segment in energy coupling. *Biochem. J.* 330:707-712.

Ketchum, C.J., and R.K. Nakamoto. 1998. A mutation in the *Escherichia coli* F_OF_1 ATP synthase rotor, γE208K, perturbs conformational coupling between transport and catalysis. *J. Biol. Chem.* 273:22292-22297.

Kim, S.H., R. Vlkolinsky, N. Cairns, and G. Lubec. 2000. Decreased levels of complex III core protein 1 and complex V beta chain in brains from patients with Alzheimer's disease and Down syndrome. *Cell Mol Life Sci*. 57:1810-6.

Kimura, Y., S. Shibasaki, K. Morisato, N. Ishizuka, H. Minakuchi, K. Nakanishi, M. Matsuo, T. Amachi, M. Ueda, and K. Ueda. 2004. Microanalysis for MDR1 ATPase by high-performance liquid chromatography with a titanium dioxide column. *Anal. Biochem.* 326:262-266.

Kinosita, K., K. Adachi, and H. Itoh. 2004. Rotation of F_1-ATPase: how an ATP-driven molecular machine may work. *Annu. Rev. Biophys. Biomol. Struct.* . 33:245-268.

Klionsky, D.J., W.S.A. Brusilow, and R.D. Simoni. 1984. *In vivo* evidence for the role of the ε subunit as an inhibitor of the proton-translocating ATPase of *Escherichia coli*. *J. Bacteriol.* 160:1055-1060.

Krebstakies, T., I. Aldag, K. Altendorf, J.C. Greie, and G. Deckers-Hebestreit. 2008. The stoichiometry of subunit c of Escherichia coli ATP synthase is independent of its rate of synthesis. *Biochemistry*. 47:6907-16.

Kuki, M., T. Noumi, M. Maeda, A. Amemura, and M. Futai. 1988. Functional domains of ε subunit of *Escherichia coli* H^+-ATPase (F_oF_1). *J. Biol. Chem.* 263:17437-17442.

Laemmli, U.K. 1970. *Nature*. 227:680-685.

Le, N.P., H. Omote, Y. Wada, M.K. Al-Shawi, R.K. Nakamoto, and M. Futai. 2000. The *Escherichia coli* ATP synthase α subunit Arg-376: the catalytic site arginine does not participate in the hydrolysis/synthesis reaction but is required for promotion to steady state. *Biochemistry*. 39:2778-2783.

Lefebvre-Legendre, L., A. Balguerie, S. Duvezin-Caubet, M.F. Giraud, P.P. Slonimski, and J.P. Di Rago. 2003. F1-catalysed ATP hydrolysis is required for mitochondrial biogenesis in Saccharomyces cerevisiae growing under conditions where it cannot respire. *Mol Microbiol*. 47:1329-39.

Lightowlers, R.N., S.M. Howitt, L. Hatch, F. Gibson, and G.B. Cox. 1987. The proton pore in the *Escherichia coli* F_oF_1-ATPase: a requirement for arginine at position 210 of the *a* subunit. *Biochim. Biophys. Acta*. 894:399-406.

Lill, H., F. Hensel, W. Junge, and S. Engelbrecht. 1996. Cross-linking of engineered subunit δ to $(\alpha\beta)_3$ in chloroplast F-ATPase. *J. Biol. Chem.* 271:32737-32742.

Löbau, S., J. Weber, S. Wilke-Mounts, and A.E. Senior. 1997. F_1-ATPase, roles of three catalytic site residues. *J. Biol. Chem.* 272:3648-3656.

Long, J.C., S. Wang, and S.B. Vik. 1998. Membrane topology of subunit *a* of the F_1F_O ATP synthase as determined by labeling of unique cysteine residues. *J. Biol. Chem.* 273:16235-16240.

Lowry, O.H., N.J. Rosebrough, A.C. Farr, and R.J. Randall. 1951. Protein measurement with the folin phenol reagent. *J. Biol. Chem.* 193:265-275.

Lündsdorf, H., K. Ehrig, P. Friedl, and H.U. Schairer. 1984. Use of monoclonal antibodies in immuno-electron microscopy for the determination of subunit stoichiometry in oligomeric enzymes: there are three α-subunits in the F_1-ATPase of *Escherichia coli*. *J. Mol. Biol.* 173:131-136.

Lunardi, J., A. Dupuis, J. Garin, J.P. Issartel, L. Michel, M. Chabre, and P.V. Vignais. 1988. Inhibition of H^+-transporting ATPase by formation of a tight nucleoside

diphosphate-fluoroaluminate complex at the catalytic site. *Proc. Natl. Acad. Sci. U. S. A.* 85:8958-8962.

Maggio, M.B., J. Pagan, D. Parsonage, L. Hatch, and A.E. Senior. 1987. The defective proton-ATPase of *uncA* mutants of *Escherichia coli*: identification by DNA sequencing of residues in the α-subunit which are essential for catalysis or normal assembly. *J. Biol. Chem.* 262:8981-8984.

Mao, H.Z., and J. Weber. 2007. Identification of the betaTP site in the x-ray structure of F1-ATPase as the high-affinity catalytic site. *Proc. Natl. Acad. Sci. U. S. A.* 104:18478-83.

Masaike, T., E. Muneyuki, H. Noji, K. Kinosita, and M. Yoshida. 2002. F_1-ATPase changes its conformations upon phosphate release. *J. Biol. Chem.* 277:21643-21649.

Matsuyama, S., J. Llopis, Q.L. Deveraux, R.Y. Tsien, and J.C. Reed. 2000. Changes in intramitochondrial and cytosolic pH: early events that modulate caspase activation during apoptosis. *Nat Cell Biol*. 2:318-25.

Matsuyama, S., Q. Xu, J. Velours, and J.C. Reed. 1998. The Mitochondrial F0F1-ATPase proton pump is required for function of the proapoptotic protein Bax in yeast and mammalian cells. *Mol Cell*. 1:327-36.

McGeoch, J.E., and G. Guidotti. 2001. Batten disease and the control of the Fo subunit c pore by cGMP and calcium. *Eur J Paediatr Neurol*. 5 Suppl A:147-50.

McLachlin, D.T., J.A. Bestard, and S.D. Dunn. 1998. The *b* and δ subunits of the *Escherichia coli* ATP synthase interact via residues in their C-terminal regions. *J. Biol. Chem.* 273:15162-15168.

McLachlin, D.T., and S.D. Dunn. 1997. Dimerization interactions of the *b* subunit of the *Escherichia coli* F_1F_O-ATPase. *J. Biol. Chem.* 272:21233-21239.

Meier, T., U. Matthey, C. von Ballmoos, J. Vonck, T. Krug von Nidda, W. Kuhlbrandt, and P. Dimroth. 2003. Evidence for structural integrity in the undecameric c-rings isolated from sodium ATP synthases. *J Mol Biol*. 325:389-97.

Meier, T., P. Polzer, K. Diederichs, W. Welte, and P. Dimroth. 2005. Structure of the rotor ring of F-Type Na+-ATPase from Ilyobacter tartaricus. *Science*. 308:659-62.

Mendel-Hartvig, J., and R.A. Capaldi. 1991a. Catalytic site nucleotide and inorganic phosphate dependence of the conformation of the ε subunit in *Escherichia coli* adenosinetriphosphatase. *Biochemistry*. 30:1278-1284.

Mendel-Hartvig, J., and R.A. Capaldi. 1991b. Nucleotide-dependent and dicyclohexylcarbodiimide-sensitive conformational changes in the ε subunit of *Escherichia coli* ATP synthase. *Biochemistry*. 30:10987-10991.

Menz, R.I., J.E. Walker, and A.G.W. Leslie. 2001. Structure of bovine mitochondrial F_1-ATPase with nucleotide bound to all three catalytic sites: implication for the mechanism of rotary catalysis. *Cell*. 106:331-341.

MicroMath_Research. 1995. MicroMath Scientist: for Experimental Data Fitting/Microsoft Windows Version 2.0. MicroMath Research, St. Louis, MO.

Miller, M.J., D. Fraga, C.R. Paule, and R.H. Fillingame. 1989. Mutations in the conserved proline 43 residue of the *uncE* protein (subunit *c*) of *Escherichia coli* F_1F_o-ATPase alter the coupling of F_1 to F_o. *J. Biol. Chem.* 264:305-311.

Miller, M.J., M. Oldenburg, and R.H. Fillingame. 1990. The essential carboxyl group in subunit *c* of the F_1F_o ATP synthase can be moved and H^+-translocating function retained. *Proc. Natl. Acad. Sci. U.S.A.* 87:4900-4904.

Minauro-Sanmiguel, F., S. Wilkens, and J.J. Garcia. 2005. Structure of dimeric mitochondrial ATP synthase: novel F0 bridging features and the structural basis of mitochondrial cristae biogenesis. *Proc Natl Acad Sci U S A*. 102:12356-8.

Mitchell, P. 1974. A chemiosmotic molecular mechanism for proton-translocating adenosine triphosphatases. *FEBS Lett.* 43:189-194.

Mitchell, P., and J. Moyle. 1967. Chemiosmotic hypothesis of oxidative phosphorylation. *Nature*. 213:137-9.

Mitome, N., T. Suzuki, S. Hayashi, and M. Yoshida. 2004. Thermophilic ATP synthase has a decamer c-ring: indication of noninteger 10:3 H+/ATP ratio and permissive elastic coupling. *Proc Natl Acad Sci U S A*. 101:12159-64.

Miwa, K., and M. Yoshida. 1989. The $\alpha_3\beta_3$ complex, the catalytic core of F_1-ATPase. *Proc. Natl. Acad. Sci. U.S.A.* 86:6484-6487.

Moore, K.J., C.M. Angevine, O.D. Vincent, B.E. Schwem, and R.H. Fillingame. 2008. The cytoplasmic loops of subunit a of Escherichia coli ATP synthase may participate in the proton translocating mechanism. *J Biol Chem*. 283:13044-52.

Moriyama, Y., A. Iwamoto, H. Hanada, M. Maeda, and M. Futai. 1991. One-step purification of *Escherichia coli* H^+-ATPase (F_oF_1) and its reconstitution into liposomes with neurotransmitter transporters. *J. Biol. Chem.* 266:22141-22146.

Moser, T.L., D.J. Kenan, T.A. Ashley, J.A. Roy, M.D. Goodman, U.K. Misra, D.J. Cheek, and S.V. Pizzo. 2001. Endothelial cell surface F1-F0 ATP synthase is active in ATP synthesis and is inhibited by angiostatin. *Proc Natl Acad Sci U S A*. 98:6656-61.

Moser, T.L., M.S. Stack, I. Asplin, J.J. Enghild, P. Hojrup, L. Everitt, S. Hubchak, H.W. Schnaper, and S.V. Pizzo. 1999. Angiostatin binds ATP synthase on the surface of human endothelial cells. *Proc Natl Acad Sci U S A*. 96:2811-6.

Nadanaciva, S., J. Weber, and A.E. Senior. 2000. New probes of the F1-ATPase catalytic transition state reveal that two of the three catalytic sites can assume a transition state conformation simultaneously. *Biochemistry*. 39:9583-9590.

Nadanaciva, S., J. Weber, S. Wilke-Mounts, and A.E. Senior. 1999. Importance of F_1-ATPase residue α-Arg-376 for catalytic transition state stabilization. *Biochemistry*. 38:15493-15499.

Nakamoto, R.K. 1996. Mechanisms of active transport in the F_OF_1 ATP synthase. *J. Memb. Biol.* 151:101-111.

Nakamoto, R.K. 1999. Molecular features of energy coupling in the F_OF_1 ATP Synthase. *News Physiol. Sci.* 14:40-46.

Nakamoto, R.K., M.K. Al-Shawi, and M. Futai. 1995. The ATP synthase γ subunit: suppressor mutagenesis reveals three helical regions involved in energy coupling. *J. Biol. Chem.* 270:14042-14046.

Nakamoto, R.K., J.A. Baylis Scanlon, and M.K. Al-Shawi. 2008. The rotary mechanism of the ATP synthase. *Arch. Biochem. Biophys.*:doi:10.1016/j.abb.2008.05.004.

Nakamoto, R.K., C.J. Ketchum, and M.K. Al-Shawi. 1999. Rotational coupling in the F_OF_1 ATP synthase. *Ann. Rev. Biophys. Biomol. Struct.* 28:205-234.

Nakamoto, R.K., C.J. Ketchum, P.H. Kuo, Y.B. Peskova, and M.K. Al-Shawi. 2000. Molecular mechanisms of rotational catalysis in the F_OF_1 ATP synthase. *Biochim. Biophys. Acta*. 1458:289-299.

Nakamoto, R.K., M. Maeda, and M. Futai. 1993. The γ subunit of the *Escherichia coli* ATP synthase: mutations in the carboxyl-terminal region restore energy coupling to the amino-terminal mutant, γMet-23→Lys. *J. Biol. Chem.* 268:867-872.

Nakanishi-Matsui, M., S. Kashiwagi, T. Ubukata, A. Iwamoto-Kihara, Y. Wada, and M. Futai. 2007. Rotational catalysis of Escherichia coli ATP synthase F1 sector. Stochastic fluctuation and a key domain of the beta subunit. *J Biol Chem*. 282:20698-704.

Nalin, C.M., and R.L. Cross. 1982. Adenine nucleotide binding sites on beef-heart F_1-ATPase: specificity of cooperative interactions. *J. Biol. Chem.* 257:8055-8060.

Nelson, N. 1992. Organellar proton-ATPases. *Curr Opin Cell Biol*. 4:654-60.

Nicastro, D., A.S. Frangakis, D. Typke, and W. Baumeister. 2000. Cryo-electron tomography of neurospora mitochondria. *J Struct Biol*. 129:48-56.

Nijtmans, L.G., N.S. Henderson, G. Attardi, and I.J. Holt. 2001. Impaired ATP synthase assembly associated with a mutation in the human ATP synthase subunit 6 gene. *J Biol Chem*. 276:6755-62.

Nishio, K., A. Iwamoto-Kihara, A. Yamamoto, Y. Wada, and M. Futai. 2002. Subunit rotation of ATP synthase embedded in membranes: a or beta subunit rotation relative to the c subunit ring. *Proc. Natl. Acad. Sci. U. S. A.* 99:13448-52.

Nishizaka, T., K. Oiwa, H. Noji, S. Kimura, E. Muneyuki, M. Yoshida, and K. Kinosita. 2004. Chemomechanical coupling in F1-ATPase revealed by simultaneous observation of nucleotide kinetics and rotation. *Nat. Struct. Mol. Biol.* 11:142-8.

Nixon, A.E., J.L. Hunter, G. Bonifacio, J.F. Eccleston, and M.R. Webb. 1998. Purine nucleoside phosphorylase: its use in a spectroscopic assay for inorganic phosphate and for removing inorganic phosphate with the aid of phosphodeoxyribomutase. *Anal. Biochem.* 265:299-307.

Noji, H., K. Häsler, W. Junge, K. Kinosita, M. Yoshida, and S. Engelbrecht. 1999. Rotation of *Escherichia coli* F_1-ATPase. *Biochem. Biophys. Res. Commun.* 260:597-599.

Noji, H., R. Yasuda, M. Yoshida, and K. Kinosita. 1997. Direct observation of the rotation of F_1-ATPase. *Nature*. 386:299-302.

Noumi, T., M. Maeda, and M. Futai. 1987. Mode of inhibition of sodium azide on H^+-ATPase of *Escherichia coli*. *FEBS Lett.* 213:381-384.

Noumi, T., M. Maeda, and M. Futai. 1988. A homologous sequence between H^+-ATPase (F_oF_1) and cation-transporting ATPases: Thr-185Asp replacement in the β subunit

of *Escherichia coli* F_1 changes its catalytic properties. *J. Biol. Chem.* 263:8765-8770.

Nowak, K.F., V. Tabidze, and R.E. McCarty. 2002. The C-terminal domain of the epsilon subunit of the chloroplast ATP synthase is not required for ATP synthesis. *Biochemistry*. 41:15130-4.

Oberfeld, B., J. Brunner, and P. Dimroth. 2006. Phospholipids occupy the internal lumen of the c ring of the ATP synthase of Escherichia coli. *Biochemistry*. 45:1841-51.

Ogilvie, I., R. Aggeler, and R.A. Capaldi. 1997. Cross-linking of the δ subunit to one of the three α subunits has no effect on functioning, as expected if δ is a part of the stator that links the F_1 and F_O parts of the *Escherichia coli* ATP synthase. *J. Biol. Chem.* 272:16652-16656.

Omote, H., N.P. Le, M.-Y. Park, M. Maeda, and M. Futai. 1995. β subunit Glu-185 of *Escherichia coli* H^+-ATPase (ATP synthase) is an essential residue for cooperative catalysis. *J. Biol. Chem.* 270:35-43.

Omote, H., M. Maeda, and M. Futai. 1992. Effects of mutations of conserved Lys-155 and Thr-156 residues in the phosphate-binding glycine-rich sequence of the F_1-ATPase β subunit of *Escherichia coli*. *J. Biol. Chem.* 267:20571-20576.

Omote, H., N. Sambonmatsu, K. Saito, Y. Sambongi, A. Iwamoto-Kihara, T. Yanagida, Y. Wada, and M. Futai. 1999. The γ-subunit rotation and torque generation in F_1-ATPase from wild-type or uncoupled mutant *Escherichia coli*. *Proc. Natl. Acad. Sci. U. S. A.* 96:7780-7784.

Oster, G., and H. Wang. 2003. Rotary protein motors. *Trends Cell Biol*. 13:114-21.

Pänke, O., K. Gumbiowski, W. Junge, and S. Engelbrecht. 2000. F-ATPase: specific observation of the rotating c subunit oligomer of EF_OEF_1. *FEBS Lett.* 472:34-38.

Pati, S., W.S.A. Brusilow, G. Deckers-Hebestreit, and K. Altendorf. 1991. Assembly of the F_o proton channel of the *Escherichia coli* F_1F_o ATPase: low proton conductance of reconstituted F_o sectors synthesized and assembled in the absence of F_1. *Biochemistry*. 30:4710-4714.

Paumard, P., J. Vaillier, B. Coulary, J. Schaeffer, V. Soubannier, D.M. Mueller, D. Brethes, J.P. di Rago, and J. Velours. 2002. The ATP synthase is involved in generating mitochondrial cristae morphology. *Embo J*. 21:221-30.

Penefsky, H.S. 1979. A centrifuged-column procedure for the measurement of ligand binding by beef heart F_1. *Methods Enzymol.* 56:527-530.

Penefsky, H.S., and R.L. Cross. 1991. Structure and mechanism of F_oF_1-type ATP synthases and ATPases. *Adv. Enzymol.* 64:173-213.

Peskova, Y.B., and R.K. Nakamoto. 2000. Catalytic control and coupling efficiency of the *Escherichia coli* F_OF_1 ATP synthase: influence of the F_O sector and ε subunit on the catalytic transition state. *Biochemistry*. 39:11830-11836.

Pogoryelov, D., J. Yu, T. Meier, J. Vonck, P. Dimroth, and D.J. Muller. 2005. The c15 ring of the Spirulina platensis F-ATP synthase: F1/F0 symmetry mismatch is not obligatory. *EMBO Rep*. 6:1040-4.

Powell, M.J.D. 1970. A FORTRAN Subroutine for Solving Systems of Nonlinear Algebraic Equations. Gordan & Breach Science Publishers, New York, NY.

Rao, R., D.S. Perlin, and A.E. Senior. 1987. The defective proton-ATPase of *uncA* mutants of *Escherichia coli*: ATP-binding and ATP-induced conformational change in mutant α-subunits. *Arch. Biochem. Biophys.* 255:309-315.

Rastogi, V.K., and M.E. Girvin. 1999. Structural changes linked to proton translocation by subunit *c* of the ATP synthase. *Nature*. 402:263-268.

Ray, M.K., I.F. Connerton, and D.E. Griffiths. 1988. DNA sequence analysis of the *Oli^r 2-76* and *Oss^r 1-92* alleles of the *Oli-2* region of the yeast *Saccharomyces cerevisiae*. Analysis of related amino acid substitutions and protein antibiotic interaction. *Biochim. Biophys. Acta*. 951:213-219.

Ren, H., and W.S. Allison. 2000. On what makes the γ subunit spin during ATP hydrolysis by F_1. *Biochim. Biophys. Acta*. 1458:221-233.

Ren, H., S. Bandyopadhyay, and W.S. Allison. 2006. The alpha3(betaMet222Ser/Tyr345Trp)3gamma subcomplex of the TF1-ATPase does not hydolyze ATP at a significant rate until the substrate binds to the catalytic site of the lowest affinity. *Biochemistry*. 45:6222-30.

Richter, M.L., and F. Gao. 1996. The chloroplast ATP synthase: structural changes during catalysis. *J. Bioenerg. Biomemb.* 28:443-449.

Rodgers, A.J.W., and R.A. Capaldi. 1998. The second stalk composed of the *b*- and δ-subunits connects F_O to F_1 via an α-subunit in the *Escherichia coli* ATP synthase. *J. Biol. Chem.* 273:29406-29410.

Rodgers, A.J.W., and M.C.J. Wilce. 2000. Structure of the γ-ε complex of ATP synthase. *Nature Struct. Biol.* 7:1051-1054.

Rondelez, Y., G. Tresset, T. Nakashima, Y. Kato-Yamada, H. Fujita, S. Takeuchi, and H. Noji. 2005. Highly coupled ATP synthesis by F1-ATPase single molecules. *Nature*. 433:773-7.

Rubinstein, J.L., J.E. Walker, and R. Henderson. 2003. Structure of the mitochondrial ATP synthase by electron cryomicroscopy. *Embo J*. 22:6182-92.

Sambongi, Y., Y. Iko, M. Tanabe, H. Omote, A. Iwamoto-Kihara, I. Ueda, T. Yanagida, Y. Wada, and M. Futai. 1999. Mechanical rotation of the *c* subunit oligomer in ATP synthase (F_OF_1): direct observation. *Science*. 286:1722-1724.

Sambrook, J., E.F. Fritsch, and T. Maniatis. 1989. Molecular Cloning: A Laboratory Manual, 2nd Ed. Cold Spring Harbor Laboratory Press, Cold Spring Harbor.

Schneider, E., and K. Altendorf. 1985. All three subunits are required for the reconstitution of an active proton channel (F_o) of *Escherichia coli* ATP synthase (F_1F_o). *EMBO J.* 4:515-518.

Schon, E.A., S. Santra, F. Pallotti, and M.E. Girvin. 2001. Pathogenesis of primary defects in mitochondrial ATP synthesis. *Semin Cell Dev Biol*. 12:441-8.

Schulenberg, B., R. Aggeler, J. Murray, and R.A. Capaldi. 1999. The γε-*c* subunit interface in the ATP synthase of *Escherichia coli*: cross-linking of the ε subunit to the *c* subunit ring does not impair enzyme function, that of γ to *c* subunit leads to uncoupling. *J. Biol. Chem.* 274:34233-34237.

Schulenberg, B., and R.A. Capaldi. 1999. The ε subunit of the F_1F_O complex of *Escherichia coli*: cross-linking studies show the same structure *in situ* as when isolated. *J. Biol. Chem.* 274:28351-28355.

Schwem, B.E., and R.H. Fillingame. 2006. Cross-linking between helices within subunit a of Escherichia coli ATP synthase defines the transmembrane packing of a four-helix bundle. *J Biol Chem*. 281:37861-7.

Seelert, H., A. Poetsch, N.A. Dencher, A. Engel, H. Stahlberg, and D.J. Muller. 2000. Structural biology. Proton-powered turbine of a plant motor. *Nature*. 405:418-9.

Senior, A.E. 1990. The proton-translocating ATPase of *Escherichia coli. Annu. Rev. Biophys. Chem.* 19:7-41.

Senior, A.E., and M.K. Al-Shawi. 1992. Further examination of seventeen mutations in *Escherichia coli* F_1-ATPase β-subunit. *J. Biol. Chem.* 267:21471-21478.

Senior, A.E., L.R. Latchney, A. Fersuson, and J.G. Wise. 1984. Purification of F_1-ATPase with impaired catalytic activity from partial revertants of *Escherichia coli uncA* mutant strains. *Arch. Biochem. Biophys.* 228:49-53.

Senior, A.E., R.S.-F. Lee, M.K. Al-Shawi, and J. Weber. 1992. Catalytic properties of *Escherichia coli* F_1-ATPase depleted of endogenous nucleotides. *Arch. Biochem. Biophys.* 297:340-344.

Senior, A.E., S. Nadanaciva, and J. Weber. 2002. The molecular mechanism of ATP synthesis by F_1F_O-ATP synthase. *Biochim. Biophys. Acta*. 1553:188-211.

Senior, A.E., J. Weber, and M.K. Al-Shawi. 1995. Catalytic mechanism of *Escherichia coli* F_1-ATPase. *Biochem. Soc. Trans.* 23:747-752.

Senior, A.E., S. Wilke-Mounts, and M.K. Al-Shawi. 1993. Lysine 155 in β-subunit is a catalytic residue of *Escherichia coli* F_1 ATPase. *J. Biol. Chem.* 268:6989-6994.

Sgarbi, G., A. Baracca, G. Lenaz, L.M. Valentino, V. Carelli, and G. Solaini. 2006. Inefficient coupling between proton transport and ATP synthesis may be the pathogenic mechanism for NARP and Leigh syndrome resulting from the T8993G mutation in mtDNA. *Biochem J.* 395:493-500.

Sheffield, P.J., S.M. Garrard, and Z.S. Derewenda. 1999. Overcoming expression and purification problems of RhoGDI using a family of "parallel" expression vectors. *Prot. Exp. Purif.* 15:34-39.

Shimabukuro, K., R. Yasuda, E. Muneyuki, K.Y. Hara, K. Kinosita, and M. Yoshida. 2003. Catalysis and rotation of F_1 motor: cleavage of ATP at the catalytic site occurs in 1 ms before 40 degree substep rotation. *Proc. Natl. Acad. Sci. U. S. A.* . 100:14731-14736.

Shin, K., R.K. Nakamoto, M. Maeda, and M. Futai. 1992. F_oF_1-ATPase γ subunit mutations perturb the coupling between catalysis and transport. *J. Biol. Chem.* 267:20835-20839.

Shirakihara, Y., A.G.W. Leslie, J.P. Abrahams, J.E. Walker, T. Ueda, Y. Sekimoto, M. Kambara, K. Saika, Y. Kagawa, and M. Yoshida. 1997. The crystal structure of the nucleotide-free $\alpha_3\beta_3$ subcomplex of F_1-ATPase from the thermophilic *Bacillus* PS3 is a symmetric trimer. *Structure*. 5:825-836.

Singh, S., P. Turnia, C.J. Bustamante, D.J. Keller, and R.A. Capaldi. 1996. Topographical structure of membrane-bound *Escherichia coli* F_1F_O ATP synthase in aqueous buffer. *FEBS Lett.* 397:30-34.

Smith, J.B., and P.C. Sternweis. 1977. Purification of membrane attachment and inhibitory subunits of the proton translocating adenosine triphosphatase from *Escherichia coli*. *Biochemistry*. 16:306-311.

Soong, R.K., G.D. Bachand, H.P. Neves, A.G. Olkhovets, H.G. Craighead, and C.D. Montemagno. 2000. Powering an inorganic nanodevice with a biomolecular motor. *Science*. 290:1555-1558.

Sorgen, P.L., M.R. Bubb, and B.D. Cain. 1999. Lengthening the second stalk of F_1F_O ATP synthase in *Escherichia coli*. *J. Biol. Chem.* 274:36261-36266.

Sorgen, P.L., T.L. Caviston, R.C. Perry, and B.D. Cain. 1998. Deletions in the second stalk of F1F0-ATP synthase in Escherichia coli. *J Biol Chem*. 273:27873-8.

Souid, A.-K., and H.S. Penefsky. 1995. Energetics of ATP dissociation from the mitochondrial ATPase during oxidative phosphorylation. *J. Biol. Chem.* 270:9074-9082.

St-Pierre, J., M.D. Brand, and R.G. Boutilier. 2000. Mitochondria as ATP consumers: cellular treason in anoxia. *Proc Natl Acad Sci U S A*. 97:8670-4.

Stahlberg, H., D.J. Muller, K. Suda, D. Fotiadis, A. Engel, T. Meier, U. Matthey, and P. Dimroth. 2001. Bacterial Na(+)-ATP synthase has an undecameric rotor. *EMBO Rep*. 2:229-33.

Sternweis, P.C. 1978. The ε subunit of *Escherichia coli* coupling factor 1 is required for its binding to the cytoplasmic membrane. *J. Biol. Chem.* 253:3123-3128.

Stock, D., A.G.W. Leslie, and J.E. Walker. 1999. Molecular architecture of the rotary motor in ATP synthase. *Science*. 286:1700-1705.

Sugino, Y., and Y. Miyoshi. 1964. The specific precipitation of orthophosphate and some biochemical applications. *J. Biol. Chem.* 239:2360-2364.

Suzuki, T., T. Murakami, R. Iino, J. Suzuki, S. Ono, Y. Shirakihara, and M. Yoshida. 2003. F0F1-ATPase/synthase is geared to the synthesis mode by conformational rearrangement of epsilon subunit in response to proton motive force and ADP/ATP balance. *J Biol Chem*. 278:46840-6.

Takeyasu, K., H. Omote, S. Nettikadan, F. Tokumasu, A. Iwamoto-Kihara, and M. Futai. 1996. Molecular imaging of *Escherichia coli* F_OF_1-ATPase in reconstituted membranes using atomic force microscopy. *FEBS Lett.* 392:110-113.

Tanabe, M., K. Nishio, Y. Iko, Y. Sambongi, A. Iwamoto-Kihara, Y. Wada, and M. Futai. 2001. Rotation of a complex of the gamma subunit and c ring of Escherichia coli ATP synthase. The rotor and stator are interchangeable. *J. Biol. Chem.* 276:15269-74.

Tang, C., and R.A. Capaldi. 1996. Characterization of the interface between γ and ε subunits of *Escherichia coli* F_1-ATPase. *J. Biol. Chem.* 271:3018-3024.

Taussky, H.H., and E. Shorr. 1953. *J. Biol. Chem.* 202:675-685.

Tomashek, J.J., O.B. Glagoleva, and W.S. Brusilow. 2004. The Escherichia coli F1F0 ATP synthase displays biphasic synthesis kinetics. *J Biol Chem*. 279:4465-70.

Tsunoda, S.P., R. Aggeler, M. Yoshida, and R.A. Capaldi. 2001a. Rotation of the *c* subunit oligomer in fully functional F_1F_O ATP synthase. *Proc. Natl. Acad. Sci. U. S. A.* 98:898-902.

Tsunoda, S.P., E. Muneyuki, Y. Amano, M. Yoshida, and H. Noji. 1999. Cross-linking of two β subunits in the closed conformation in F_1-ATPase. *J. Biol. Chem.* 274:5701-5706.

Tsunoda, S.P., A.J. Rodgers, R. Aggeler, M.C. Wilce, M. Yoshida, and R.A. Capaldi. 2001b. Large conformational changes of the epsilon subunit in the bacterial F1F0 ATP synthase provide a ratchet action to regulate this rotary motor enzyme. *Proc Natl Acad Sci U S A*. 98:6560-4.

Turina, P., R. Aggeler, R.S.-F. Lee, A.E. Senior, and R.A. Capaldi. 1993. The cysteine introduced into the α subunit of the *Escherichia coli* F_1-ATPase by the mutation αR376C is near the α-β subunit interface and close to a noncatalytic nucleotide binding site. *J. Biol. Chem.* 268:6978-6984.

Turina, P., and R.A. Capaldi. 1994. ATP hydrolysis-driven structural changes in the γ-subunit of *Escherichia coli* ATPase monitored by fluorescence from probes bound at introduced cysteine residues. *J. Biol. Chem.* 269:13465-13471.

Ueno, H., T. Suzuki, K. Kinosita, Jr., and M. Yoshida. 2005. ATP-driven stepwise rotation of FoF1-ATP synthase. *Proc Natl Acad Sci U S A*. 102:1333-8.

Uhlin, U., G.B. Cox, and J.M. Guss. 1997. Crystal structure of the ε subunit of the proton-translocating ATP synthase from *Escherichia coli*. *Structure*. 5:1219-1230.

Valiyaveetil, F.I., and R.H. Fillingame. 1998. Transmembrane topography of subunit *a* in the *Escherichia coli* F_1F_O ATP synthase. *J. Biol. Chem.* 273:16241-16247.

Vik, S.B. 2000. What Is the Role of epsilon in the Escherichia coli ATP Synthase? *J Bioenerg Biomembr*. 32:485-91.

Vik, S.B., and B.J. Antonio. 1994. A mechanism of proton translocation by F_1F_O ATP synthases suggested by double mutant of the *a* subunit. *J. Biol. Chem.* 269:30364-30369.

Vik, S.B., J.C. Long, T. Wada, and D. Zhang. 2000. A model for the structure of subunit a of the Escherichia coli ATP synthase and its role in proton translocation. *Biochim Biophys Acta*. 1458:457-66.

Vonck, J., and E. Schaefer. 2008. Supramolecular organization of protein complexes in themitochondrial inner membrane. *Biochim. Biophys. Acta*:doi:10.1016/j.bbamcr.2008.05.019.

Wada, T., J.C. Long, D. Zhang, and S.B. Vik. 1999. A novel labeling approach supports the five-transmembrane model of subunit a of the Escherichia coli ATP synthase. *J Biol Chem*. 274:17353-7.

Walker, J.E., and V.K. Dickson. 2006. The peripheral stalk of the mitochondrial ATP synthase. *Biochim Biophys Acta*. 1757:286-96.

Wang, H., and G. Oster. 1998. Energy transduction in the F_1 motor of ATP synthase. *Nature*. 396:279-282.

Watanabe, R., R. Iino, K. Shimabukuro, M. Yoshida, and H. Noji. 2008. Temperature-sensitive reaction intermediate of F1-ATPase. *EMBO Rep.* 9:84-90.

Watts, S.D., C. Tang, and R.A. Capaldi. 1996. The stalk region of the *Escherichia coli* ATP synthase: tyrosine 205 of the γ subunit is in the interface between the F_1 and F_O parts and can interact with both the ε and *c* oligomer. *J. Biol. Chem.* 271:28341-28347.

Webb, M.R., C. Grubmeyer, H.S. Penefsky, and D.R. Trentham. 1980. The stereochemical course of phosphoric residue transfer catalyzed by beef heart mitochondrial ATPase. *J. Biol. Chem.* 255:11637-11639.

Weber, J. 2006. ATP synthase: subunit-subunit interactions in the stator stalk. *Biochim Biophys Acta*. 1757:1162-70.

Weber, J., and Senior, A. E. 2003. ATP synthesis driven by proton transport in F_1F_O-ATP synthase. *FEBS Lett.* 545:61-70.

Weber, J., C. Bowman, and A.E. Senior. 1996. Specific tryptophan substitution in catalytic sites of *Escherichia coli* F_1-ATPase allows differentiation between bound substrate ATP and product ADP in steady-state catalysis. *J. Biol. Chem.* 271:18711-18718.

Weber, J., C. Bowman, S. Wilke-Mounts, and A.E. Senior. 1995. α-Aspartate 261 is a key residue in noncatalytic sites of *Escherichia coli* F_1-ATPase. *J. Biol. Chem.* 270:21045-21049.

Weber, J., A. Muharemagic, S. Wilke-Mounts, and A.E. Senior. 2003. F_1F_O-ATP synthase: binding of δ subunit to a 22-residue peptide mimicking the N-terminal region of α subunit. *J. Biol. Chem.* 278:13623-13626.

Weber, J., S. Nadanaciva, and A.E. Senior. 2000. ATP-driven rotation of the γ subunit in F_1-ATPase. *FEBS Lett.* 483:1-5.

Weber, J., and A.E. Senior. 1996. Binding and hydrolysis of TNP-ATP by *Escherichia coli* F_1-ATPase. *J. Biol. Chem.* 271:3474-3477.

Weber, J., and A.E. Senior. 1997. Catalytic mechanism of F_1-ATPase. *Biochim. Biophys. Acta*. 1319:19-58.

Weber, J., and A.E. Senior. 2000. ATP synthase: what we know about ATP hydrolysis and what we do not know about ATP synthesis. *Biochim. Biophys. Acta*. 1458:300-309.

Weber, J., and A.E. Senior. 2001. Bi-site catalysis in F_1-ATPase: Does it exist? *J. Biol. Chem.* 276:35422-35428.

Weber, J., and A.E. Senior. 2004. Fluorescent probes applied to catalytic cooperativity in ATP synthase. *Methods Enzymol*. 380:132-52.

Weber, J., S. Wilke-Mounts, R.S.-F. Lee, E. Grell, and A.E. Senior. 1993. Specific placement of tryptophan in the catalytic sites of *Escherichia coli* F_1-ATPase provides a direct probe of nucleotide binding: maximal ATP hydrolysis occurs with three sites occupied. *J. Biol. Chem.* 268:20126-20133.

Weber, J., S. Wilke-Mounts, S. Nadanaciva, and A.E. Senior. 2004. Quantitative determination of direct binding of b subunit to F1 in Escherichia coli F1F0-ATP synthase. *J Biol Chem*. 279:11253-8.

Weber, J., S. Wilke-Mounts, and A.E. Senior. 2002. Quantitative determination of binding affinity of delta-subunit in Escherichia coli F1-ATPase: effects of mutation, Mg2+, and pH on Kd. *J Biol Chem*. 277:18390-6.

White, H.D., B. Belknap, and M.R. Webb. 1997. Kinetics of nucleoside triphosphate cleavage and phosphate release steps by associated rabbit skeletal actomyosin,

measured using a novel fluorescent probe for phosphate. *Biochemistry*. 36:11828-11836.

Wilkens, S., D. Borchardt, J. Weber, and A.E. Senior. 2005. Structural characterization of the interaction of the delta and alpha subunits of the Escherichia coli F1F0-ATP synthase by NMR spectroscopy. *Biochemistry*. 44:11786-94.

Wilkens, S., and R.A. Capaldi. 1998a. ATP synthase's second stalk comes into focus. *Nature*. 393:29.

Wilkens, S., and R.A. Capaldi. 1998b. Solution structure of the ε subunit of the F_1-ATPase from *Escherichia coli* and interactions of this subunit with β subunits in the complex. *J. Biol. Chem.* 273:26645-26651.

Wilkens, S., F.W. Dahlquist, L.P. McIntosh, L.W. Donaldson, and R.A. Capaldi. 1995. Structural features of the ε subunit of the *Escherichia coli* ATP synthase determined by NMR spectroscopy. *Nature Struct. Biol.* 2:961-967.

Wise, J.G., L.R. Latchney, A.M. Ferguson, and A.E. Senior. 1984. Defective proton ATPase of *uncA* mutants of *Escherichia coli.* 5'-adenylyl imidodiphosphate binding and ATP hydrolysis. *Biochemistry*. 23:1426-1432.

Wise, J.G., L.R. Latchney, and A.E. Senior. 1981. The defective proton-ATPase of *uncA* mutants of *Escherichia coli*: studies of nucleotide binding sites, bound aurovertin fluorescence, and labeling of essential residues of the purified F_1-ATPase. *J. Biol. Chem.* 256:10383-10389.

Wise, J.G., and E. Senior. 1985. Catalytic properties of the *Escherichia coli* proton adenosinetriphosphatase: evidence that nucleotide bound at noncatalytic sites is

not involved in regulation of oxidative phosphorylation. *Biochemistry*. 24:6949-6954.

Wise, J.G., and P.D. Vogel. 2008. Subunit b-dimer of the Escherichia coli ATP synthase can form left-handed coiled-coils. *Biophys J*. 94:5040-52.

Xiong, H., D. Zhang, and S.B. Vik. 1998. Subunit ε of the *Escherichia coli* ATP synthase: novel insights into structure and function by analysis of thirteen mutant forms. *Biochemistry*. 37:16423-16429.

Yagi, H., N. Kajiwara, H. Tanaka, T. Tsukihara, Y. Kato-Yamada, M. Yoshida, and H. Akutsu. 2007. Structures of the thermophilic F1-ATPase epsilon subunit suggesting ATP-regulated arm motion of its C-terminal domain in F1. *Proc Natl Acad Sci U S A*. 104:11233-8.

Yasuda, R., T. Masaike, K. Adachi, H. Noji, H. Itoh, and K. Kinosita. 2003. The ATP-waiting conformation of rotating F1-ATPase revealed by single-pair fluorescence resonance energy transfer. *Proc. Natl. Acad. Sci. U. S. A.* 100:9314-8.

Yasuda, R., H. Noji, K. Kinosita, and M. Yoshida. 1998. F_1-ATPase is a highly efficient molecular motor that rotates with discrete 120° steps. *Cell*. 93:1117-1124.

Yasuda, R., H. Noji, M. Yoshida, K. Kinosita, and H. Itoh. 2001. Resolution of distinct rotational substeps by submillisecond kinetic analysis of F_1-ATPase. *Nature*. 410:898-904.

Yoshida, M., E. Muneyuki, and T. Hisabori. 2001. ATP synthase--a marvellous rotary engine of the cell. *Nat. Rev. Mol. Cell Biol.* 2:669-677.

Yoshida, M., H. Okamoto, N. Sone, H. Hirata, and Y. Kagawa. 1977. Reconstitution of thermostable ATPase capable of energy coupling from its purified subunits. *Proc. Natl. Acad. Sci. U.S.A.* 74:936-940.

Zhang, Y., and R.H. Fillingame. 1994. Essential aspartate in subunit *c* of F_1F_O ATP synthase: effect of position 61 substitutions in helix-2 on function of Asp^{24} in helix-1. *J. Biol. Chem.* 269:5473-5479.

Zhang, Y., and R.H. Fillingame. 1995. Subunits coupling H^+ transport and ATP synthesis in the *Escherichia coli* ATP synthase: cys-cys cross-linking of F_1 subunit ε to the polar loop of F_1F_o subunit *c*. *J. Biol. Chem.* 270:24609-24614.

Zhang, Y., M. Oldenburg, and R.H. Fillingame. 1994. Suppressor mutations in F_1 subunit ε recouple ATP-driven H^+ translocation in uncoupled Q42E subunit *c* mutant of *Escherichia coli* F_1F_o ATP synthase. *J. Biol. Chem.* 269:10221-10224.

Zhou, Y., T.M. Duncan, and R.L. Cross. 1997. Subunit rotation in *Escherichia coli* F_OF_1-ATP synthase during oxidative phosphorylation. *Proc. Natl. Acad. Sci. U. S. A.* 94:10583-10587.

Zimmermann, B., M. Diez, M. Borsch, and P. Graber. 2006. Subunit movements in membrane-integrated EF0F1 during ATP synthesis detected by single-molecule spectroscopy. *Biochim Biophys Acta*. 1757:311-9.

Zimmermann, B., M. Diez, N. Zarrabi, P. Graber, and M. Borsch. 2005. Movements of the epsilon-subunit during catalysis and activation in single membrane-bound H(+)-ATP synthase. *Embo J*. 24:2053-63.